Energy Efficiency of Soft Pneumatic Extension Actuators

Jelle de Vries

physics of functional complex matter

Delft University of Technology

Energy Efficiency of Soft Pneumatic Extension Actuators

by

Jelle de Vries

to obtain the degree of

Master of Science
in Mechanical Engineering

at the Delft University of Technology,
to be defended publicly on Tuesday August 31, 2021 at 13:30 AM.

Student number:	4292987	
Thesis committee:	Dr. ir. A. Sakes,	TU Delft, chair, supervisor
	Dr. D. Dodou,	TU Delft
	Dr. ir. J. T. B. Overvelde,	AMOLF, supervisor

An electronic version of this thesis is available at http://repository.tudelft.nl/.

TU Delft Delft University of Technology

Preface

I attempt an arduous task;
but there is no worth in that which is not a difficult achievement.

Ovidius

It's done. It's over.
After eight years of work I still can barely believe it has finally come to an end. It hasn't always been easy, especially during this last year and a half. The pandemic certainly has taken its toll, both mentally and physically. I would like to thank everyone who has guided and supported me during these trying times.

First of all I would like to thank Bas Overvelde, your guidance and trust in me have helped me throughout this entire journey but mostly when I was at the end of my rope. Next, I would like to thank Luuk van Laake, thanks to your infinite curiosity and enthusiasm, I never had to fear running out of ideas for additional investigation. Furthermore, I would like to thank Aimée Sakes nudging my research in the right direction to make sure it would hold up to the standards that are to be expected at TU Delft.

It should go without saying that I want to thank everyone in the Soft Robotic Matter group. Each and everyone of you has been amazing in your own way. Thank you guys and gals for making this such an awesome and supportive working environment. I loved all the random useless discussions we had during this time. I would like to restate the most important equation I found: 1 Slice = 1 Sandwich!

Finally, I want to thank the most important person in my life, my amazing girlfriend Nikkie. You have made all of this possible, for without you, I am nowhere. I love you.

Thank you all!

Jelle de Vries
Leiden, August 2021

Abstract

Mobile soft robots show great potential for exploration of unknown and hard to navigate environments. Sadly, most of these robots are currently being held back by their power sources and control systems. These components, which are usually quite heavy and bulky, need to be integrated before mobile soft robots can cut their tethers and explore the world autonomously. Soft robots should be mindful of their energy consumption to minimize the requirements on the power supply. However, the efficiency of their actuators is still a not well understood area of research. We attempt to pave the road for future research into this subject by developing a testing protocol based on a simplified analytical model. We built an experimental setup and investigated the efficiency of soft pneumatic extension actuators. We found that actuator designs which reduce axial stiffness produced higher efficiency. Additionally, we found that efficiency increases with load, until it is limited by the buckling load. Unfortunately, these two conditions seem to conflict with each other since a lower axial stiffness also reduced the buckling load. Future actuator designs should therefore try to combine a low axial stiffness with high load bearing capabilities. Also, this research should be extended to different classes of soft actuators as well as investigating non-ideal circumstances. We believe this research aids in the general understanding of efficiency of soft actuators and act as a stepping stone for future research.

Contents

1
Introduction

Soft robotics is an upcoming area of research which shows great potential for complementing the field of traditional rigid robotics. Its main application areas are medical instruments [9], rehabilitation devices [25], grippers [35], manipulators [41], and locomotion [22]. Advantages of soft robots include safe interaction with humans, adaptability, and the ability to deal with unknown environments. These desirable properties stem from the materials used in soft robotics. Most commonly, hyperelastic materials are used which allow for extremely large deformations, exhibit high damage tolerance, and showcase excellent compliance. However, non-linear material responses combined with large deformations significantly increase the difficulty of modeling such robots. Furthermore, soft robots cannot achieve the same levels of precision commonly seen in rigid robots. Nevertheless, soft robots can complete tasks without the need for high precision and controllability due to their inherent compliance. The ability to perform tasks due to material properties and structure is referred to as embodied intelligence [21].

Robotic systems are comprised of multiple individual components which are combined into a complete unit. These components include actuation, sensing, processing, and power. Developments in all of these areas have greatly improved over the last years and integration of these components has started to become more important [32]. However, most soft robots are still connected to a stationary power supply or processing unit. The next step is for soft robots to cut their tethers and start exploring the world autonomously. To do so, untethered soft robots still have hurdles to overcome [33]. To cut the cord to the fixed world all the aforementioned components need to be integrated into one system. Robots need to be strong enough to carry their load and posses adequate power production and supply. Energy efficiency of soft robots is thus an important subject as a higher energy efficiency results in lower power requirements. This in turn allows for usage of smaller and lighter power sources which also lowers power requirements. Selection of suitable and efficient power sources [1] as well efficiency of complete locomotion systems [36] has been discussed. However, efficiency of individual actuators has so far been relatively understudied and no clear guidelines exist.

The goal of this research is gain more insight into the energy efficiency of soft actuators. We will investigate how energy is transfered, stored, and dissipated over a complete actuation cycle. Additionally, we will study the influence of different designs and parameters on the energy distribution. We start with highlighting possible applications of soft robotics and discussing different classes of soft actuators.

1.1. Soft Robotics

As mentioned before, soft robotics provide specific benefits within certain applications. One of the biggest advantages of soft robots is the safe interaction with humans which offers excellent potential within rehabilitation devices. As an example, figure 1.1 shows such a device. Polygerinos et al. [31] have developed this device as an assistance and rehabilitation device for people with hand disabilities. Five hydraulic soft actuators, each one individually designed to mimic the motion path of the corresponding finger, are placed on top of the hand to provide additional bending force to the fingers. The soft nature of the actuators means that the assistance force is provided without heavily restricting the natural motion path of the fingers. Figure 1.1a-c show different exercises encountered in rehabilitation training while figure 1.1d-f show grasping of every day objects of different shape and weight.

Figure 1.1: "The soft robotic glove in: A. index finger–thumb opposition contact, B. small finger–thumb opposition contact, C. index finger flexion, D. grasping a bottle of water using all fingers, E. picking up a telephone using all fingers, except of the small, and F. grasping of a television remote control using a tripod pinch." [31]

Another application where soft robotics can excel is as grippers and manipulators. Figure 1.2a shows a fully 3D printed pneumatic actuator with conformal grasping [39]. This novel bending actuator design was enhanced using bio-inspired fin ray structures which help conform to the grasped object. Soft grippers can be used to grasp objects without having any knowledge about size or shape. The compliant structure will form itself to the object and provide good grasping. This particular gripper can lift an electric drill weighing 1.6 kg, shown in figure 1.2a. Even delicate objects can be grabbed without damaging them. Figure 1.2b shows different objects, including an egg, being lifted. Soft grippers can be mounted on a rigid arm or alternatively on a soft manipulator. An example of a (partly) soft manipulator is shown in figure 1.2c. The OctArm [15] consists of three segments which are comprised of six (first two segments) or three (third segment) McKibben extensor muscles. When inflated, the McKibben muscles will extend due to the angle of the braided mesh. A segment will bend towards one side when the muscles on the opposite side of the OctArm actuate. The three segments combined with the 360 degrees rotational base provide excellent dexterity and manoeuvrability. Figure 1.2d shows the OctArm picking up a traffic cone and placing it on top of another cone. In this example the manipulator is able to perform the task without a gripper but combining the manipulator with a gripper makes it able to also perform more delicate tasks.

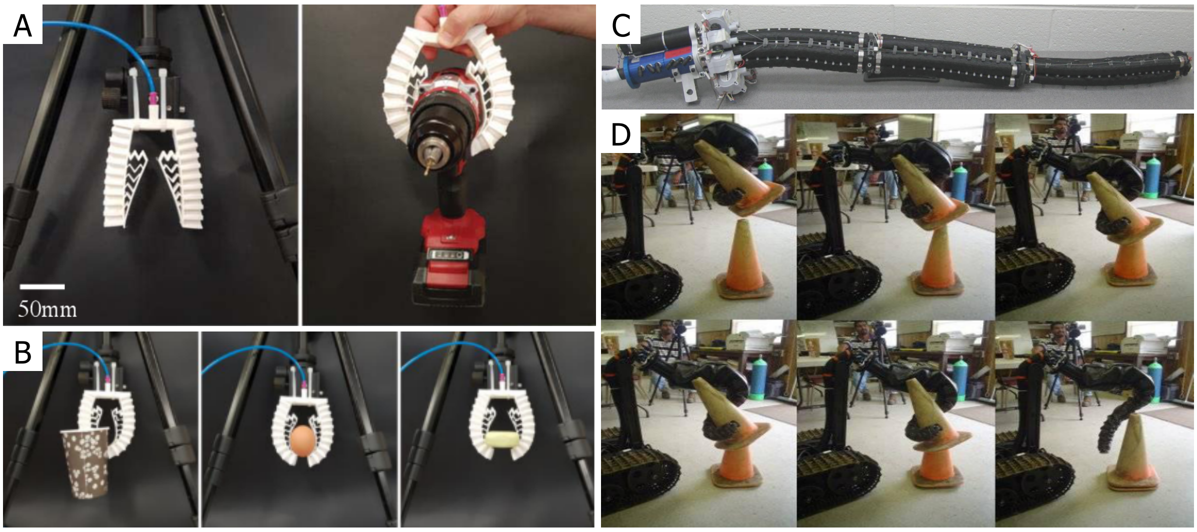

Figure 1.2: A. 3D printed soft gripper unactuated (left) and gripping a 1.6 kg drill (right) [39], B. 3D printed soft gripper picking up a cup (left), an egg (middle), and a bar of soap (right) [39], C. OctArm VI [15], D. OctArm performing a pick and place task using a traffic cone [15].

The final example of an application where the inherent compliance of soft robots can be advantageous is locomotion. The inherent compliance helps soft robots easily navigate irregular and unknown landscapes without complicated control strategies. Figure 1.3a shows a soft quadruped walking robot [12]. The robot has four legs, each made using three extension bellows actuators. By actuating a single bellows the tip of the leg can be steered in a specific direction to take a step. The four legs take alternating steps and thereby move the robot forward. Another example of a walking robot is the multigait soft robot designed by Shepherd et al. [34]. It is comprised of five bending actuators, four actuators as legs and one as a spine. The addition of the active spine makes different gait patterns possible. Figure 1.3b shows the robot using an undulating gait pattern to crawl underneath a glass plane.

For both these examples the robot is still tethered to a stationary pressure source and control system. To be useful in actual practical applications it is necessary for locomotion robots to operate autonomously. Tolley et al. [40] expand on the research of Shepherd et al. by integrating all components on-board. This includes pressure source, energy storage, control system, and sensors. Figure 1.3c shows the autonomous robot exploring an indoor area and also demonstrates the robots resilience to damage (in this case being run over by a car). The final example of locomotive soft robots does not walk or crawl but rather swims. The Soft Robotic Fish (SoFi) by Katzschmann et al. [20] is a remote controlled robot used to study fish in a non invasive manner. The components for the SoFi are shown in figure 1.3d. Forward motion is achieved through the use of a bidirectional hydraulic bending actuator based on the tail fin of fish.

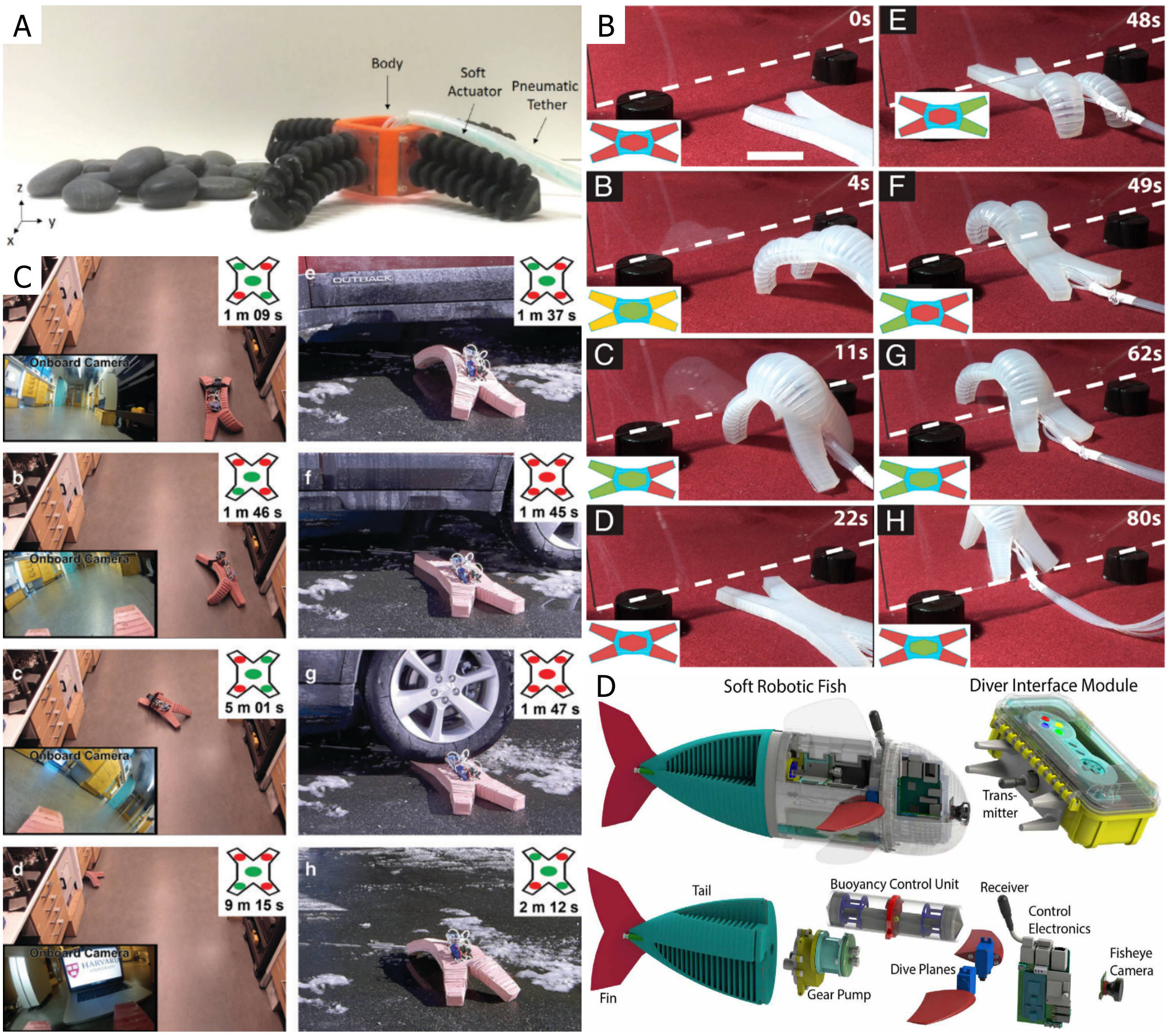

Figure 1.3: A. Soft quadruped walking robot [12]. B. Multigait soft robot [34]. C. Resilient Untethered soft robot [40]. D. SoFi [20]

1.2. Soft Actuators

Any soft robot relies on its actuators to perform motion or tasks. The actuators are the muscles of the robot. Most research within the field has been aimed towards the development of new and better actuators. Soft actuators can be based on a number of working principles. Boyraz et al. [5] have identified five of these working principles. They compared these working principles on eight selection criteria. The actuator types reviewed include shape-memory alloys (SMAs), fluidic elastomer actuators (FEAs), shape memory polymers (SMPs), dielectric/electrically-actuated polymers (DEAPs) and electro-magnetic/magnetic actuators (E/MAs). The selection criteria which were assessed are compliance, topology-geometry, scalability, energy efficiency, operation range, modality, controllability and technological readiness level.

- Shape-memory alloys are composite metals that can recover their initial state after being deformed. This is achieved by heating the material above a transition temperature which restores the remembered shape. The shape is maintained by cooling the material below the transition temperature. Challenges involving SMAs are the innate hysteresis and the slow response time.
- Fluidic elastomer actuators are rubber-like structures with a hollow inner cavity. Increasing the pressure inside the cavity through a fluidic medium (most commonly air or water) causes the actuator to deform. The response to the pressure stimulus is determined by the topology of the actuator. FEAs can display extreme strain levels of up to 700%. However, their highly non-linear behaviour poses significant challenges regarding modeling and control.
- Shape memory polymers are similar to SMAs in that they can recover their initial state when exposed to a thermal stimulus. Differences lie in their mechanical properties where SMPs have larger recovery strains (>300% vs <8%) but lower recovery stresses (1-10 MPa vs 1 GPa). Furthermore, SMAs exhibit better biocompatibility which is especially important for medical applications. Downsides with these materials are the non-linear and sometimes still unidentified behaviour and the rate of heat transfer limiting the actuation speed.
- Dielectric-electrically actuated polymers show similar levels of compliance as FEAs but actuation is achieved very differently. DEAPs start to deform when placed in a large electric field, similar to piezoelectric actuators. The electric field can be applied by means of flexible electrodes placed directly on the DEAP. When working with high voltage the electric breakdown of the material becomes an obstacle. Additionally, durability of DEAPs is also an issue.
- Electro-magnetic/magnetic actuators can work using ferromagnetic particles, a flexible coil, or a liquid metal coil embedded in an elastomer substrate. When an E/MA is subjected to an external magnetic field it will deform and apply a force. Although promising, E/MAs are a relatively recent discovery and have not been explored to their full potential. Currently they are only produced at small scale and scalability is a yet unaddressed problem. However, E/MAs do boast the highest reported power density (22.3-309.3 kW/m^3) but at the cost of energy efficiency (0.0049-0.03%).

Once the actuator types were reviewed with respect to the selection criteria their applicability in different domains is scored. Scoring is based on the selection criteria most relevant to specific domain. Table 1.1 shows the scores given by Boyraz et al. [5]. From this table we can conclude FEAs are a suitable choice for most applications. Their wide range applicability combined with their ease of manufacturing (FEAs can be produced through mould casting using a variety of commercially available silicons) and simple actuation principle means FEAs are an excellent choice of actuator. This research will thus focus on FEAs.

Actuator	Medical	Industrial	Haptic-Interface	Active Safety in Automotive
SMA	*	*	*	*
FEA	***	***	***	***
SMP	**	*	***	**
DEAP	**	**	**	***
E/MA	*	**	*	**

Table 1.1: Scoring of actuator types based on application domain with (***) as highest score and (*) as lowest score [5]

Gorissen et al. [14] have reviewed FEAs more in depth. They refer to FEAs as elastic inflatable actuators (EIAs). Four aspects of EIAs were addressed: design and modeling, fabrication techniques, control, and applications. EIAs work using an inflatable void surrounded by soft materials with Young's moduli between 10^5 and 10^7 Pa. Sometimes stiffer materials acting as strain limiting layers are added. By changing the topology of the actuator, and optionally the placement of strain limiting material, different motions can be achieved. Figure 1.4 shows the different motions identified by Gorissen et al. which include extension, contraction, twisting, and bending. Furthermore, some actuators have been proposed which transcend the classes described here and can achieve multiple different motion paths based on specific inputs [2, 44, 26].

Inflating any void will result in expansion. The difficulty lies in transforming this omni-directional expansion into a desired motion. For extension actuators this can be achieved by restraining or limiting the expansion along lateral axes or by enhancing the expansion along the longitudinal axis. Limiting the lateral expansion can be done by dividing an actuator into segments or chambers [29, 13]. The walls between these chambers help constrain the expansion. Another way to limit the expansion is by adding stiffer material placed such that lateral expansion is limited without affecting axial expansion too much [3, 17]. Enhancing the expansion along the longitudinal axis can be done using corrugated side walls [10, 19]. This way the actuator walls will first bend at the peaks and valleys of the corrugation which lowers the longitudinal stiffness.

Contraction actuators can be made in multiple different ways. The first is to apply a vacuum instead of a positive pressure [23, 38]. Tactics similar to the extension actuator can be used to direct the contraction along the longitudinal axis. The second way is to use positive pressure but convert, through an inextensible material, the lateral expansion to longitudinal contraction [6, 48]. The last way to achieve contraction is by using an extension actuator but inverting the actuation [16]. The initial state of the actuation is with a high internal pressure and to achieve contraction the pressure is lowered and the elastic energy stored in the actuator provides contraction.

Twisting actuators can display pure torsion or a screwing motion. The screwing motion can be retracting [18] or protracting [4]. The retraction motion is achieved through a combination of vacuum and slanted buckling walls. Protraction motion is in this case achieved by using a fiber based design having a different braiding angle for the clockwise fibers than for the counterclockwise fibers. Protraction can also be realised by spiralling two extension actuators around a longitudinal axis. If the extension is then constrained pure torsion is achieved [45].

An inflatable bending actuator can be made by adapting an extension or contraction actuator. If an extension actuator is inflated it will extend. But if there is an asymmetry in the axial stiffness the side of the actuator with the lower stiffness will extend more and the actuator bends towards the stiffer side [14]. This asymmetry can be created by using a corrugated pattern on one side of the actuator [28, 46], integration of a strain limiting layer [30, 47], or eccentrical placement of the inflatable void [37, 7].

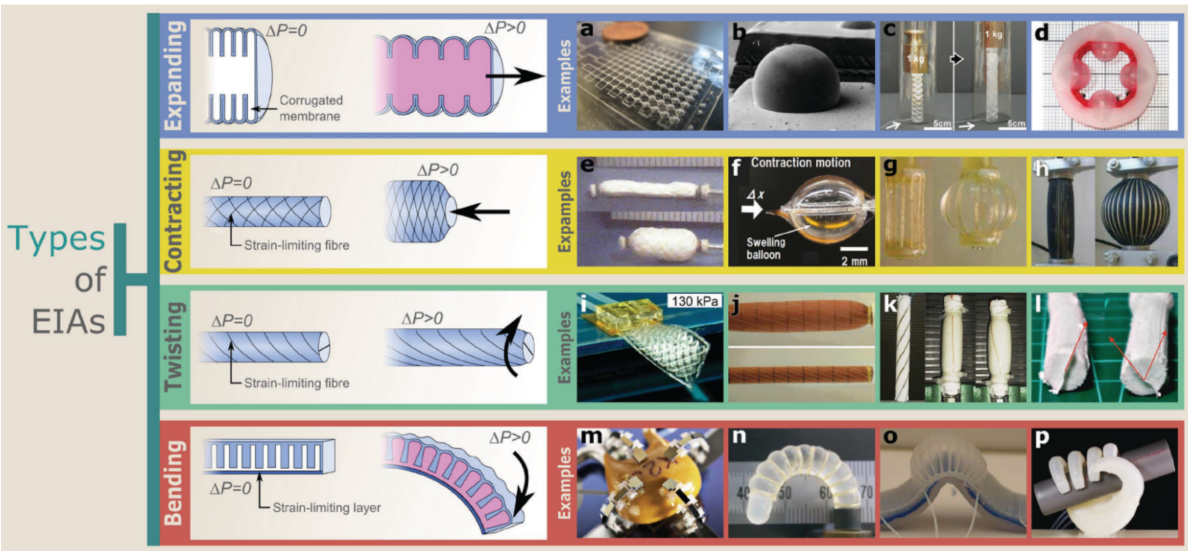

Figure 1.4: Classification of EIAs based on their motion paths as described by Gorissen et al. [14]

1.3. Energy efficiency

Energy efficiency is an important aspect for untethered soft robots. For locomotion robots to become untethered and explore autonomously all of their components need to be embedded. Each component has its own efficiency which contributes to the overall efficiency of the entire robot. The actuator is one of the main components where energy losses occur. Actuators are the main moving parts of the robot and thus also the biggest source of dissipation. Materials commonly used in soft robotics are classified as viscoelastic materials meaning they dissipate energy internally during deformation [11]. Furthermore, the high compliance allows soft actuators to deform greatly but not all of this deformation gets translated to work. Investigating how efficient soft actuators are and, more importantly, how to improve this is important.

However, few researchers have taken up to investigate this important property. Furthermore, different experimental methods have been used to determine the energy efficiency in soft pneumatic actuators. Efficiency is not a standardized quantity and cannot be directly measured. Therefore, efficiency is greatly dependent on the definition and measurement setup which are being used. To illustrate this importance three articles will be discussed. Each of them uses a different definition and experimental procedure to determine efficiency.

Wehner et al. [43] have characterized different properties McKibben artificial muscles, a type of contraction actuator. Efficiency tests were performed using an Instron tensile testing machine. A specimen was placed in the machine and inflated to a set pressure (551 kPa). Using the Instron machine the specimen was allowed to contract at a prescribed rate. After achieving full contraction the specimen was forced back to its initial length. This cycle was repeated multiple times to ensure repeatable behaviour. After the first cycle the specimen showed very repeatable behaviour. A hysteresis in the force-displacement curve was observed and the energy loss over one cycle was calculated as the area inside this hysteresis loop. They found the efficiency of these actuators to be 65%-75%, dependent on actuator length. A point of criticism could be that this procedure does not resemble an actuation cycle since generally fluidic actuators are controlled using pressure or volume input.

Chun et al. [8] did use volume as the input for their pneu-net bending actuator. The experimental design they used was to connect a weight via a rope and pulley to the end of the actuator. Using a syringe with water a volume input was provided to actuate the pneu-net. Parameters include material stiffness, internal wall thickness, and applied load. The weight was lifted and the efficiency was calculated as the ratio of work done by lifting the weight over the hydraulic input energy provided. Efficiency was found to be highest for the more compliant material. Also, an efficiency optimum was observed when weight was varied. The maximum efficiency measured was 2.8%. Obviously, this is significantly lower than Wehner et al. reported. Using an actual actuation can explain for some of the discrepancy. However, Chun et al. only considered the lifting of the weight ending in the fully actuated position. Here, a large part of the input energy is stored in the elastically deformed material and thus regarded as energy lost. Measuring the stored energy provides a more complete representation of the actuator.

Lin et al. [24] also preformed efficiency measurements. They characterized their vacuum-powered soft linear actuator strengthened by granular jamming (J-VSLA). In their experiments a weight was lifted by applying a volume input. The efficiency was calculated as the work done during lifting divided by the input energy. Additionally, dissipation during a complete cycle of lifting and lowering was calculated as the difference between input energy and the recovered energy divided by the input energy. For the energy efficiency around 30% was found, while for the energy dissipation between 25% and 35% was found. This means 35%-45% of the input energy was stored in the actuator indicating this is indeed an important aspect to consider. However, the weight is connected to the actuator at all times. This means that over a complete actuation cycle the energy efficiency would be zero since the total sum of work is zero. Having a load which is only applied during activation would improve the analysis even further.

1.4. Project goals and thesis outline

In this section we will define the objective of this study and the distinct research questions associated with this objective. Furthermore, we will provide an outline of this thesis and relate the sections to the objective and research questions. The main goal of this study is to *gain a more complete and in-depth understanding of the energy efficiency of soft pneumatic actuators.* To reach this goal we aim to answer three research questions:

1. The first research question is *how can we define and measure efficiency to provide a complete representation of a soft pneumatic actuator?* In section 2.1 we present the actuators used in this research and their fabrication process. Then, in section 2.2 we present a analytical model of an actuator during an actuation cycle. Using this model we discuss all the energy contributions and formulate the equations needed to describe them. From here, two distinct definitions of efficiency are presented as well as the quantities needed to be measured. Section 3.1 presents the design of the experimental setup to measure these quantities. Furthermore, we describe the operating procedure for the experiments.
2. The second research question is *how is energy distributed during an actuation cycle and what are the main causes of energy loss?* Section 3.2 shows the actuator behaviour during a single actuation cycle. Furthermore, we quantify each of the energy contributions separately during a series of experiments. Lastly, we ensure the validity of our assumptions by tuning the settings for the experiments.
3. The third research question is *how do different design parameters affect actuator efficiency and work?* In chapter 4, we show the results for the experiments. Sections 4.1 through 4.4 each consider a specific actuator design, as described in section 2.1.1, and highlight the effects of the relevant design parameters at different loads and inputs. In section 4.5 we take a step back and look at all actuators from a broader perspective and compare the different types to each other.

Chapter 5 discusses the steps taken to answer these questions and presents our conclusions based on the results. Furthermore, we provide some general guidelines for effective design and use of soft actuators. Finally, we will discuss some potential areas for future research.

2

Actuators

In this chapter we will discuss the actuators used during this research. First, we will discuss the design of the actuators which will be created and tested. Following that, we will explain the fabrication process in detail. Lastly, we introduce the analysis of the actuators where we discuss a simplified model of the actuation cycle, highlight the possible causes of energy losses in this cycle, explain the equations to characterize these energy losses, and present two definitions of efficiency.

2.1. Actuator design and fabrication

We already narrowed the scope of this research to FEAs. However, even within this section of soft actuators there are still a number of classes of actuators, each with their own sub-types. For sake of feasibility only one of these classes will be investigated. We have made the choice for extension actuators. The linear motion path simplifies the setup design. Additionally, all types of extension actuator are, unlike contraction actuators, powered using positive pressure. This allows for a more straightforward control scheme and comparison between actuator types.

2.1.1. Actuator designs

As mentioned previously in section 1.2, three different types of extension actuators can be identified. These are: chamber actuators, corrugated actuators, and multi-material actuators. Additionally, we will also make a baseline actuator which will be used to compare the performance between designs. For this baseline actuator we will also vary other design parameters such as wall thickness and material properties.

Baseline design

The baseline actuator will be as simple as possible. This way, we can determine the effects of the different design strategies more easily. The actuator is a hollow cylinder with three geometrical design parameters: length (L), inner radius (R), and wall thickness (t). Figure 2.1 shows the design of the base actuator and indicates these design parameters. The fourth design parameter is the material used for the actuator.

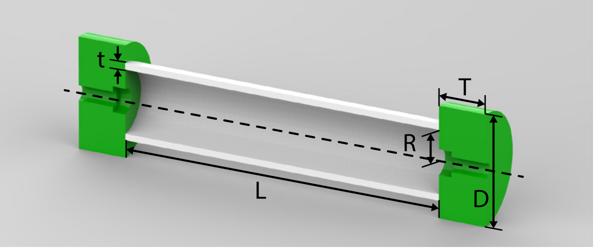

Figure 2.1: Cross-sectional view of the baseline actuator. The dashed line indicates the central axis of the actuator. The length L, inner radius R, wall thickness t, block diameter D, and block thickness T are indicated as well.

Two blocks of stiffer rubber are attached to either side which allow for the actuator to be placed in the experimental setup described in section 3.1. These blocks are purposely made relatively thick to ensure their stiffness is significantly larger than the tube section. These blocks will be the same for all actuators to ensure a consistent interaction with the measurement setup. The holes on both ends allow the water-soluble inner mould to be flushed out. Section 2.1.2 will explain the fabrication process in more detail.

Chamber design

The first actuator design that will be investigated is the chamber design. Here, the inside of the baseline actuator will be subdivided into discrete chambers by placing walls. Figure 2.2 shows a cross-section of the chamber design. Three new design parameters are important for this specific design: radius of the hole in the chamber wall (r), chamber wall thickness (t_w), and chamber length (L_{cham}). The lower limit for the radius of the hole in the wall is constrained by the structural integrity of the inner mould. The chamber wall thickness and chamber length are dependent on each other as the sum of the length of all chambers and the thickness of all walls combined must be equal to the total length of the actuator. We have chosen for a constant wall thickness and to vary the number of chambers. The length of chambers changes to accommodate the number of chambers. However, all chambers within an actuator will have equal length.

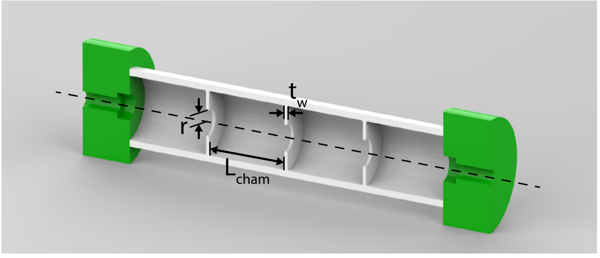

Figure 2.2: Cross-sectional view of the chamber design actuator. The relevant parameters are hole radius r, chamber wall thickness t_w, and chamber length L_{cham}.

Corrugated design

The second actuator design to investigate is the corrugated design. The wall of the corrugated actuator is not straight like the baseline actuator, but follows a wavy pattern. Figure 2.3 shows a cross-section of the corrugated design. The wave pattern has a sine-like shape with the ends transitioning to a straight cylinder. This ensures similar boundary conditions for all actuators. This design features two important parameters: wavelength (λ) and amplitude (A). We have chosen to keep the wavelength constant for all the actuators and vary the amplitude. Near the ends the waving pattern transitions to a cylinder so the ends are consistent with the other designs. The wavelength has been chosen such that an odd harmonic wave fits in the length between the transitions. An odd harmonic was chosen to keep the actuator symmetrical.

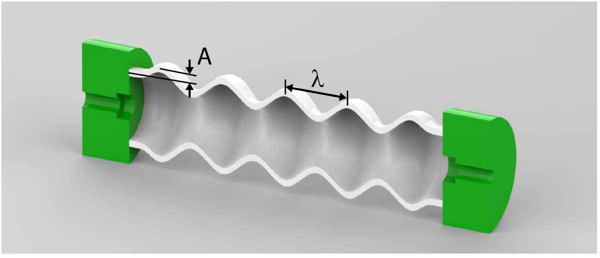

Figure 2.3: Cross-sectional view of the corrugated design actuator. The relevant parameters are amplitude A and wavelength λ.

Multi-material design

The final actuator design which we will investigate is the multi-material actuator. The inside of this actuator is the same as the baseline actuator. However, the outside of the actuator is wrapped with another (stiffer) material acting as strain-limiting fibers. The multi-material actuator design is shown in figure 2.4 Commonly, the materials used for these fibers have such a high stiffness that they can be considered inextensible. The only parameter associated is the braiding angle between the fiber and the longitudinal axis of the actuator. In this case we will not consider the fiber to be inextensible which makes the stiffness of the fiber relevant. The stiffness is dependent on the diameter and material of the fiber. The braiding angle (α) and fiber diameter (d) are kept constant and the stiffness is varied by changing the fiber material.

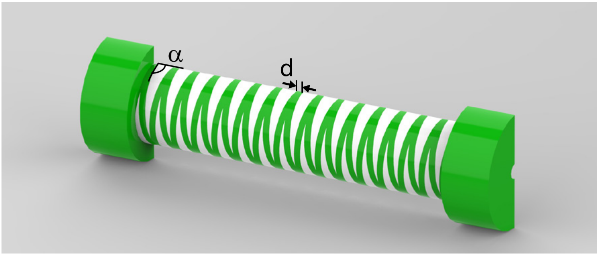

Figure 2.4: Side view of the multi-material design actuator. The relevant parameters are fiber diameter d and braiding angle α.

Actuator dimensions

We have many different design parameters, even after narrowing it down. The effects of changing some parameters might be correlated to other parameters. However, it is not feasible to fabricate and test all distinct combinations of parameters. Therefore, we will vary only one parameter at a time while keeping all others constant. Table 2.1 shows all the design parameters sorted by actuator design and how they will be varied. The bold values indicate the dimensions of the baseline actuator. We can indicate each individual actuator by a simple abbreviation of the specific symbol and value since only one parameter is varied at once. For example, actuator N8 is a chamber design actuator with 8 chambers and all other dimension as specified by the bold values in table 2.1.

Actuator	Parameter	Symbol	Value	unit
Baseline	Material	-	EF50,**DS10**,DS20,DS30	-
	Length	L	50,**100**,150	mm
	Wall thickness	t	1,**2**,3	mm
	Inner radius	R	**10**	mm
	Block diameter	D	**35**	mm
	Block thickness	T	**15**	mm
Chamber	Number of chambers	N	**1**,2,4,8,16,32	-
	Chamber wall thickness	t_w	**1**	mm
	Hole radius	r	**4**	mm
Corrugated	Amplitude	A	**0**,1,2,3,4	mm
	Wavelength	λ	**20**	mm
Multi-Material	Fiber material	-	**None**,ED22,ED32,SS45	-
	Fiber diameter	d	**1**	mm
	Braiding angle	α	**85**	°

Table 2.1: Dimensions for all actuators. Bold values indicate the dimensions for the baseline actuator

2.1.2. Fabrication method

The fabrication method used for production of the actuators is known as reaction injection moulding. In this method a pre-polymer is injected into a mould. The part is removed from the mould once the material is cured. Combining two materials or creating inner cavities using this method is often done by creating separate parts and gluing them together. We want to avoid using glue since manual gluing often introduces inaccuracies during manufacturing. Our solution to this problem involves a two step moulding process and the use of a water-soluble inner mould.

The moulds are designed using the 3D CAD modelling software SolidEdge (Siemens). The outer moulds are 3D printed from Veroclear (Stratasys) using the Eden 260VS printer (Stratasys). The polyjet printing technique allows for high accuracy, large design freedom, and fast printing times. The inner mould is made from Ultrafuse BVOH (BASF) printed using an Ultimaker 3 (Ultimaker). The inner mould is printed as two halves to improve printability. These halves are fused together by making the surface wet, slightly dissolving the material, and sticking the two parts together. The outer mould is used to align the two parts.

Figure 2.5a shows all the mould parts needed to make one actuator. We mentioned a two step moulding process is used. First, the active (middle) part of the actuator is cast. The frontcap and backcap are attached to the inner mould and placed in the bottom half of the first mould. The top half of the first mould is placed and using six M4 nuts and bolts the mould is closed tight. The plug is inserted all the way through the frontcap. This prevents any silicone from clogging the hole in the inner mould. Figure 2.5b shows the fully assembled first mould.

Two-component platinum-cure silicones are used to cast the actuators. Following the instructions, the two components are stirred thoroughly. After stirring, the materials are degassed using vacuum. When casting, the two components pass through a static mixing nozzle which mixes the components during injection. The first mould is placed upright before casting. The injection hole is located near the lower end of the mould while holes in the frontcap allow air to escape. Injection is done slowly to avoid formation of air bubbles.

The first part is then left to cure. The curing times for this part range from 3 hours (EF50) to 16 hours (DS30). However, the first part is not left for the entire curing time. It is taken out of the mould 30 minutes before the end of the curing time. At this point, the material is cured enough to be taken out of the mould without losing its shape but has not completed bonding all polymer molecules. The first part is shown in figure 2.5c with the inner mould still inside. The first part, with inner mould, is then placed in the bottom half of the second mould. The plug is inserted and the top half is placed. Figure 2.5d shows the fully assembled second mould. Elite Double 32 (Zhermack) is used for the end blocks since this has a relatively high shore hardness and a fast curing time of only 20 minutes. The combination of the partially cured first part and the uncured second material allows for cross-linkage of molecules to occur at the interface. This leads to a strong bonding between materials and a clean and airtight connection.

The finished actuator is removed from the mould once the second material has fully cured, shown in figure 2.5e. The actuator is placed in an oven to complete the post curing process as prescribed by the manufacturer. The inner mould is still present inside the actuator. After post curing the actuator is connected to a water pump to flush the water-soluble mould out of the actuator. The actuator is then dried and ready for use.

Figure 2.5: Casting process used to make a single actuator. A. Overview of all the required mould parts. 1) Top half of first mould. 2) Frontcap. 3) Bottom half of first mould. 4) Backcap. 5) Plug. 6) Inner mould. 7) Bottom half of second mould. 8) Top half of second mould. B. Fully assembled first mould. Frontcap (2) and backcap (4) are attached to the inner mould (6). This is placed between the top half (1) and bottom half (3) of the first mould. The plug (5) in inserted. Nuts and bolts are used to close the mould tightly. C. Inner mould with the first part of the cast after removing the outer mould parts. D. The inner mould with the first part of the actuator is placed in the bottom half of the second mould (7). The plug (5) is placed and the top half of the second mould (8) closes the mould. E. Finished actuator after removing the second outer mould.

2.2. Actuator analysis

The efficiency of an actuator is a measure of how well input energy is converted into useful work. As mentioned previously in section 1.3, efficiency and energy are quantities which cannot be directly measured. Furthermore, efficiency changes with definition which, in turn, is application dependent. Our goal is to provide a complete overview of the energy paths during a full actuation cycle. To do so, we design an actuator cycle in which an actuator does work.

Firstly, we will discuss what the actuation cycle will look like and how we can analyse it. Secondly, we investigate how energy is distributed during the actuation cycle. Finally, we will make some assumptions to simplify the analysis and present the equations which lead to the definition of efficiency.

2.2.1. Actuation cycle

Figure 2.6a shows a simplified model of our system. The actuator can be seen as a cylinder with a variable volume V_{act}. Our input to the system will be a specific amount of air. This input can be represented by a second cylinder with volume V_{input}, which is connected to the actuator. The air in these two volumes together forms the pneumatic domain, highlighted in blue. A high pressure is indicated with an increased colour intensity. The cylinder representing the actuator has two pistons where the air interacts with the material and a third piston where the material interacts with the environment. The material domain is highlighted in orange where the increased colour intensity denotes a high strain. The first piston represents the radial expansion where material is deformed but no useful work is done. The second piston is connected to the third piston which interacts with the load. The third piston is where work is done which is in the mechanical domain, highlighted in pink. The springs and dampers between the first piston and the cylinder, as well as between the second and third piston, represent the viscoelastic material properties where some energy is stored elastically and some is dissipated.

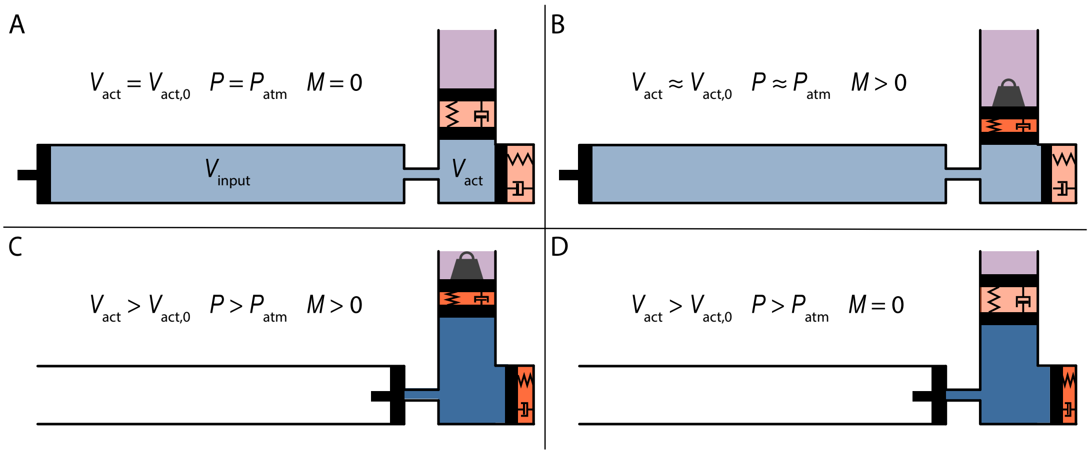

Figure 2.6: Four phases of a single actuation cycle. We can consider our system as a closed system of two coupled cylinders. The left cylinder represents the air input with volume V_{input}. The right cylinder represents the actuator with volume V_{act}. The blue part represents the air in the system, the orange part the material, and the pink part the environment. A. The starting state for the actuation cycle. The volume in the actuator is equal to its unloaded volume, the pressure is equal to atmospheric pressure, and the load is zero. B. State after the loading phase. During loading a weight is placed on the actuator, deforming it. The deformation might cause slight changes in volume and pressure, but they will still be approximately equal to initial conditions. C. State after the inflation phase. During inflation we push the input volume into the actuator, thus increasing the volume and the pressure in the actuator. D. State after the unloading phase. The weight is removed, increasing volume further and decreasing pressure. The last phase is the deflation phase. Here, the input volume is removed from the actuator, returning to the situation in A.

Four distinct phases can be identified in the actuation cycle. The first phase is the loading phase. Here, a load is applied to the actuator which causes the material to deform. Depending on the actuator design, this deformation can also change the volume and pressure in the actuator. However, these changes are fairly small so that actuator volume and pressure remain approximately constant. Figure 2.6b shows the system after the loading phase. The second phase is the inflation phase. Here, we apply the input to the system. In the model this is represented by a piston pushing into the input cylinder. The air is pushed into the actuator as the piston moves. This increases the volume and pressure in the actuator and lifts the weight. Figure 2.6c shows the system after the inflation phase. The third phase is the unloading phase. In this phase the load is removed from the actuator. This causes the volume to increase and the pressure to decrease. Figure 2.6d shows the system after the unloading phase. The last phase is the deflation phase. Here, the system is returned to the initial conditions.

2.2.2. Energy paths

Figure 2.7 shows a schematic overview of the possible energy paths during operation of an actuator. Each of the three physical domains has its own sources of potential energy loss. The first domain is the pneumatic domain. This is where we apply the input energy (E_{in}) of the system. The air interacts with the walls of the tubes as it flows through the system. This flow friction is our first source of energy loss (E_{flow}). To increase the pressure in the actuator the air has to be compressed. Compression of air requires energy. This is the second energy loss ($E_{\text{compression}}$). The second domain is the material domain. This represents the energy stored or dissipated in the material itself. The viscoelastic material can be characterized by an elastic component (E_{elastic}), which is stored, and a viscous component (E_{viscous}), which is dissipated through internal damping. The third domain is the mechanical domain. Here, the first source of energy loss is the energy required to increase the speed of the system (E_{kinetic}). The second source is the energy dissipated through contact friction (E_{friction}). Finally, the energy that remains is the useful work (W) done by the actuator.

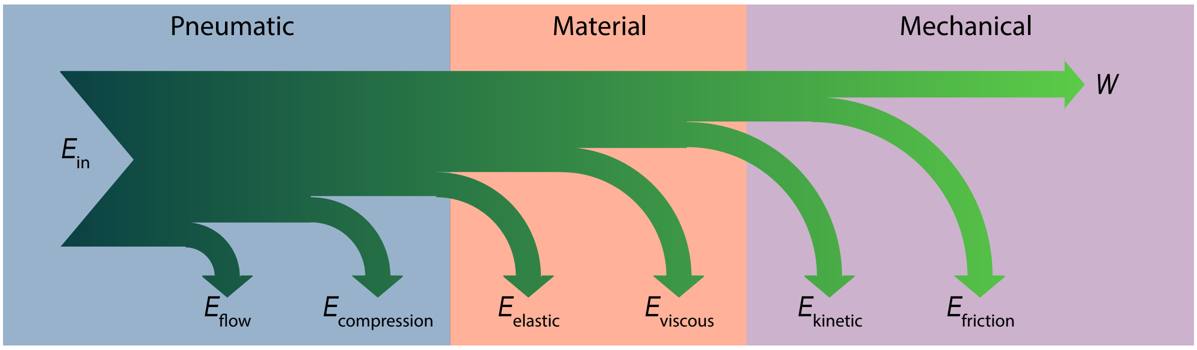

Figure 2.7: Energy paths in a soft pneumatic actuator. In the pneumatic domain there is the input energy (E_{in}) which is the air flow into the system. E_{flow} represents the energy lost by means of friction as the air flows through the tubing. $E_{\text{compression}}$ is the energy required to compress the air. The rest of the energy flows into the material. Deformation in the viscoelastic material can be described by two components. E_{elastic} is the energy which is elastically stored in the material and E_{viscous} is the energy dissipated internally. The remaining energy is used to mechanically interact with the environment. Some energy is used to overcome inertia as the system is gaining speed. This energy is denoted as E_{kinetic}. E_{friction} is the energy dissipated through friction. The remaining energy is the useful work (W) done by the actuation.

2.2.3. Efficiency definition

To simplify our analysis we will make two assumptions. The first assumption is that *we will consider air to behave like an ideal gas*. Air can be considered an ideal gas at standard conditions (0 °C and 1 bar absolute pressure) [27]. Since we only deviate slightly from these conditions we can assume air to always behave like an ideal gas. The second assumption is that *we will conduct the experiments in a quasi-static manner*. This means the system is in constant equilibrium. We will check the validity of this assumption in section 3.2.

Next, we will discuss how to describe each source of energy loss, what definition of efficiency we will use, and which quantities we will need to measure. We start with the input energy. To find this energy we start from the work required to push the piston of the left cylinder:

$$E_{\text{in}} = \int F ds \tag{2.1}$$

where F is the force on the piston (N) and s is the distance the piston travels. The force on the piston is equal but opposite to the pressure inside the cylinder times the area of the piston so we find:

$$E_{\text{in}} = \int -PAds \tag{2.2}$$

The area times the distance travelled by the piston is equal to the volume change:

$$E_{\text{in}} = \int -PdV_{\text{input}} \tag{2.3}$$

Since we are in a closed system the volume out of the input should be equal to the volume into the actuator. So we find:

$$E_{\text{in}} = \int PdV_{\text{act}} \tag{2.4}$$

We only input energy during the inflation phase. The energy input to the system is therefore:

$$E_{\text{in}} = \int_{V_{\text{B}}}^{V_{\text{C}}} PdV_{\text{act}} \tag{2.5}$$

Where E_{in} is the input energy (J), P is the pressure (Pa), and V_{act} is the volume in the actuator (m^3). To find the input energy we need to measure the pressure and the volume. The pressure can be measure using a pressure sensor but the volume cannot be directly measured. However, we can measure the flow to the actuator using a flow sensor and integrate with respect to time to find the volume.

$$V_{\text{act}} = V_{\text{act,0}} + \int Qdt \tag{2.6}$$

Where V_{act} is the volume in the actuator, $V_{\text{act,0}}$ is the initial volume of the actuator, and Q is the volumetric flow rate into the actuator (m^3/s).

Next, we consider the energy loss caused by flow resistance (E_{flow}). The energy loss for flow through a pipe is proportional to the head loss through the pipe. In this case the head loss is only determined by the friction. For this the Darcy-Weisbach equation can be used:

$$h_{\text{f}} = f\frac{Lv^2}{2D} \tag{2.7}$$

Where h_{f} is the head loss (J/kg), f is the dimensionless friction-coefficient, L is the length of the tube (m), v is the average flow speed (m/s), and D is the hydraulic diameter of the the tube (m). To find the average flow speed we use the volumetric flow rate and divide by the cross-sectional area of the tube:

$$v = \frac{Q}{\pi r^2} \tag{2.8}$$

To find the total energy loss we multiply the head loss with the total mass of air that passed through the tube.

$$E_{\text{flow}} = \rho Q h_{\text{f}} t \tag{2.9}$$

Where E_{flow} is the energy loss through fluid friction (J), ρ is the density of air (kg/m^3), and t is the flow time (s). For each component we can estimate the order of magnitude to find an approximation of the energy loss.

$$v = \frac{10^{-6}}{10^0 * 10^{-3^2}} = 10^0 \tag{2.10}$$

$$h_{\text{f}} = 10^{-1} * \frac{10^{-2} * 10^{0^2}}{10^0 * 10^{-3}} = 10^0 \tag{2.11}$$

$$E_{\text{flow}} = 10^0 * 10^{-6} * 10^0 * 10^2 = 10^{-4} \tag{2.12}$$

The second potential energy loss in the pneumatic domain is the energy loss caused by compression of the air. The quasi-static condition means we will assume a reversible and isothermal process. We start with the first law of thermodynamics:

$$\Delta U = Q - W \tag{2.13}$$

Where ΔU is the change in internal energy (J), Q is the energy supplied to the system as heat (J), and W is the thermodynamic work done by the system (J). Because of the isothermal assumption we know $\Delta U = 0$. Furthermore, we can calculate the work done by the system as:

$$W_{\mathrm{B}\to\mathrm{C}} = -\int_{V_\mathrm{B}}^{V_\mathrm{C}} PdV \tag{2.14}$$

The ideal gas law states:

$$P = \frac{nRT}{V} \tag{2.15}$$

Substituting 2.15 into 2.14 and solving the integral gives:

$$W_{\mathrm{B}\to\mathrm{C}} = -nRTln(\frac{V_\mathrm{C}}{V_\mathrm{B}}) \tag{2.16}$$

We prefer to express the work in terms of pressure since pressure is directly measurable but volume is inferred. Rewriting 2.15 and combining with 2.16 gives:

$$W_{\mathrm{B}\to\mathrm{C}} = -nRTln(\frac{P_\mathrm{B}}{P_\mathrm{C}}) \tag{2.17}$$

From equation 2.13 we know that, if there is no change in the internal energy, the work done to compress the air leaves the system as heat. This energy is lost during inflation and, in the ideal case, recovered during deflation.

$$E_{\mathrm{compression}} = Q_{\mathrm{B}\to\mathrm{C}} = W_{\mathrm{B}\to\mathrm{C}} \tag{2.18}$$

Over a full cycle this will equate to zero since the initial and final pressure are the same. However, during the cycle heat will flow in and out of the system. The heat flow is used in section 3.2.3 for checking the quasi-static assumption.

Now, we move on to the material domain. The first potential energy loss is E_{elastic}. $E_{\mathrm{compression}}$ and E_{elastic} are the only reversible terms in the energy path. We can measure the energy of the output flow during deflation, similar to E_{in}. If we subtract the heat flowing into the system as the air expands we find the elastically stored energy.

$$E_{\mathrm{elastic}} = -\int_{V_\mathrm{D}}^{V_\mathrm{A}} PdV_{\mathrm{act}} - nRTln(\frac{P_\mathrm{D}}{P_\mathrm{A}}) \tag{2.19}$$

The viscous term in the material domain cannot be measured or calculated. It can only be inferred once we know al the other terms.

$$E_{\mathrm{viscous}} = E_{\mathrm{in}} - E_{\mathrm{elastic}} - E_{\mathrm{kinetic}} - E_{\mathrm{friction}} - W \tag{2.20}$$

Next, we continue to the mechanical domain. Here, we start with E_{kinetic}:

$$E_{\mathrm{kinetic}} = \frac{1}{2}mv^2 \tag{2.21}$$

Where m is the mass of the moving object (kg) and v is its speed (m/s). Similar to E_{flow}, we can estimate the order of magnitude of the different components to find an a approximation of E_{kinetic}.

$$E_{\mathrm{kinetic}} = 10^0 * 10^0 * 10^{-3^2} = 10^{-6} \tag{2.22}$$

The last potential source of energy loss is the friction at the interface between the actuator and the environment. If we can measure the friction force directly we can calculate the energy dissipation as follows:

$$E_{\mathrm{friction}} = -\int_L \vec{F}_\mathrm{f} d\vec{s} \tag{2.23}$$

If we constrain the motion and force to be along one direction this simplifies to:

$$E_{\mathrm{friction}} = \int_L F_{\mathrm{f}} dx \tag{2.24}$$

Where E_{friction} is the energy loss from friction (J), L is the path over which we integrate, F_{f} is the friction force (N), and x is the position (m). The useful work done by the actuator is calculated in a similar way as the friction loss:

$$W = \int_L F dx \tag{2.25}$$

Where W is the work done (J) and F is the force from the load (N). Lastly, we will define efficiency. Two definitions of efficiency can be formulated. The first is the open loop efficiency. Here, all energy that is not transfered to the useful work is considered as wasted:

$$\eta_{\mathrm{ol}} = 100 * \frac{W}{E_{\mathrm{in}}} \tag{2.26}$$

Where η_{ol} is the open loop efficiency (%), W is the useful work (J), and E_{in} is the input energy (J). If we combine equations 2.26, 2.25, and 2.5 we find the final expression for the open loop efficiency:

$$\eta_{\mathrm{ol}} = 100 * \frac{\int_L F dx}{\int_{V_{\mathrm{B}}}^{V_{\mathrm{C}}} P dV_{\mathrm{act}}} \tag{2.27}$$

The second definition of efficiency we will use is the closed loop efficiency. Here we assume all the energy extracted during deflation can be recycled.

$$\eta_{\mathrm{cl}} = 100 * \frac{\int_L F dx}{\int_{V_{\mathrm{B}}}^{V_{\mathrm{C}}} P dV_{\mathrm{act}} + \int_{V_{\mathrm{D}}}^{V_{\mathrm{A}}} P dV_{\mathrm{act}}} \tag{2.28}$$

Where η_{cl} is the closed loop efficiency (%). From equations 2.27 and 2.28 we can see we need to measure four important quantities to fully characterize the efficiency of our actuators. Mechanically, we need to measure the force on the actuator and the displacement of the load. Pneumatically, we need to measure the pressure inside the actuator and the volume of the actuator. However, directly measuring the volume in the actuator is not feasible. By measuring the flow into and out from the actuator and integrating according to equation 2.6 we can still find the volume.

3

Experimental setup

In this chapter the experimental setup is presented. First, we discuss the design of the experiment. We highlight the considerations that were taken into account during the design, show the mechanical setup and the fluidic circuit, and go through the experimental procedure step-by-step. Second, we performed a series of experiments to validate the setup. We show the details of a single actuation cycle for the baseline actuator, characterize the friction in the setup, investigate the effect of load as well as the effect of the inflation speed.

3.1. Experimental design

The setup can be divided into a mechanical part and a fluidic part. Both sides have some specific requirements. First, the mechanical part should be able to hold the actuator by its end blocks without placing any strain on the actuator. Second, the goal is to find the maximum efficiency as an extension actuator. Therefore, sideways and bending motion should be constrained since this would reduce the work in the direction of extension. Third, the first and third phase of the actuation cycle involve loading and unloading the actuator. The mechanical setup should be able to apply and remove a load. This must be done slowly to ensure the quasi-static assumption. The load should be variable to investigate the dependency of the efficiency on the load. Last, the mechanical setup should be able to measure the load and the distance it travels.

The fluidic side should supply the inflow of air to the actuator. Again, this should be slow enough for the quasi-static assumption to hold. During loading and unloading the actuator should be closed so we need a way to shut the inflow and outflow on or off. The fluidic side should measure the pressure in the actuator as well as the inflow and outflow.

3.1.1. Mechanical setup

The mechanical setup is shown in figure 3.1. The frame of the setup is an anodized metal plate with a grid pattern of holes. This allows for a modular approach where additions are easily realised. The rest of the components are either store bought or 3D printed in PLA on the Ultimaker 3. The actuator (7) is held by the bottom clamp (9) and the top clamp (4). The bottom clamp is attached to frame and will be the stationary side. The top clamp is mounted on a linear slider (MGN12C, HIWIN) which runs on the linear slider rail (MGNR12R, HIWIN).

The load is applied in the form of weights. The weight is placed on a weight carrier (3), which is also mounted on a linear slider on the same rail as the top clamp. This ensures a repeatable placement of load as well as prevents any off-axis loads. The weight carrier is connected with a nylon fishing wire (highlighted in red) to a geared stepper motor (14) with a gear ratio of 15:1 (17HS15-1684S-HG15, stepperonline). The gearbox ensures that no slip occurs at higher loads and acts as a brake when the power is disconnected. The wire is attached to the motor pulley (8) and runs along two pulleys (1). After loading we want no interaction between the load and the motor. Therefore, the cable should be slack. Guides are placed at the pulleys to avoid the cable running off the pulley when it is slack. A second weight carrier (6) was installed to be able to apply pulling forces. This is meant for contraction actuators and will not be used during our experiments.

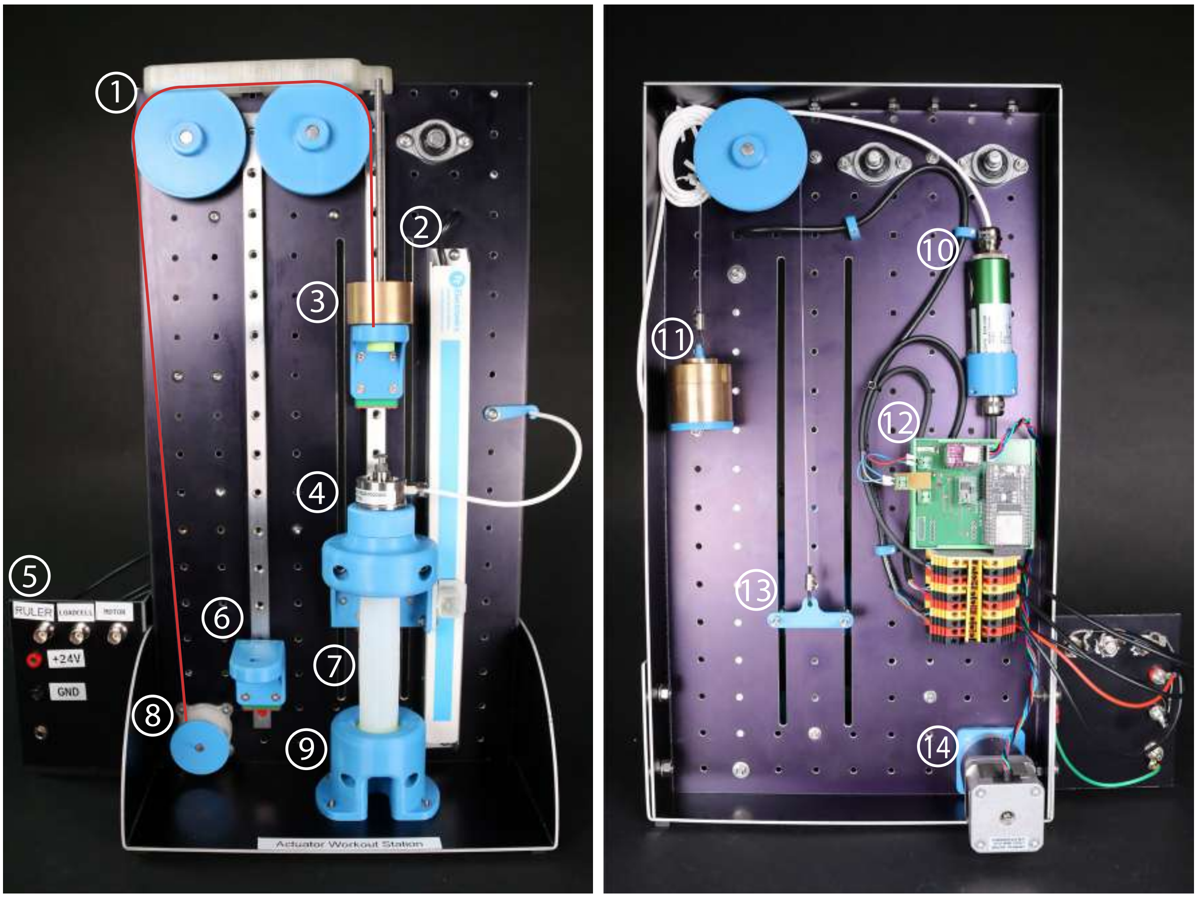

Figure 3.1: Front side (left) and back side (right) of the mechanical setup. Important components are indicated. 1) Cable (highlighted in red), pulleys, and guide. 2) Contactless position sensor, stationary part. 3) Right weight carrier. Connected to the cable. 4) Top actuator clamp. Holds the load cell and the moving part for the ruler. 5) Electrical connector panel. Connectors for two measurements signals and one control signal as well as connectors for the the power supply and grounding of the metal back plate. 6) Left weight carrier, used in the tension configuration (not used in the shown configuration). 7) Actuator. 8) Motor pulley and cable guide. 9) Bottom actuator clamp. 10) Amplifier for the load cell signal. 11) Counterweight. Used to balance the weight of the top actuator clamp (4). 12) Control unit for the stepper motor. Includes a microcontroller and motor driver. 13) Coupling between top actuator clamp (4) and counterweight (11). 14) Stepper motor.

The weight of the top clamp is compensated to avoid the clamp applying a load on the actuator. The clamp is connected to a coupling (13) on the back side of the setup. Here, a counterweight (11) is suspended to cancel the weight of the top clamp and the top block of the actuator.

To measure the force a bi-directional load cell (8427-5020-N000S000, Burster) is placed on top of the top clamp. The signal wire runs around to the back side where it is connected to the signal amplifier (10) (9236-V000, Burster). To measure the displacement we use a contactless linear position sensor (AP0-250-002-000, AB ELEKTRONIK). The stationary part (2) is mounted on the frame while the moving part is attached to the top clamp. A contactless solution was chosen to prevent additional friction. To control the stepper motor we implement a control board (12) with a microcontroller (ESP32-DEVKITC-32D, Espressif Systems) and stepper motor driver (DRV8825, Texas Instruments). All signals and the power input are gathered at the connector panel (5).

3.1.2. Fluidic circuit

The fluidic side is a not as intricate as the mechanical side. It is shown in figure 3.2. The air supply (1) is provided by a mass flow controller (SLA5850ST1AB102A1, Brooks Instrument). To switch the inflow to the actuator on and off we use a solenoid valve (2) (VDW250-5G-2-01N-L, SMC). To activate the solenoid a switching relay is used. The switching of the solenoid causes high peak flow which we want to avoid. To compensate for this, a variable inflow restriction (5) is used. The switching of the outflow is done similarly with a variable outflow restriction (6) and a second solenoid valve (8). A

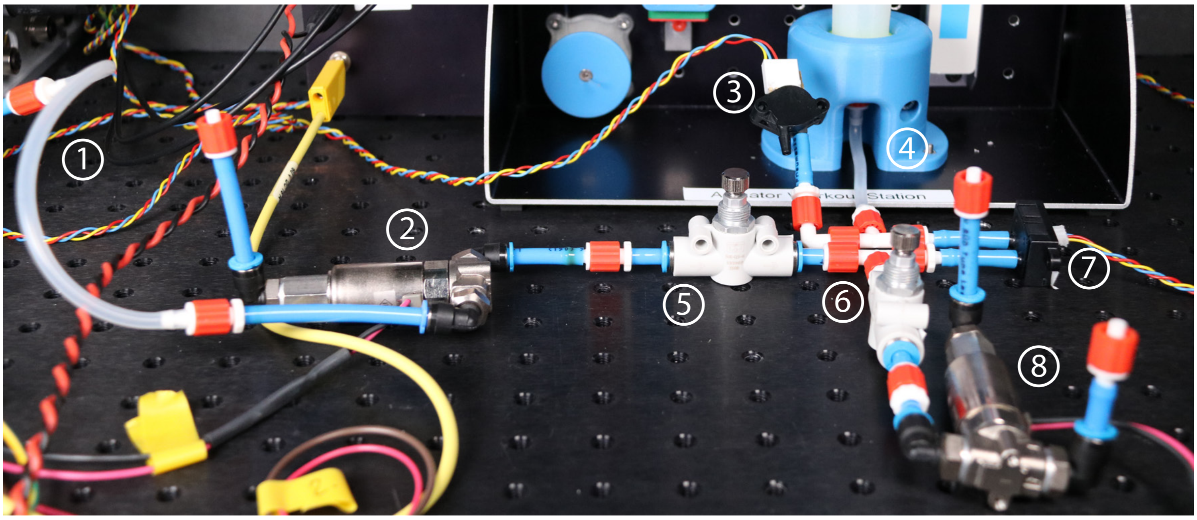

Figure 3.2: The fluidic circuit used for the experiments. 1) Inflow of air. 2) Solenoid valve for inflation. 3) Pressure sensor. 4) Flow to the actuator. 5) Variable inflow restriction. 6) Variable outflow restriction. Bi-directional flow sensor. 8) Solenoid valve for deflation.

pressure sensor (3) (MPX5100DP, NXP) is used to measure the pressure as close to actuator inlet (4) as possible. The airflow into and out from the actuator is measured using a bi-directional flow sensor (7) (Zephyr HAFBFL0750, Honeywell). The flow sensor is used to calculate the volume in the actuator by integration. The flow sensor is calibrated using the mass flow controller to reduce errors which might accumulate when integrating. All the measurement and control signals, both from the mechanical and fluidic setup, are collected and sent out by a data acquisition box (NI USB-6212, National Instruments).

3.1.3. Experimental procedure

Conducting an experiment begins as follows: an actuator is chosen, the top end is plugged, and the bottom end is connected to a tube. The actuator is placed in the clamps as shown in figure 3.3. The tube is connected to the fluidic circuit and all the connections in the circuit are tightened to ensure no leakage occurs. The appropriate weight is chosen and placed on the weight carrier. Using the motor, the carrier with weight is lifted to the top of the rail. This allows for a consistent starting place over experiments.

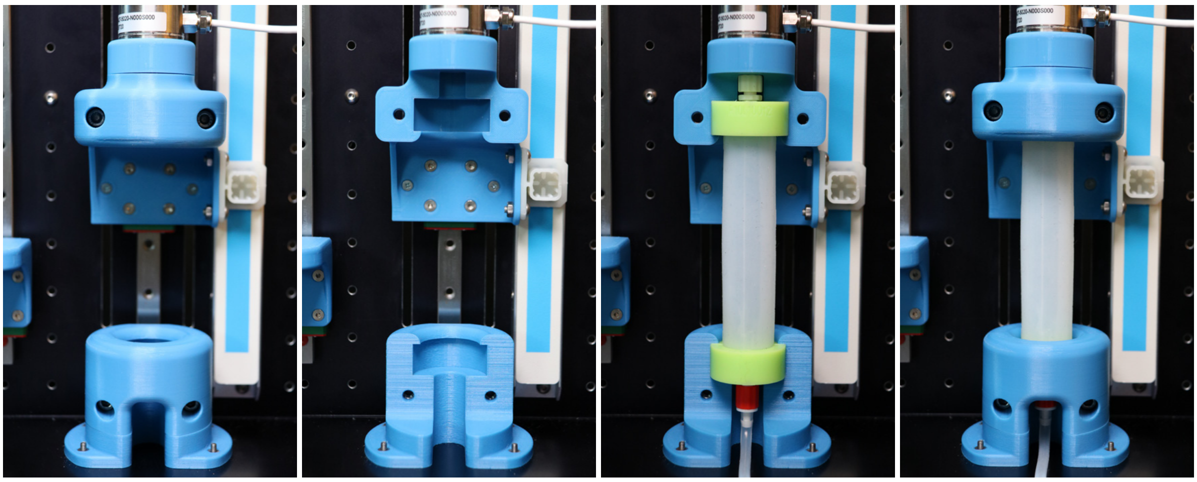

Figure 3.3: Procedure showing proper placement of the actuator. First, removing the front halves of the clamps. Second, placing the actuator (with a plug in the top and a tube connected to the bottom) and pushing it in until snug. Third, placing the front halves of the clamps and tighten the bolts alternately until hand tight.

Each experimental run one actuator is tested using one weight. However, multiple actuation cycles are tested in succession using different input volumes. The input volume is controlled by setting the flow speed on the mass flow controller and switching the inflation solenoid on for a specified amount of time. Each measurement with a specific input value is repeated three times to increase accuracy. At the start of each run, while nothing is happening, ten seconds of data is taken which is used in the data processing to remove any DC offsets on the sensors. Then, a dummy cycle is performed. This cycle is used to manually tune the inflow and outflow resistance. The inflow resistance is adjusted so that the flow is sufficiently damped to avoid overshooting peak flows as the valve switches. The outflow resistance is adjusted to ensure the actuator deflates within a reasonable time while avoiding excessively high peak flows. The data taken during the dummy cycle is discarded.

During the actuation cycles, the air flow is set once and left to stabilize. We lower the weight until the cable is slack and the weight is fully supported by the actuator. The inflation solenoid is activated and the air flow is directed to the actuator. After the desired time the solenoid is deactivated and the actuator is left to stabilize. The motor is used to lift the weight off the actuator. The deflation solenoid is activated after unloading, venting the actuator to the atmosphere. The solenoid is left open until the actuator is fully deflated.

3.2. Experimental validation

To validate the results found during experiments we first perform tests to see if the results can be trusted. In the first test we performed a single actuation cycle using the baseline actuator to see how the sensor values vary during a complete actuation cycle. In the second test we investigate the influence of the friction of the top clamp and how the loading affects the behaviour of the actuator. In the last test we repeat the same actuation cycle multiple times using different inflation speeds and monitor the effects.

3.2.1. Single cycle

Figure 3.4 shows the data of this single cycle. The top graph shows the sensor values with respect to time. The two smaller graphs below show the pressure-volume curve and the force-distance curve. The four phases discussed in figure 2.6 are indicated as well. Figure 3.5 shows the actuator in each of the four phases.

First the mass flow controller (yellow line) is set to the set point. The actuator is still in phase A with no load and atmospheric pressure. The load is placed on the actuator. The force (blue line) increases while the distance (red line) becomes negative as the actuator is compressed. The load stabilises and the actuator is in phase B. The digital signal for the actuation solenoid (light green line) is set to high and the flow (pink line) increases until it reaches the same value as the mass flow controller. The pressure (purple line) builds up rapidly and the volume (brown line) increases gradually. The force increases slightly as the friction on the weight carrier is overcome. The distance starts to increase once friction is overcome. Pressure, volume, and distance increase until the actuation is turned off and the flow goes to zero. The actuator is in phase C. We see a slight pressure drop as the system relaxes. Then, when we remove the load, the force decreases to zero while the distance increases even further. Removing the load also decreases the pressure slightly. The actuator is now in phase D. From here the digital signal for the deflation solenoid (dark green line) is set to high and the flow becomes negative. Pressure, volume, and distance gradually decrease until the actuator is fully at rest. Note that the starting conditions are not completely recovered after the full cycle as the elastic restoring force equals the friction on the top clamp before the actuator reached its free length. The actuator is now in phase A'.

3.2.2. Effects of friction and load

The second test we performed was to find the influence of the friction of the top clamp and to see the inherent dissipation of the actuator. Two more measurements were taken. During the first measurement the actuator was clamped only in the bottom clamp. The actuator was inflated and deflated while the top block was left to freely move. During the second measurement the actuator was held by both clamps. Again, it was inflated and deflated but no load was placed on the actuator. The pressure-volume curve from these measurements are shown in figure 3.6 together with the data from the previous test where a mass of 200 grams was used.

We can see that the yellow line ("No Clamp") and the blue line ("No Weight") are almost identical.

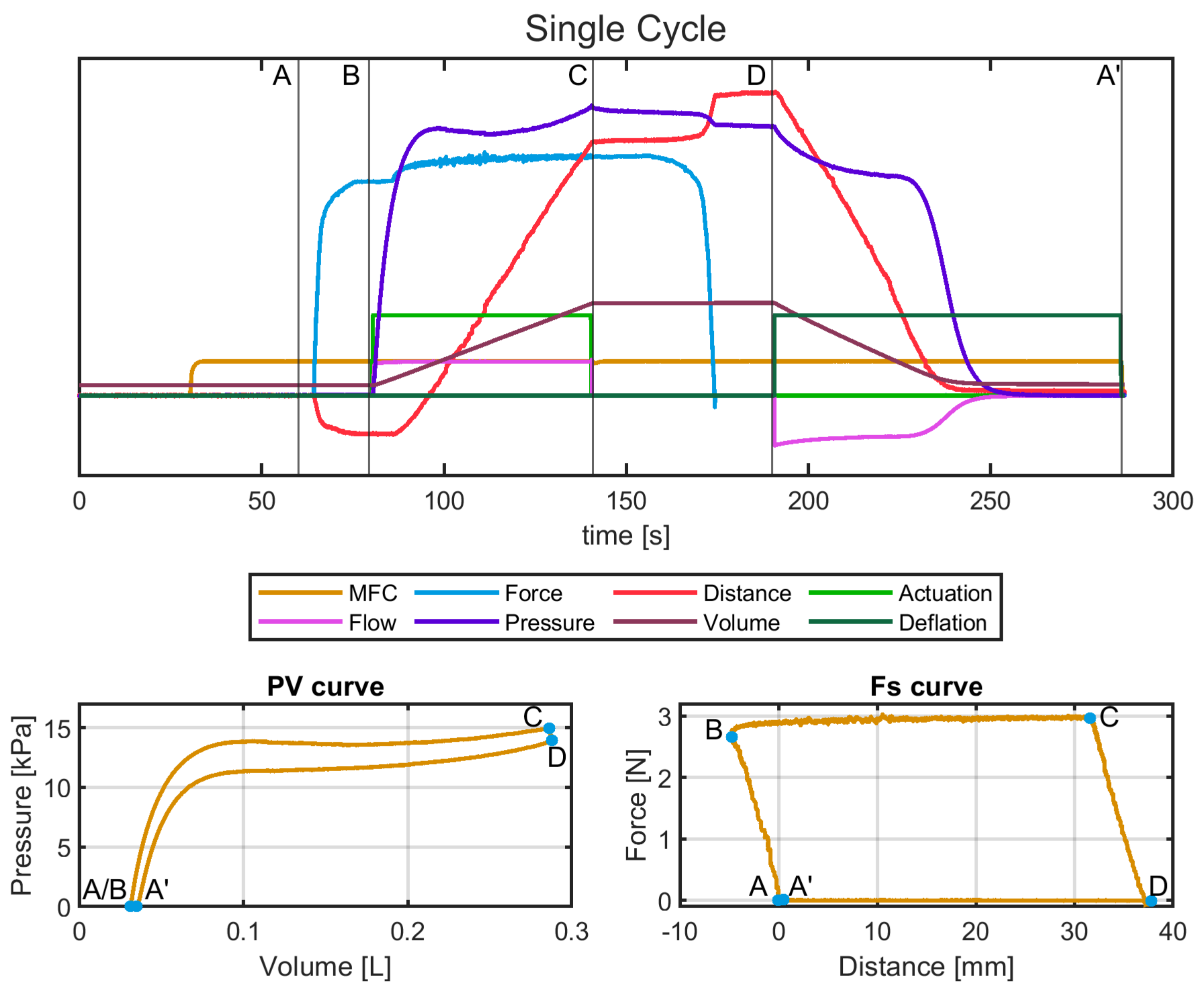

Figure 3.4: Sensor data during the course of a single actuation cycle. Top image shows the scaled data. The different phases of the actuator during a cycle, as described in section 2.2, are indicated. Bottom left image shows the pressure volume curve. Bottom right image shows the force displacement curve.

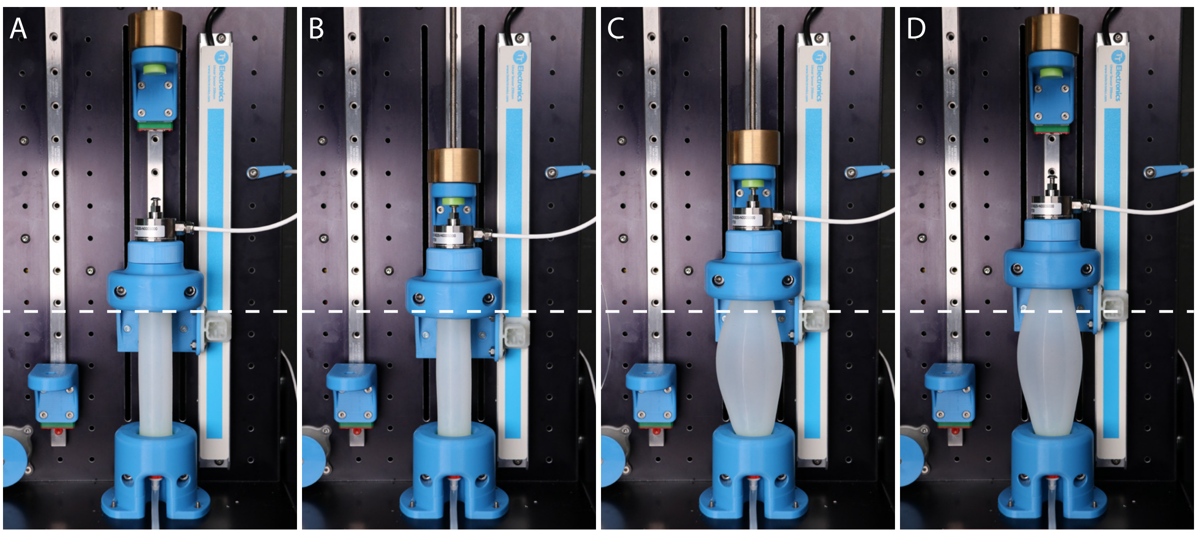

Figure 3.5: Baseline actuator shown in each of the four phases of the actuation cycle. A. Initial conditions. B. After loading. C. After inflation. D. After unloading.

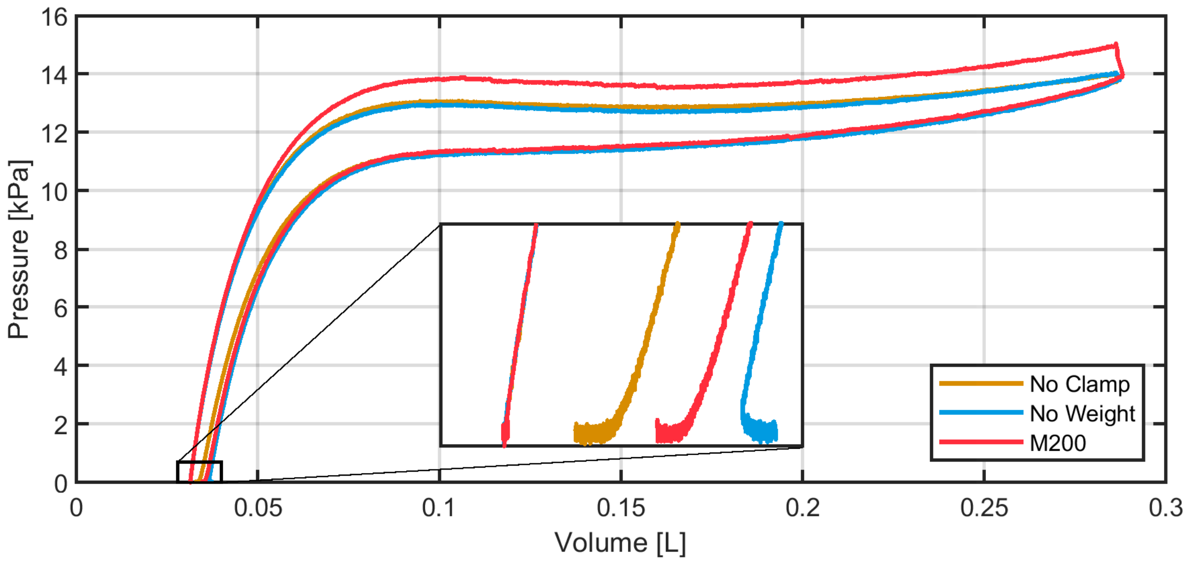

Figure 3.6: Pressure-Volume curve for three different cycles with the same actuator. In the first run, "No Clamp", the actuator is connected only to the bottom clamp of the setup and inflated while freely deforming. In the second run, "No Weight", the actuator is connected to both the bottom and top clamp. However, during this run no load is applied to the actuator. During the last run, "M200", The actuator is tested as normal. This is the same data as shown in figure 3.4.

Some small differences can be seen. In the magnified section we can see the volume of the yellow line almost returns to the initial volume whereas the blue line shows a bigger discrepancy. This can be attributed to the friction on the top clamp. Furthermore, we see that the yellow line has higher pressures than the blue line at the same volume. This is because in the no clamp experiments the actuator feels the load of the top block which is compensated for by the top clamp. Higher loads cause higher pressure, this is also observed when we compared the first two lines to the red line ("M200"). The main difference lies in the part of the curve where inflation occurs. The deflation follows the same path since the load is removed at this point.

Using the equations formulated in section 2.2 we can provide a more quantitative view of these three cycles. We calculated the energy input during inflation E_{in}, the energy output during deflation E_{out} (which is the sum of $E_{\text{compression}}$ and E_{elastic}, the heat produced by compression of air during inflation $E_{\text{compression}}$, the total work done during a full cycle W, the energy dissipation during a full cycle E_{diss}, the dissipation as a percentage of the input energy, the open cycle efficiency η_{ol}, and the closed cycle efficiency η_{cl}. Table 3.1 shows these values for each of the three cycles.

The only difference between the first two cycles is the use of the top clamp and the friction associated with it. The difference in dissipated energy of the first two cycles is therefore equal to the energy loss caused by the friction. We can see that this difference is relatively small (approximately 0.1% of the input energy) and thus we will consider this energy loss to be negligible.

When we compare between the cycle with load and the ones without, we mainly notice a higher input energy while the outflow energy is relatively similar. $E_{\text{compression}}$ is only determined by the maximum pressure. While the load does increase the maximum pressure slightly, it is not enough to cause a significant change in $E_{\text{compression}}$.

Useful work is done now that a load is applied to the actuator. However, we can see the total work is relatively low compared to E_{in}. This is reflected in the open loop efficiency for which we found

	E_{in} (J)	E_{out} (J)	$E_{\text{compression}}$ (J)	W (J)	E_{diss} (J)	Dissipation (%)	η_{ol} (%)	η_{cl} (%)
No Clamp	3.16	2.82	0.0335	-	0.341	10.8	-	-
No Weight	3.14	2.79	0.0336	-	0.344	11.0	-	-
M200	3.34	2.84	0.0356	0.108	0.394	11.8	3.22	21.4

Table 3.1: Quantitative data for the three cycles shown in figure 3.6 including the energy input, energy outflow, heat transfer during compression of air, work, dissipated energy,

an value of 3.22%. This is similar to the efficiency found by Chun et al. [8]. When looking at the dissipated energy we see this has also increased. However, when expressing the dissipated energy as a fraction of the input energy it has barely changed. The small difference can be attributed to the loading and unloading phase. Here, additional deformation is placed on the actuator which causes additional dissipation. When we calculate the closed loop efficiency we find it to be significantly higher than for the open loop, 21.4% vs 3.22%.

3.2.3. Changing inflation speed

The third and last test investigates the influence of the flow speed provided by the mass flow controller. The same cycle as before is repeated eight times. Each time a different set point for the flow speed is used. The time between opening and closing of the inflation valve is scaled so theoretically the total amount of air injected into the actuator should be constant. In practice, the amount of air will vary due to the transient behaviour which occurs when switching the solenoid. The pressure-volume curve for each cycle is shown in figure 3.7a. The end range is enlarged to better compare the curves. A large difference between 0.1 SLPM and the rest of the curves can be seen. This is caused by more air being put into the actuator. More important is the fact that for flow speeds from 0.1-0.3 SLPM the curves follow an identical path. At flow speeds higher than this we notice that some deviation starts to happen. This indicates that air is injected faster than the material can deform, causing additional dissipation.

An additional consideration which depends on the inflation speed is the heat production during inflation. $E_{\text{compression}}$ is the energy required to compression the air to a higher pressure. The isothermal assumption means that the internal energy of the air does not change. Therefore, $E_{\text{compression}}$ is fully converted to heat and transfered through the actuator wall to the environment. For the isothermal assumption to be completely true the generated heat should be instantly dispersed to the surroundings. In reality this is not possible since heat transfer is reliant on a temperature difference. However, if heat is transfered fast enough the assumption is still valid.

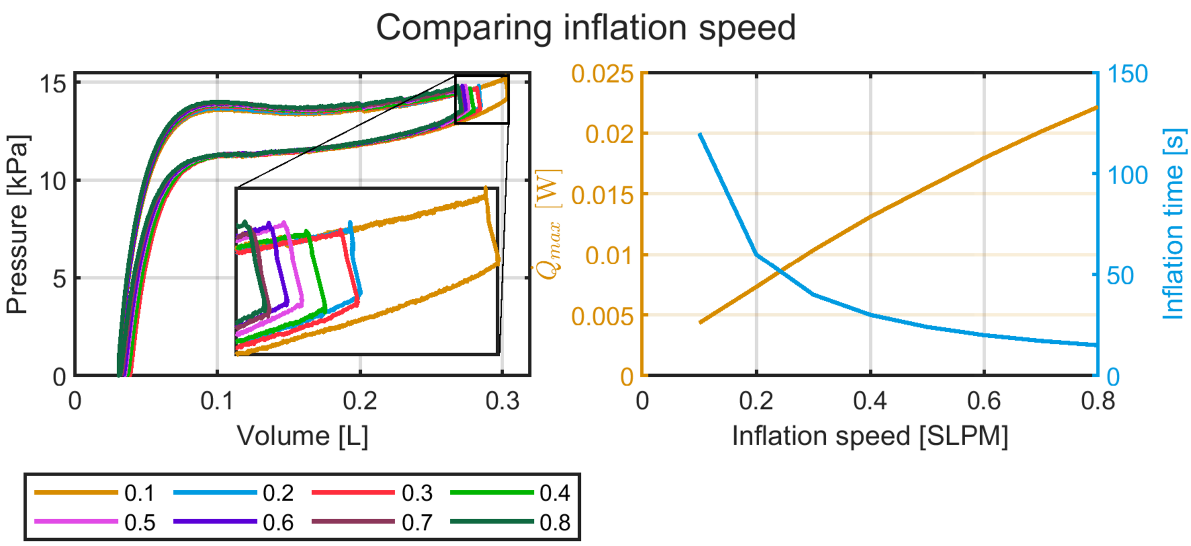

Figure 3.7: Left. Pressure-Volume curves of eight runs of the same actuator with the same load. Each cycle a different set-point for the flow speed of the mass flow controller is used. A detailed view of the end range is shown for clarity. Right. Maximum required heat flow rate and inflation time as a function of the inflation speed.

Figure 3.7b shows the maximum heat production rate and the time needed to inflate the actuator versus the inflation speed. We can see a gradual increase in the maximum heat production as the inflation speed increases. From figure 3.7a we know that the maximum flow speed is 0.3 SLPM. For this flow speed we find the maximum heat production is approximately 0.01 W. Using this, we can check our isothermal assumption. If all heat is transfered through the actuator wall we can use Fourier law for heat conduction in cylindrical shells to find the temperature difference needed to generate heat transfer equal to the heat production.

$$\dot{Q} = 2k\pi l \frac{\Delta T}{ln(\frac{r_2}{r_1})} \tag{3.1}$$

Where $\dot{Q}$ is the heat transfer (W), *k* is the material conductivity (W/mK), *l* is the length (m) of the cylinder, ΔT is the temperature difference (K) between inside and outside of the cylinder, and r_1 and r_2 are the inner and outer radius (m), respectively. Material conductivity for silicone is approximately 0.2 W/mK. If we plug this and the other known parameters in we can solve for the temperature difference.

$$\Delta T = 0.01 * \frac{ln(\frac{12e-3}{10e-3})}{2 * 0.2 * \pi * 100e-3} = 0.0145 \text{ [K]} \tag{3.2}$$

This temperature difference is small enough to validate the isothermal assumption. Even at higher pressures, which can occurs in different actuators, the temperature difference is unlikely to even exceed one degree Kelvin. Therefore, the heat production is not critical when it comes to the choice of inflation speed.

From figure 3.7a we know that the maximum flow speed is 0.3 SLPM and in figure 3.7b we see that the inflation time is inversely proportional to the inflation speed. A shorter inflation time is preferable since a shorter total runtime means more experiments can be conducted. However, changing inflation speed from 0.1 to 0.2 SLPM provides a larger reduction in inflation time than changing from 0.2 to 0.3 SLPM. Furthermore, we do not know if all actuators show consistent behaviour for inflation speeds up to 0.3 SLPM. Ultimately, the inflation speed was set to 0.2 SLPM to allow for some safety margin.

4

Results

In this chapter we will show the results of the experiments as described in section 3.1.3. Each parameter is investigated separately. First, we look at the baseline actuator where we investigate the influence of wall thickness, material, and length. Second, the performance of the chamber design with varying number of chambers is evaluated. Third, the corrugated design with different amplitudes is studied. Fourth, the effect of different fiber material for the multi-material design is studied. Finally, we try to generalise and look at the class of extension actuators as a whole and make a comparison between the different actuator designs.

4.1. Baseline actuator

We begin with the baseline actuator. Figure 4.1 shows the baseline actuator at the end of each of the four phases of the actuation cycle (A-D) as described in section 2.2. Figure 4.1a shows the actuator in the initial conditions. Figure 4.1b shows the actuator after loading. We notice a slight compression caused by the load. Figure 4.1c shows the actuator after inflation. Some axial extension can be seen but mainly we see a significant radial expansion. Figure 4.1d shows the actuator after unloading. The compression imposed by the loading is recovered as extension during unloading. For this design three different parameters are investigated since these parameters affect all other designs as well.

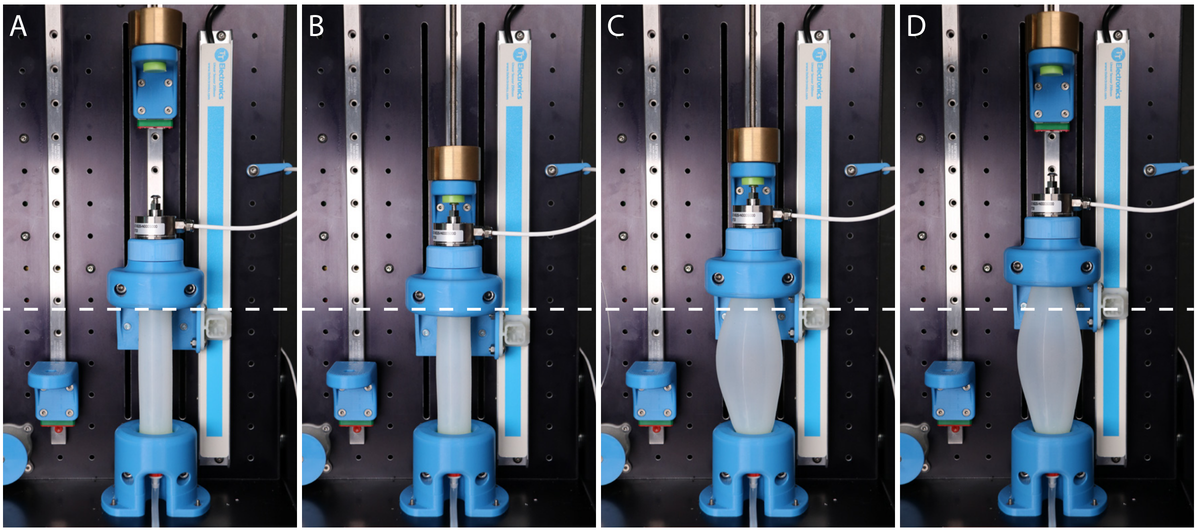

Figure 4.1: Baseline actuator shown in each of the four phases of the actuation cycle. The white dashed line indicates the starting height. A. Initial conditions. B. After loading. C. After inflation. D. After unloading.

4.1.1. Wall thickness

The first design parameter we investigated is the wall thickness, which is varied between one and three millimeter. Different loads are used, and for each load a range of input volumes is used. Figure 4.2 shows the results for these experiments. From left to right we show the closed loop efficiency, the open loop efficiency, and the work. Each point represents the mean over three actuation cycles as well as the standard deviation.

The top row shows the results for the specific load case where no additional weight is added to the carrier which results in a load of roughly one newton. The independent variable for the top row, which is determined by the inflation time, is presented as the input volume (V_{input}) divided by the initial actuator volume ($V_{\text{act,0}}$). The efficiency increases as the wall thickness decreases since less material is deformed. Changing from t3 to t2 provides a small increase, while changing from t2 to t1 gives a larger increase. Qualitatively, the closed loop and open loop show relatively similar behaviour. Quantitatively, closing the loop drastically improves the efficiency, which is expected since the elastic energy is recovered without affecting the input energy or work. Furthermore, both efficiencies reach a plateau at higher inputs, while for lower inputs the efficiency begins to drop. This can be related to the work, as it shows a linear increase with the input without much influence from the wall thickness. The work starts to approach zero as the input decreases, and if no work is done the efficiency must also be zero.

The bottom row shows the results for different loads at a specific input. We chose the input volume five times larger than the initial actuator volume ($V_{\text{input}}/V_{\text{act,0}} \approx 5$) since this is about where the plateau starts. Each actuator was loaded using increasing weights until buckling occurred. As the weight increases we observe an increase in efficiency for both closed loop and open loop. For the open loop this relation appears linear, while the closed loop shows an effect of diminishing increase. A smaller wall thickness provides a higher efficiency at equal weight. However, the smaller wall thickness drastically reduces the buckling load, and as the weight increases the actuators with a larger wall thickness become more efficient. The work scales linearly with the load with the only major effect of the wall thickness being the maximum load and thus the maximum work done. And so, to do most work in the most efficient way, we would reduce the wall thickness while trying to maximize buckling load.

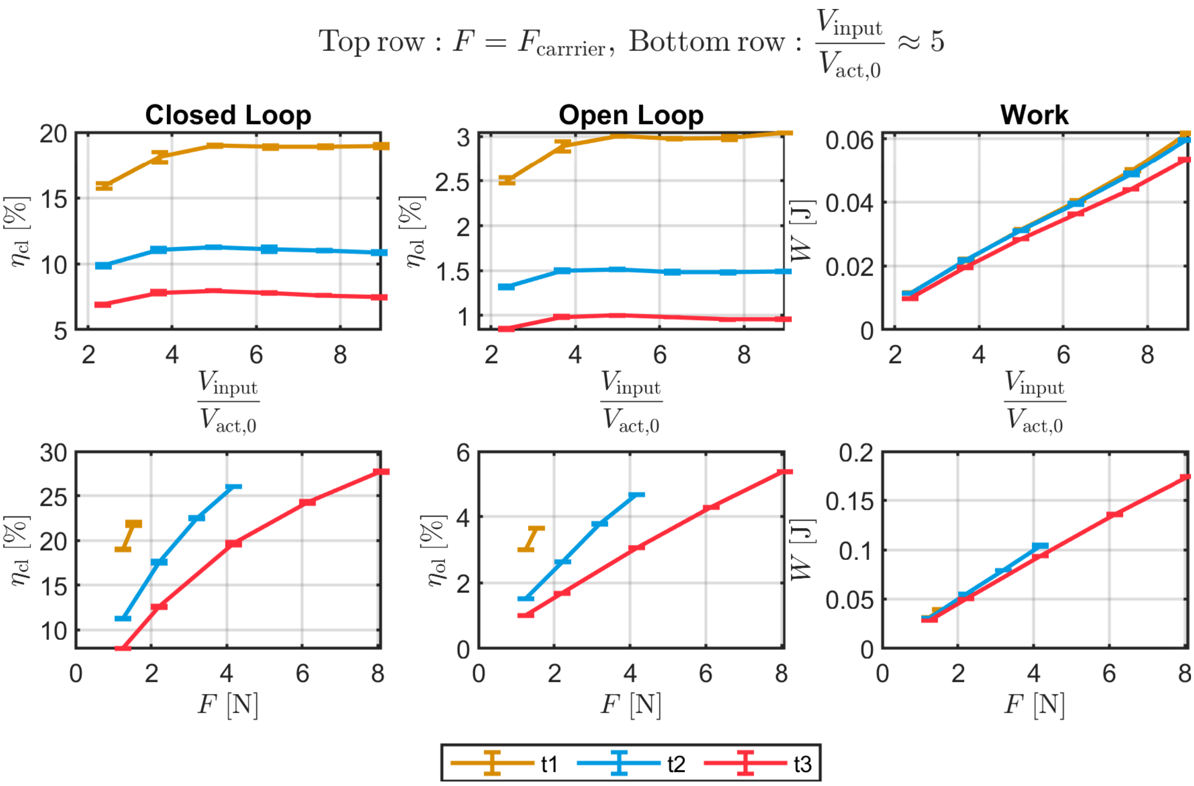

Figure 4.2: Results for the experiments with varying wall thickness. Each point represents the mean and standard deviation over three cycles. From left to right we show the closed loop efficiency, open loop efficiency, and work. The top row shows the load case where only the weight of the carrier is applied with varying inputs. The input is shown as the input volume (V_{input}) divided by the initial actuator volume ($V_{\text{act,0}}$). The bottom row shows the results for input value of 6 with varying loads.

4.1.2. Material

The second parameter we investigate is the material. Four different materials are tested where Eco-Flex 50 has the lowest stiffness and Dragon-Skin 30 has the highest stiffness. Figure 4.3 shows the results in the same format as figure 4.2. The results for the changing wall thickness showed a plateau in efficiency for larger input volumes and the beginning of a decline in efficiency at lower input volumes. The range of input volumes is shifted downwards for the next experiments to get a better understanding of the actuator efficiency at these lower input volumes. We see that the efficiency decreases drastically as the input volume becomes lower. This can be expected since early on in the inflation phase most of the input energy is used to increase the pressure in the actuator. Most of the elongation occurs once the pressure is high enough. Interestingly, Eco-flex 50 has the highest efficiency at large inputs volumes, while it has the lowest, negative, efficiency at the smallest input volume. The negative efficiency is explained by the negative work that is done by the actuator during the loading phase. The total work, and thus efficiency, becomes negative if the final length of the actuator is less than the initial length (i.e. when the actuator is compressed by the load but the pressure does not become high enough to overcome friction).

The work shows an initial startup behaviour where work only increases slightly with increasing input. After the startup behaviour the gradient increases. Work depends slightly on the material, specifically comparing Eco-Flex 50 to Dragon-Skin 30. However, Dragon-Skin 10 and 20 shows a practically identical input-work relation. The lower stiffness material gives a higher efficiency at equal weight. For different weights we see an increase in efficiency for increasing weight. However, the maximum efficiency before buckling decreases with increasing weight. Eco-Flex 50 is so flexible that any meaningful weight added to the carrier causes buckling. Work still increases linearly with load while the material is of no importance.

These results are very similar the the results for changing wall thickness where a lower stiffness, either from smaller wall thickness or more compliant material, increases efficiency but decreases the buckling load. In theory, we would expect an optimum in the efficiency for varying load since at no load

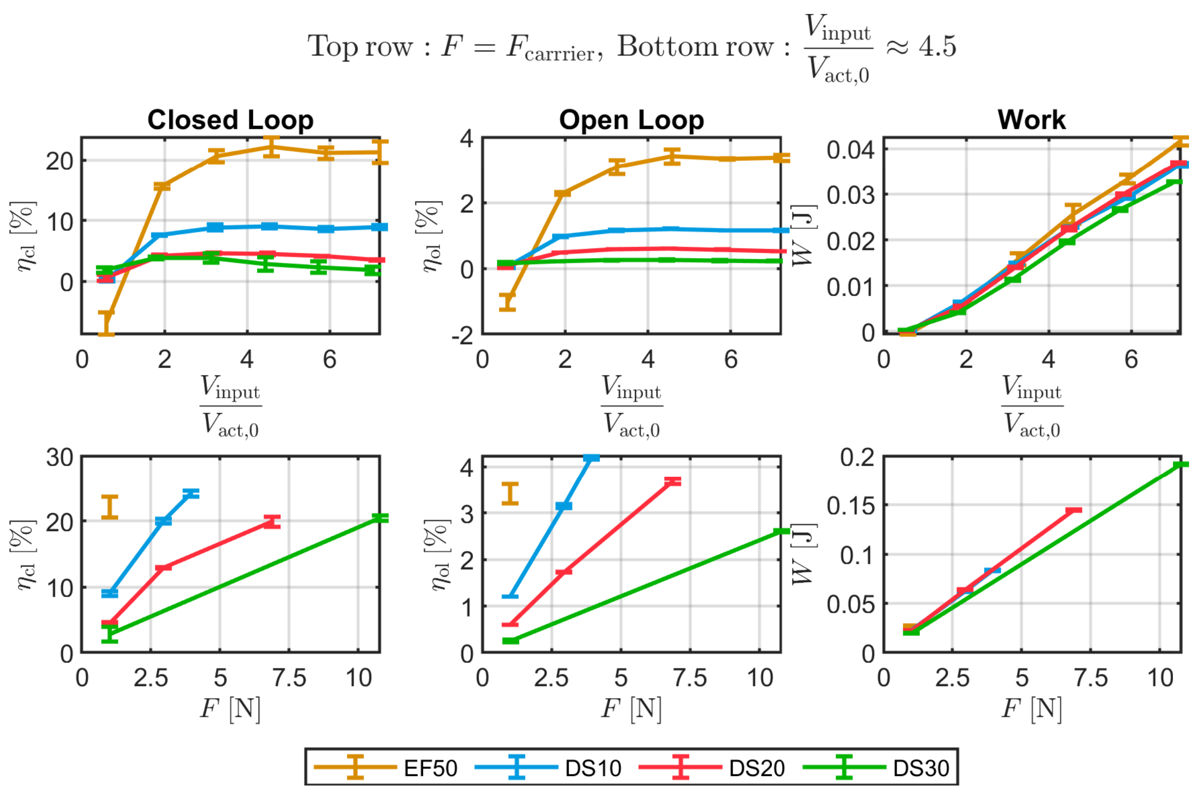

Figure 4.3: Results for the experiments with varying materials. Each point represents the mean and standard deviation over three cycles. From left to right we show the closed loop efficiency, open loop efficiency, and work. The top row shows the load case where only the weight of the carrier is applied with varying inputs. The input is shown as the input volume (V_{input}) divided by the initial actuator volume ($V_{\text{act,0}}$). The bottom row shows the results for input value of 5.5 with varying loads.

no work can be done, but similarly at infinite load no displacement can occur and thus no work can be done. Somewhere between zero and infinite load there should be a maximum in efficiency. However, this optimum in efficiency is not observed in the results. The load, and thus the efficiency, are limited by the buckling load.

4.1.3. Length

The third and last parameter we investigate for the baseline actuator is the length. Figure 4.4 shows the results for these experiments. Both closed loop and open loop efficiency show only small differences for changes in length while closed loop shows slightly larger differences. Again, efficiency increases linearly with increasing weight for the open loop, while closed loop shows diminishing returns.

The main effect of the changes in length is shown in the work. The longer actuator did more work than the shorter ones due to the larger stroke achieved by the longer actuator. However, the longer actuator requires a larger input volume due to the larger initial volume and, as a consequence, has a higher input energy demand. Thus, in applications, the length of the actuator should be matched to the required stroke. If the actuator is too short the required stroke might not be achievable, whereas too long an actuator only needs a small input volume which could reduce the efficiency if the input volume is too small.

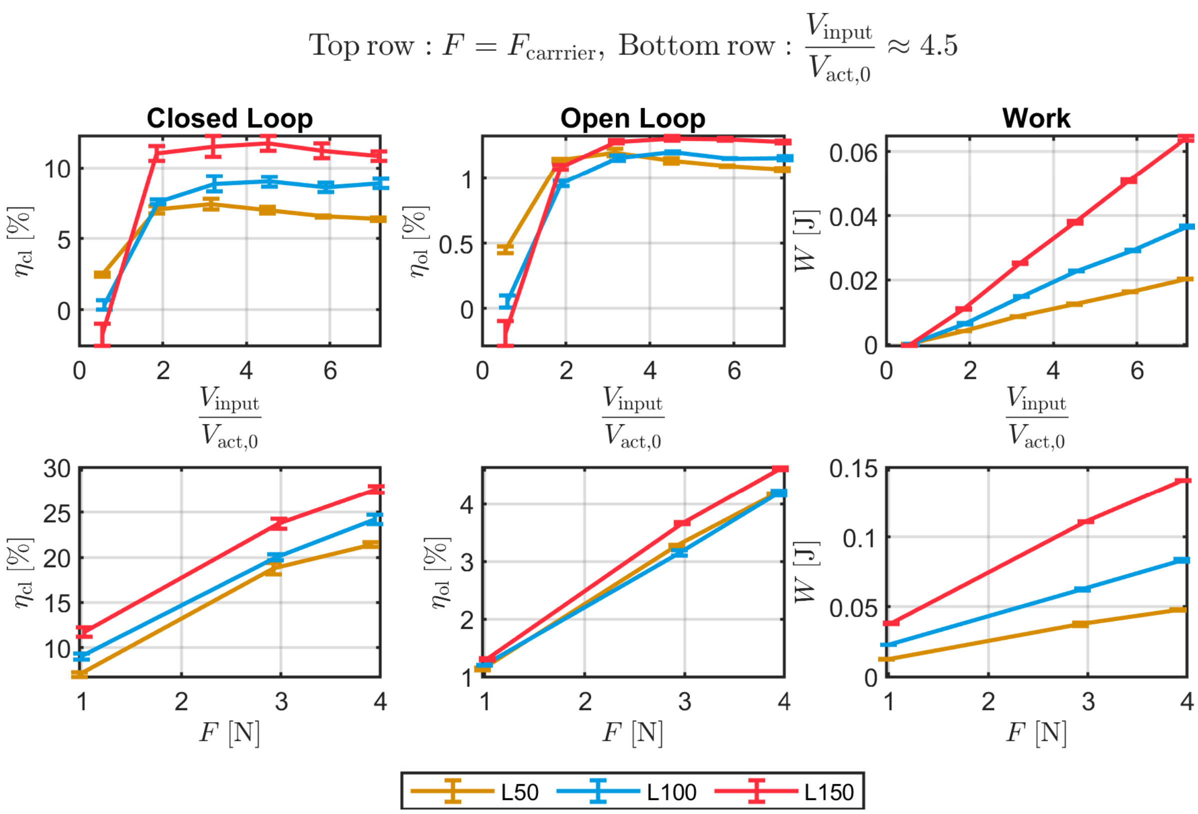

Figure 4.4: Results for the experiments with varying length. Each point represents the mean and standard deviation over three cycles. From left to right we show the closed loop efficiency, open loop efficiency, and work. The top row shows the load case where only the weight of the carrier is applied with varying inputs. The input is shown as the input volume (V_{input}) divided by the initial actuator volume ($V_{\text{act,0}}$). The bottom row shows the results for input value of 5.5 with varying loads.

4.2. Chamber

The first actuator design to deviate from the baseline actuator is the chamber design. The inside of the actuator is separated into distinct air chambers by placing walls inside the actuator. The intent of this design is to enhance efficiency by increasing the radial stiffness without affecting the axial stiffness. This way, deformation should be directed along the longitudinal axis, increasing work. Figure 4.5 shows the four phases (A-D) for the N8 chamber actuator. The effect of the walls is visible in figures 4.5c-d as the white lines which are opposing the radial expansion. However, still some flexibility remains.

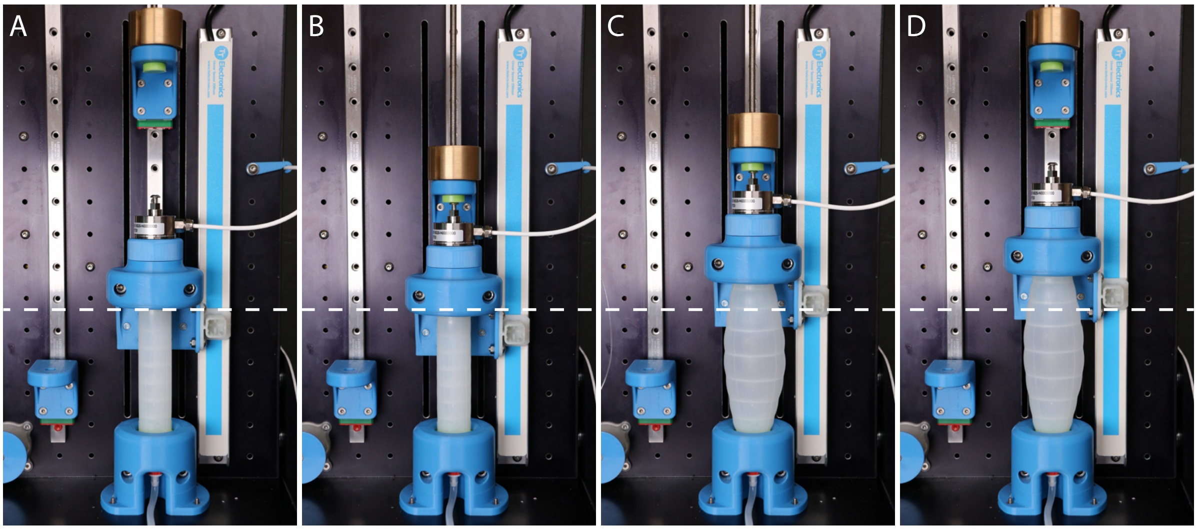

Figure 4.5: Chamber actuator N8 shown in each of the four phases of the actuation cycle. The white dashed line indicates the starting height. A. Initial conditions. B. After loading. C. After inflation. D. After unloading.

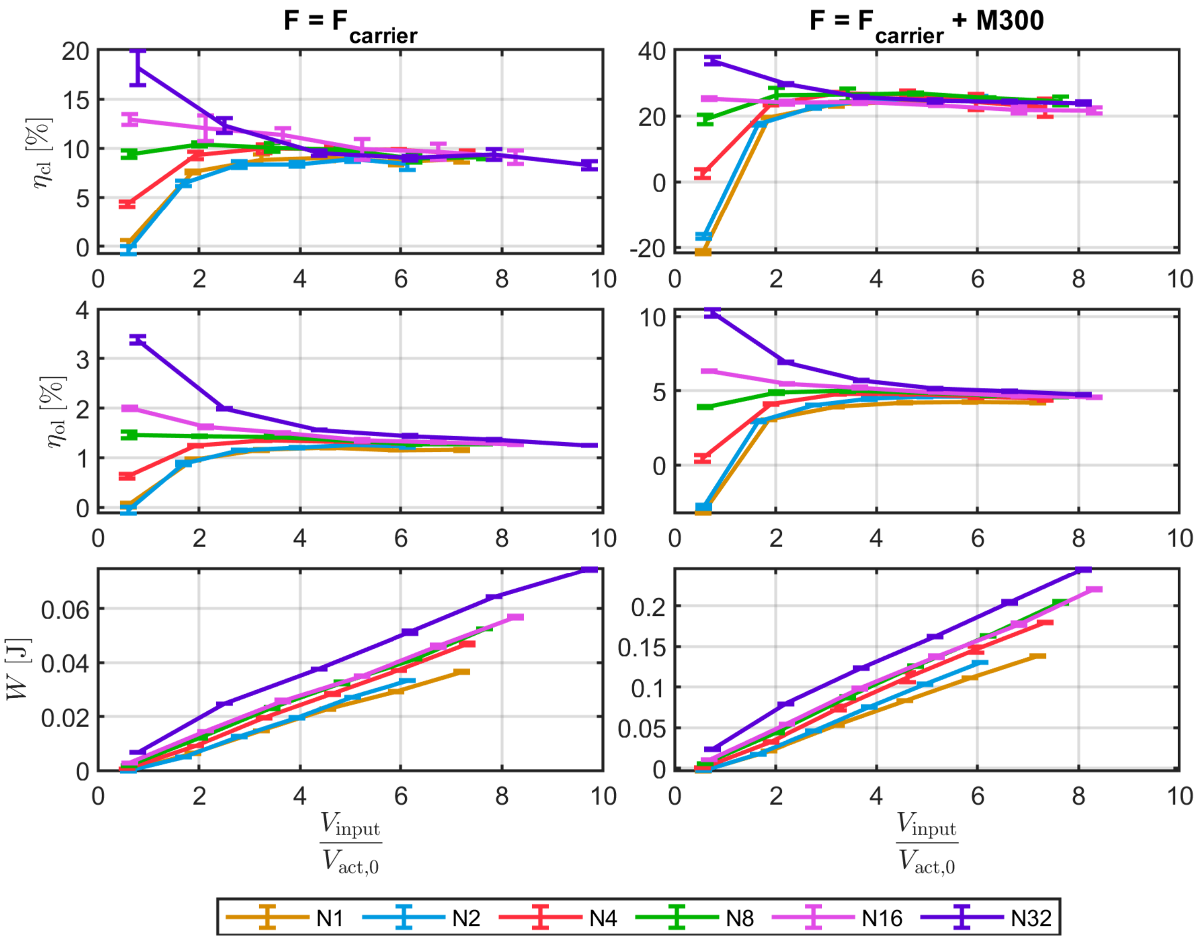

Figure 4.6: Results for the experiments with varying number of chambers. Each point represents the mean and standard deviation over three cycles. The results for the load case where only the carrier is used is shown on the left. The load case where 300 grams was added to the carrier is shown on the right. From top to bottom we show the closed loop efficiency, the open loop efficiency, and the work for varying inputs. The input is shown as the input volume (V_{input}) divided by the initial actuator volume ($V_{\mathrm{act,0}}$).

The addition of chamber walls does not drastically affect the buckling load. Because of this and the relatively large number of actuators in this category, six in total, only two load cases are tested. For the first case only the weight of the carrier is used, while for the second case 300 grams is added to the carrier (the maximum load tested for the baseline actuator). The results for these experiments are shown in figure 4.6. The results for the first load case are shown in the left column and the results for the second load case are shown in the right column. From top to bottom we show the closed loop efficiency, open loop efficiency, and work. All are shown as a function of the input volume.

For low input volumes something interesting happens. Actuators with few chambers show a decline in efficiency compared to high input volumes, while actuators with more than eight chambers show an increase in efficiency. This indicates that, for actuators with more chambers, volume increase is initially directed along axial extension as opposed to radial expansion. At high input volumes, the efficiency of all actuators converges, thus reducing the effect of the chambers on the efficiency.

A possible explanation for this is that during the initial part of the inflation phase the shape of the actuator is changing until an optimal shape with a balance between axial and radial stresses is reached. Then, the actuator inflates further but only changes size while the shape remains constant. For actuators with more chambers this optimal shape is likely more elongated than for actuators with fewer chambers due to the increased radial stiffness. This means that actuators with more chambers initially expand more axially than radially while actuators with fewer chambers are the opposite. Furthermore, when we look at the open loop efficiency for the first load case the N8 actuator shows a constant efficiency, irrespective of the input. The same actuator for the second load case shows a slight decrease in efficiency at low input volumes. This could indicate that the optimal shape is shorter for higher loads which would reduce the benefit of the chambers.

Unlike efficiency, work is always slightly increased by the increased number of chambers, regardless of input. Presumably, this is caused by the increased extension early in the inflation phase which raises the work. The difference between actuators remains approximately constant over the full range of input volumes which appears to validate this assumption.

4.3. Corrugated

The second design that we tested is the corrugated design. Here, the wall of the actuator has a waving pattern where the controlled variable is the amplitude of the wave. The idea behind this concept is that the axial stiffness is lowered, making it easier to extend, while retaining the same radial stiffness. As we started tests using these actuators we quickly noticed that the corrugation greatly reduced the buckling load. To still effectively test the actuators we slightly changed the experimental procedure.

Normally, the weight was lowered until fully supported by the actuator. For these tests we lower the weight until the load is partially supported by the actuator but not completely. From there we start

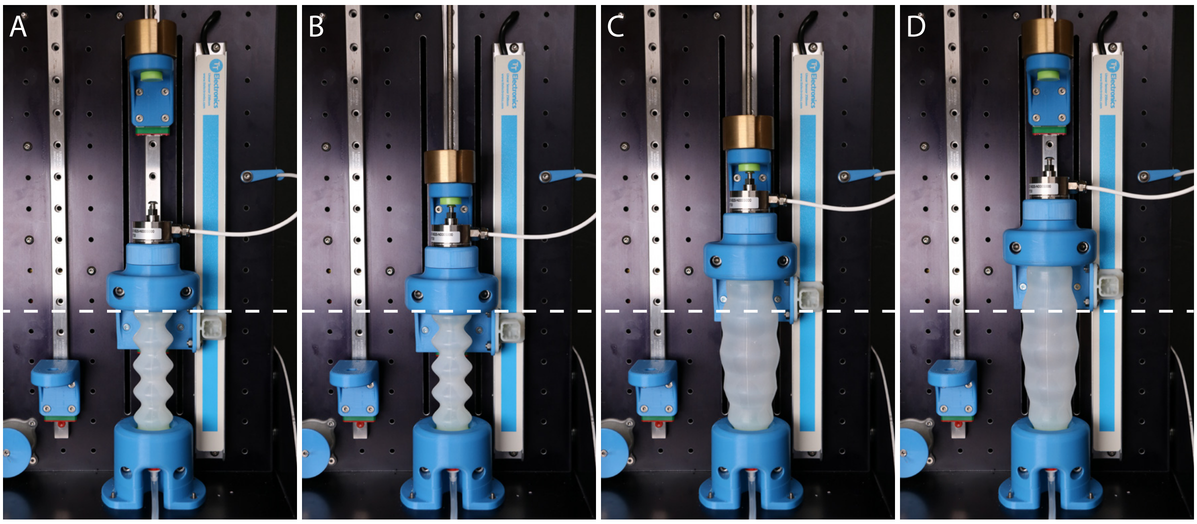

Figure 4.7: Corrugated actuator A3 shown in each of the four phases of the actuation cycle. The white dashed line indicates the starting height. A. Initial conditions. B. After loading. C. After inflation. D. After unloading.

to inflate the actuator. This way, the actuator is partly inflated before supporting the entire load which raises the maximum load. However, the corrugation still negatively affects the buckling load and if the load is too high the actuator starts to buckle as soon as the inflation starts.

Figure 4.7 shows the four phases (A-D) for the A3 corrugated actuator. From figure 4.7a to 4.7b little to no difference can be seen since the load was stopped early. The actuator after inflation is shown in figure 4.7c. The actuator extends significantly, while the radial expansion is rather limited. Furthermore, the actuator keeps the corrugated pattern even when inflated.

For the corrugated actuators three weights are tested. The results are shown in figure 4.8. The left, middle, and right column show the results for the load cases where nothing, 50 grams, and 100 grams are added to the carrier, respectively. From top to bottom we show the closed loop efficiency, open loop efficiency, and work. The corrugated actuators show similar behaviour to the chamber actuators where for actuators with small amplitude the efficiency at low input volumes drops while for actuators with a larger amplitude the efficiency increases. The amplitude for which this change in behaviour occurs seems to be load dependent. The A2 actuator shows an increased efficiency at low input when no added load or 50 grams added load is used. When 100 grams added load is used the efficiency remains approximately constant for all inputs.

At higher inputs the efficiencies start to plateau. However, unlike the chamber actuators, these efficiencies do not converge but show a consistently higher efficiency for higher amplitudes of corrugation. There are two possible explanations for this different behaviour. The first explanation is that it could be an artifact of the change in experimental procedure. The second, more likely, explanation is that

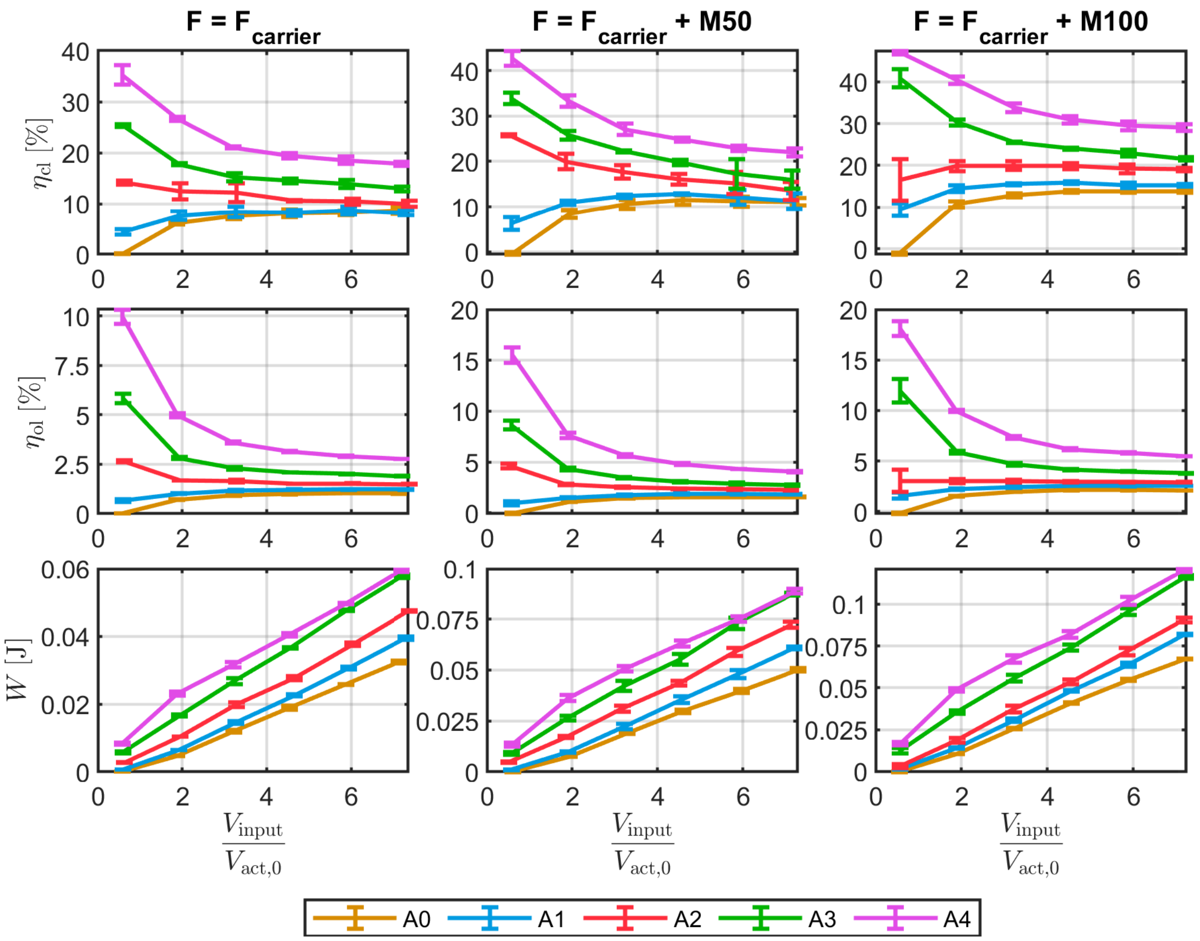

Figure 4.8: Results for the experiments with varying amplitude of corrugation. Each point represents the mean and standard deviation over three cycles. The results for the load case where only the carrier is used is shown on the left. The load case where 50 grams was added to the carrier is shown in the middle. The load case where 100 grams was added is shown on the right. From top to bottom we show the closed loop efficiency, open loop efficiency, and work for varying inputs. The input is shown as the input volume (V_{input}) divided by the initial actuator volume ($V_{\text{act},0}$).

it is caused by the corrugated pattern which remains discernible even after inflation. The corrugated pattern means that the actuator behaves almost like a mechanism with regard to axial extension. Most of the extension is accomplished by unfolding of the actuator as opposed to stretching of the material which concentrates deformation and stresses near the peaks of corrugation and reduces the total strain energy.

To get a better view of the influence of the amplitude as a function of the load we look at the work and efficiencies for the maximum input volume used ($V_{input}/V_{act,0}$ ≈7.2). These results are shown in figure 4.8. We can see that both the efficiency and work increase with load. Furthermore, both increase more as the load increases further. We believe this is caused by the change in experimental procedure. Normally, negative work would be done during loading and additional positive work is done during unloading. In these experiments however, the loading phase is skipped so no negative work is done while the positive work from unloading is still done. This advantage increases with load for two reasons. The first is that a higher load provides more work in general and the second is that the actuator was more compressed due to higher loads and thus more extension is realised during unloading.

$$\frac{V_{\text{input}}}{V_{\text{act},0}} \approx 7.2$$

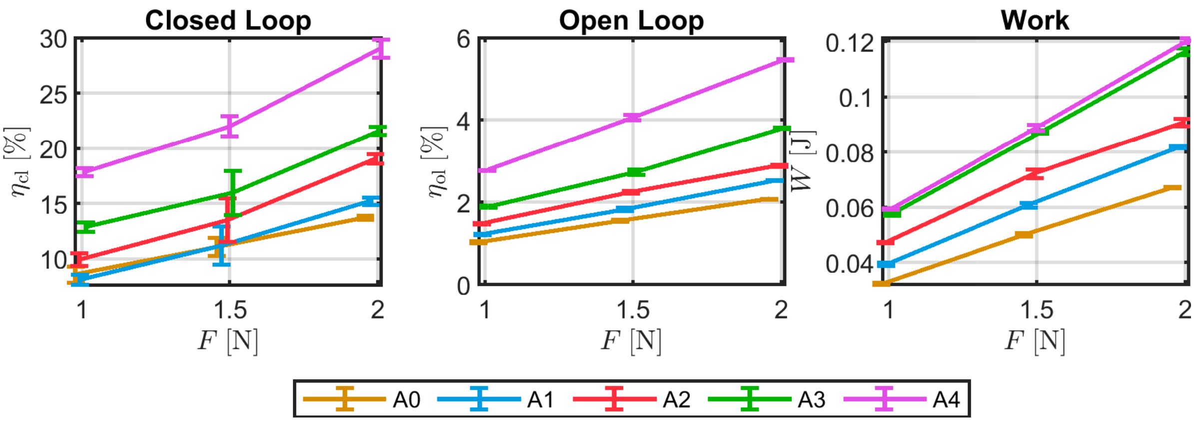

Figure 4.9: Results for the experiments with varying amplitude of corrugation. The input is set to the maximum input tested. The closed loop efficiency, open loop efficiency, and work are shown as a function of the load.

4.4. Multi-Material

The final actuator design that is tested is the multi-material design. The multi-material design has fibers made from a second, stiffer, rubber wrapped around the actuator. These fibers should restrict the radial expansion without drastically impeding the axial expansion. Figure 4.10 shows the ED32 actuator during the four phases (A-D) of the actuation cycle. Figures 4.10c and d show the actuator in the inflated state. Unlike the chamber and corrugated designs, there is no significant effect of the multi-material design visible.

The fiber actuators were tested early on in the project. At this point in time we still performed the experiments with the testing protocol used for experiments with varying wall thickness. Due to time constraints the tests were not repeated using the updated testing protocol which means there is no data available for input volumes smaller than two times the initial actuator volume.

Four actuators, with increasing stiffness of the fiber material, are compared. The results for the experiments using the multi-material actuators are shown in figure 4.11. The top row shows the results for the load case where only the carrier is used and the input is varied. The bottom row shows the results at an input of 5.9 for varying load.

The results for the multi-material actuators are fairly similar to each other. We see some hints that indicate the higher stiffness fibers might increase the efficiency at low input and reduce the efficiency at higher inputs. However, without seeing a larger range of input volume and fiber stiffnesses no clear conclusion can be drawn. For the work the results are more clear. We can see that the stiffer fibers slightly increase the work done. This advantage increases as the load increases.

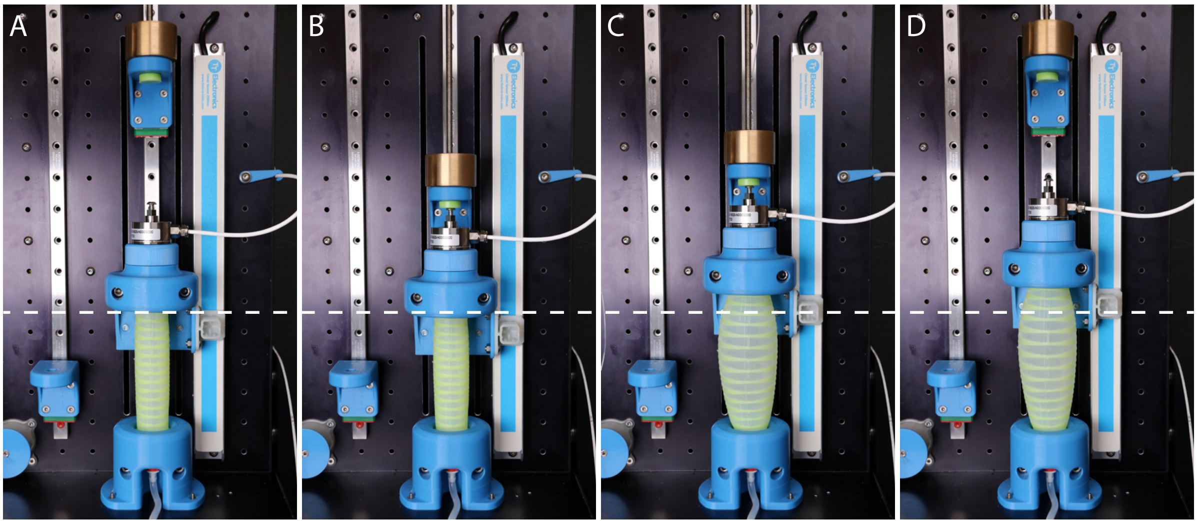

Figure 4.10: Multi-material actuator ED32 shown in each of the four phases of the actuation cycle. The white dashed line indicates the starting height. A. Initial conditions. B. After loading. C. After inflation. D. After unloading.

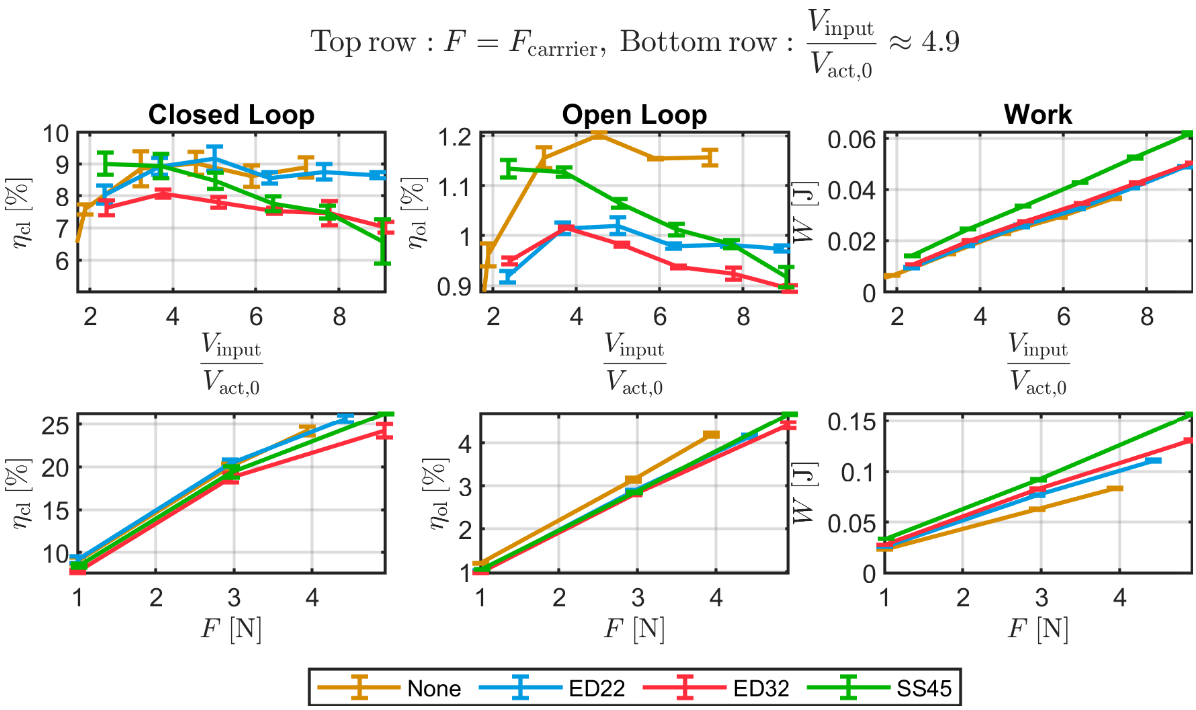

Figure 4.11: Results for the experiments with the multi-material actuators. Each point represents the mean and standard deviation over three cycles. From left to right we show the closed loop efficiency, open loop efficiency, and work. The top row shows the case where only the weight of the carrier is applied with varying inputs. The input is shown as the input volume (V_{input}) divided by the initial actuator volume ($V_{\text{act,0}}$). The bottom row shows the results for input value of 5.9 with varying loads.

4.5. Combining and Comparing

As a last step we will make a comparison between the different types of actuators. Figure 4.12 shows each of the four types of actuator after the inflation phase. All actuators are given the same input and load. The dashed lines indicate the axial extension that is achieved by the actuators. The baseline actuator, shown in figure 4.12a, and the multi-material actuator, shown in figure 4.12d, achieve approximately the same extension. The corrugated actuator, shown in figure 4.12b, and the chamber actuator, shown in figure 4.12c, both achieve a greater extension than the other two actuators. All three actuator designs reduce the radial expansion compared to the baseline actuator. However, a smaller radial expansion does not necessarily equate to a higher efficiency.

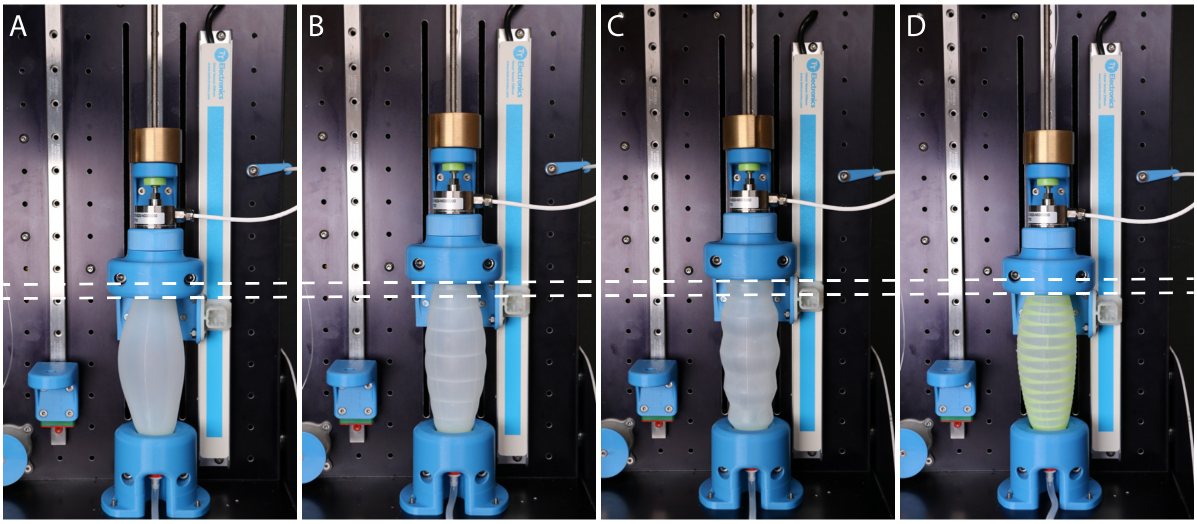

Figure 4.12: The four different actuator types after the inflation phase. Each actuator was provided the same input volume and carries the same load. A. Baseline actuator. B. Chamber actuator N8. C. Corrugated actuator A3. D. Multi-material actuator ED32.

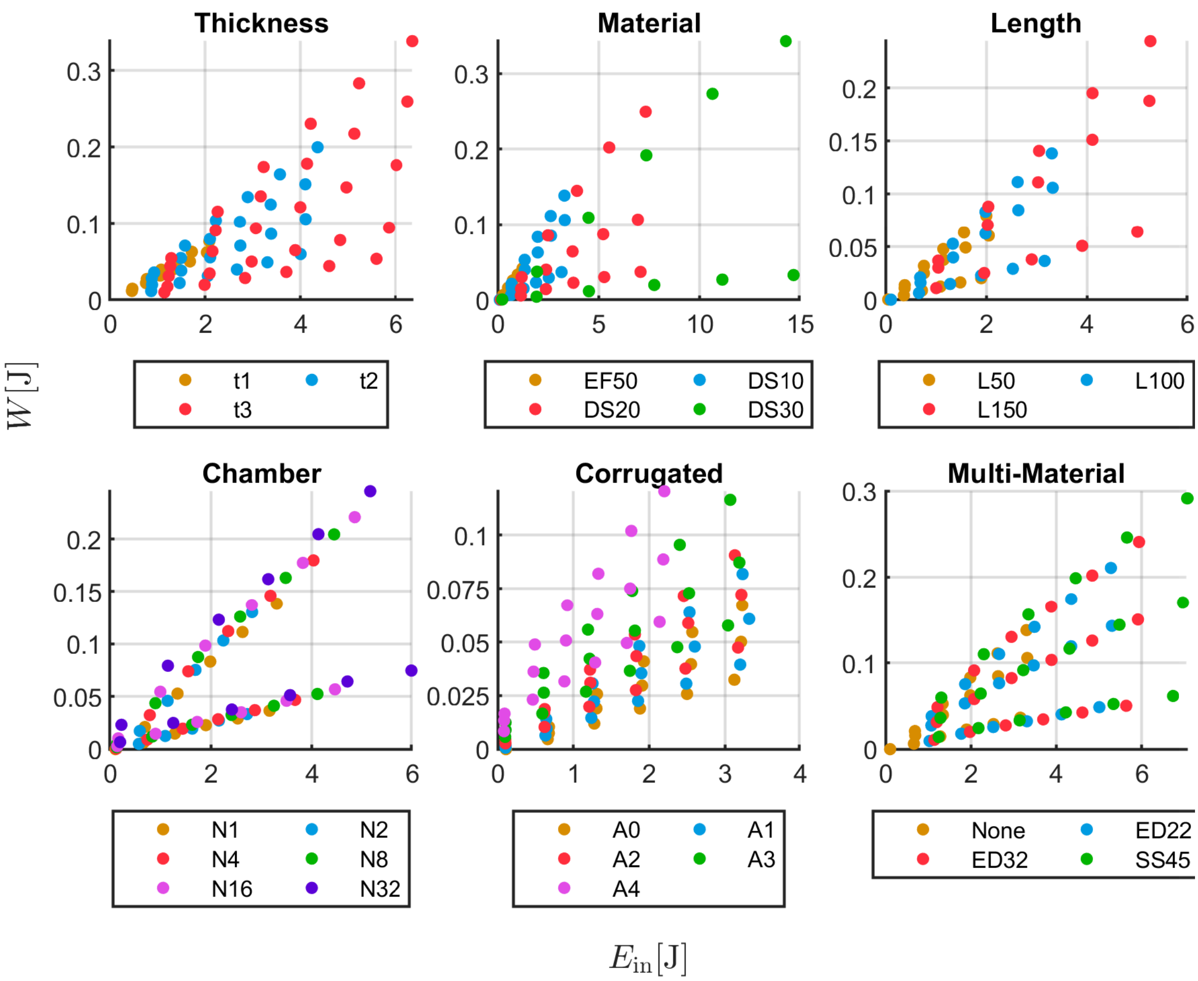

Figure 4.13: The work done versus the dissipated energy over the full actuation cycle for all experiments. Each point represents the average over three cycles at a specific input, load, and actuator combination.

The results from all experiments were grouped in figure 4.13 to compare between actuator designs. We plot the work against the input energy for each of the design parameters. Each point represents the mean over three cycles at a specific combination of input volume, load, and design parameter value. A higher input energy, for the same design parameter value, generally corresponds to a higher input volume while higher work is indicative of a higher load. Since open loop efficiency is determined by the ratio of work to input energy, we want work to be high and input energy to be low to obtain a high efficiency.

The best performing (highest efficiency) actuators trend towards the top left corner of the plot. From these plots we can see the most effective way to increase work without drastically increasing the input energy is to simply increase the load. However, load cannot be increased indefinitely since the actuator will not be able to support loads that exceed the critical buckling load. In practice, the load is usually imposed by the requirements of the specific application. Therefore, to reach the highest possible efficiency given a certain load, the actuator should be designed as such that the critical buckling load is slightly above the required load. To reduce the input energy without sacrificing work actuator stiffness can be reduced, for example by reducing the wall thickness or using a more compliant material. The best way to reduce input energy seems to be using the corrugated design and increasing the amplitude of corrugation. All three of these methods decrease the input energy but also reducing the buckling load. Again, buckling load seems to be the limiting factor to further increase efficiency.

While open loop efficiency is only dependent on the work and the input energy, closed loop efficiency is also dependent on the energy dissipation. We plot this energy dissipation versus the input energy in figure 4.14 to make a comparison between the different types of actuators. From this plot

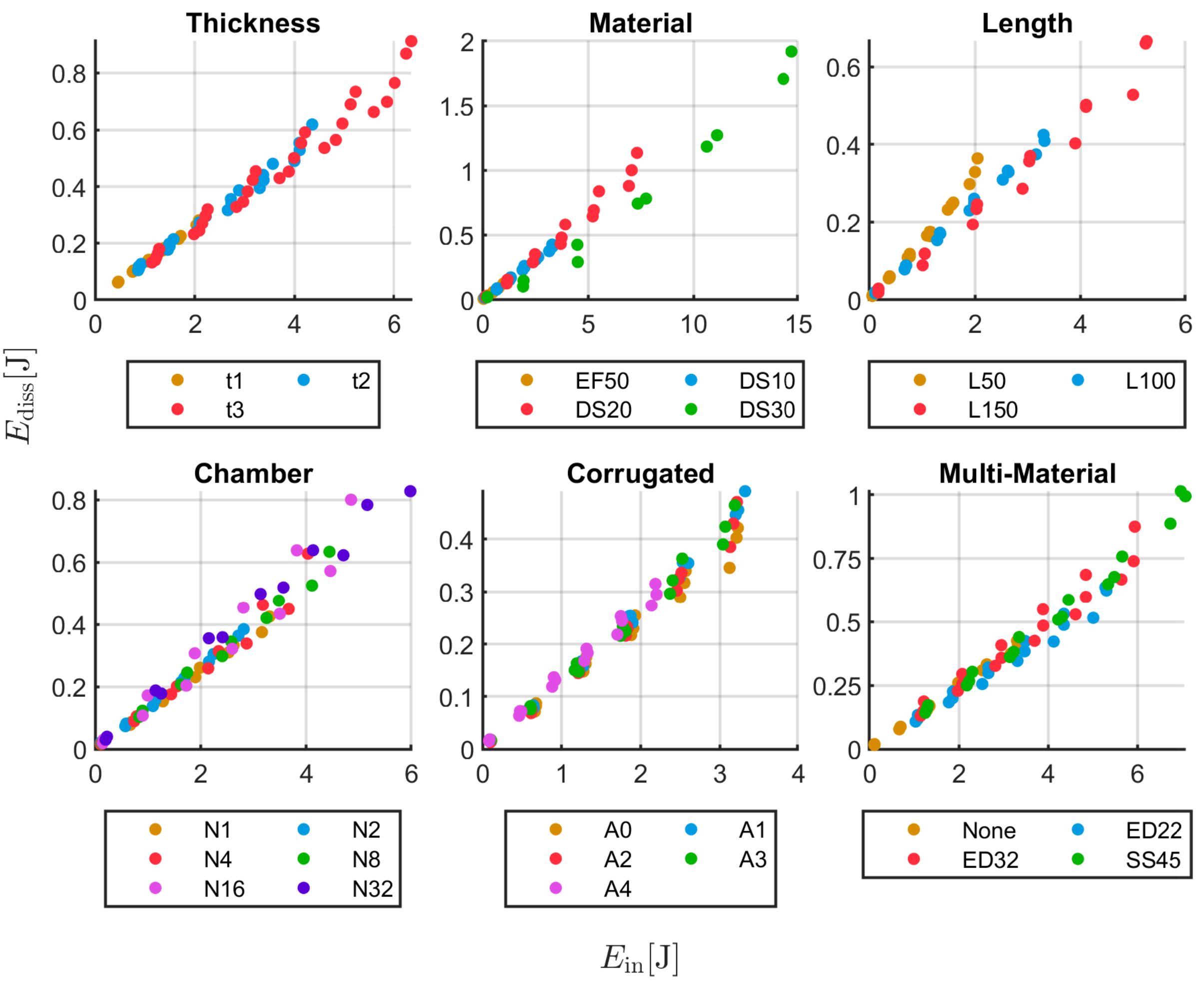

Figure 4.14: The work done versus the dissipated energy over the full actuation cycle for all experiments. Each point represents the average over three cycles at a specific input, load, and actuator combination.

it becomes clear that the energy dissipation for these types of actuator increases linearly with input energy. Furthermore, we can see that the ratio of dissipated energy to input energy remains almost constant for all actuators and input volumes. The only relevant deviation from this constant ratio that can be seen is for changes in load. However, this deviation is still small, especially compared to the increase in work related to the load increase.

In general, we see higher loads result in higher work while only slightly raising the dissipation. Increased stiffness, either from wall thickness or materials, raise the dissipated energy and required energy input while also raising the maximum work. However, the efficiency at equal load does become lower. Longer actuators mainly increase the stroke, and thus the work, but also increase the required input volume. More chambers in an actuator raises the energy input while maintaining the efficiency, thus increasing work. A higher amplitude of corrugation lowers the energy input, and thus the dissipated energy, while raising the work. However, the maximum work is limited due to the lower buckling load.

5
Discussion and conclusions

The objective of this research was to *gain a more complete and in-depth understanding of the energy efficiency of soft pneumatic actuators.* In this last chapter we will revisit the research questions that were formulated in section 1.4 to achieve this understanding. For each question we briefly discuss the process and results which lead to our conclusions. We will finalize by providing some possible directions for future work

Revisiting our research questions

The first research question was *how can we define and measure efficiency to provide a complete representation of a soft pneumatic actuator?* We began in section 2.1 by showing the actuators used in this research. We focused on extension actuators to keep the work manageable. In section 2.1.1 we presented a baseline extension actuator as well as three distinct design variations: the chamber, corrugated, and multi-material designs. Each design comes with its own set of design parameters which could all be related back to the baseline actuator. Section 2.1.2 discussed the fabrication method used to produce the actuators.

In section 2.2 we presented a simplified analytical model to describe the actuators. Here, we separated the analysis into three physical domains: pneumatic, material, and mechanical. For these domains we determined all possible causes of energy loss. We derived an expression for each potential energy loss and made some assumptions to simplify the analysis. The main assumption is that *we assume that the entire experiment is performed in a quasi-static manner.* This assumption means that dynamic effects and thermodynamic irreversibilities are avoided. It also means that any efficiency found in this research should be considered as an upper limit since these dynamic and thermodynamic effects would induce additional losses.

Two definitions of efficiency were presented. The open loop efficiency only considers the energy input and how much of this energy is converted to work. The second definition, the closed loop efficiency, assumes that all of the stored energy can be reused. The closed loop efficiency considers how much of the unrecovered energy is converted to work. In reality, not all of the stored energy can be recovered. An additional energy harvesting system, which also has inherent energy losses, is needed. Such a system and its efficiency were previously described by Wang et al. [42].

In section 3.1 we presented our design for an experimental setup to characterize linear motion actuators. Here, an actuator can be held in place while a stepper motor slowly lowers a weight to apply a load. The motion of both the actuator and load are constrained to minimize off-axis loading. In real world applications this condition might not be met, in which case we expect the efficiency to decrease. Again, we are testing in an ideal case scenario so we can consider the results as an upper limit for efficiency.

The second research question was *how is energy distributed during an actuation cycle and what are the main causes of energy loss?* In section 3.2 we performed some preliminary tests to show the behaviour of the actuator during a full actuation cycle. Three situations were tested and compared to quantify the contribution of each energy loss.

In the first situation, the actuator was inflated without doing any work. We found that most of the input energy (88%) was recovered during deflation and that very little energy (1%) was used to compress the air itself. The majority of energy is thus stored elastically in the material. The remaining energy (11%) could only have been dissipated in the viscoelastic material.

In the second situation, the actuator was only working against the friction in the setup. This work was related to the friction force on the top actuator clamp which could not be measured directly. By comparing this second situation to the first we could approximate the energy dissipation caused by this friction. We found this energy loss negligible compared to the total energy input (0.1%) and excluded it from the rest of our experiments. This friction is a property of this specific setup. For use in applications the friction should be reevaluated and characterized in the context of the particular application.

In the third situation, a complete actuation cycle, including loading and unloading, was performed. From the pressure-volume curve we found that a higher pressure was required to achieve the same volume compared to the unloaded situation. This higher pressure results in a greater energy input demand. However, the second and third situation behaved identical after the third situation had unloaded. This could be seen in the energy recovered during deflation which was very similar for both situations. We did observe more dissipation in the third situation which could be attributed to the additional deformations caused by the loading and unloading. However, the increase in dissipation relative to the input energy was rather minimal. So the main cause of energy loss for the open loop efficiency is the elastic energy. For the closed loop efficiency it would depend on the efficiency of the recovery. However, the unrecoverable energy would still be the greatest source of energy loss if we assume 44% [42] efficiency of recovery.

The third research question was *how do different design parameters affect actuator efficiency and work?* For each of the different designs we tested some specific design parameters. For all of the parameters we varied both load and input volume. For the baseline actuator, which was a simple cylindrical tube, we investigated three parameters: wall thickness, material, and length. We found that, for the baseline actuator at input volumes approximately equal to the initial actuator volume, both the closed loop and open loop efficiency are close to 0% or even below. We believe this is caused by the actuator first being pressurized and expanding radially before the weight starts moving. An interesting way to circumvent this low efficiency region could be to never fully deflate the actuator but always keep it slightly pressurized.

At higher input volumes we saw that efficiency reaches a plateau. Presumably, the actuator is expanding almost uniformly and the efficiency is only determined by the stiffness. This could be seen when comparing different wall thicknesses and materials. Stiffer actuators, either through thicker walls or stiffer materials, plateau at lower efficiency levels. However, this only applies at equal load. As load increases we observed an increase in efficiency for all actuators. We tested each actuator with increasing loads until buckling occurred and although the more compliant actuator showed a higher efficiency initially, the stiffer actuators could withstand significantly higher loads. For thicker walls the load could even be increased so much that the maximum efficiency became higher than the maximum efficiency obtained for the thinner walls. Unlike changing the wall thickness, changing to a stiffer material did not raise the maximum efficiency. We assume that the geometric relations are of greater influence than the material properties.

We found that work increases linearly, both with increasing load as well as increasing input volume. Furthermore, increasing the stiffness of the actuator has no influence on the work for a specific load or input volume. However, the stiffer actuators can handle higher loads which will result in more work being done. The only way to increase the work being done by the actuator is to change the length. A longer actuator will provide more extension, and thus more work than a shorter actuator at the same normalized input volume. However, the length seems to have little influence on the efficiency.

The first design which diverged from the baseline actuator was the chamber design where the actuator is divided into distinct chambers separated by thin walls. Here, we investigated the influence of the number of chambers. The walls placed inside the actuator act as local radial stiffeners and adding more walls should keep increasing the radial stiffness. The results of these experiments showed an effect of the increasing radial stiffness mainly for low input volumes. The efficiency of the baseline actuator, which has only one chamber, decreases for lower input volumes while the efficiency decreased less as the number of chambers increased. If the number of chambers increased beyond a certain transition point the efficiency would actually start to increase as the input volume decreased. We believe that the increased radial stiffness limits radial deformation while the actuator is being pressurized. As the actuator is inflated further, it expands more uniformly and the effect of the chambers diminishes. This was clearly visible as the efficiency of all actuators converged towards a single value as the input volume increased.

The second design used a corrugated wall to reduce the axial stiffness. The design parameter investigated was the amplitude of the corrugating wave. The reduction in axial stiffness limited the maximum pressure inside the actuator. The lower pressure reduces the radial deformation while pressurizing and thus increases the efficiency at lower input volume, much like the chamber actuators. However, for higher input volume the efficiency did not converge but the efficiency for each actuator plateaued at a different value. The reduced radial deformation only contributes at the low input volume but the corrugated pattern remained during the complete range of motion, reducing energy requirements and increasing efficiency. A bigger amplitude always increased the efficiency but also decreased the critical buckling load. Here, a trade-off arises between efficiency and load capacity.

The third and last design was the multi-material design. Here, a combination of two materials was used. The more compliant of the two materials was used to create the cylindrical actuator while the second, stiffer, material was used as a fiber wrapped around the outside. The idea behind this concept was to increase the radial stiffness, similar to the chamber design. Unfortunately, the results for this design were inconclusive. A larger range of input volumes would help highlight possible differences between the current actuators. Additionally, achieving a larger stiffness ratio between the bladder material and the fiber material could also accentuate any possible differences.

When looking at the class of extension actuators as a whole we found that the relation between input energy and work is mainly determined by actuator stiffness and the applied load. The two ways to increase efficiency are to lower stiffness or increase load. However, actuators with a lower stiffness suffer from a reduction in critical buckling load so there is a limit to how much stiffness can be decreased without compromising the load bearing capacity. Furthermore, we found that the relation between input energy and dissipated energy remains mostly constant and is only slightly affected by load and actuator design. Therefore, the best way to increase energy efficiency is to try and reduce the energy requirements (i.e. lower actuator stiffness). Again, the critical buckling load appears to be the limiting factor. A good way to realise the lowest possible stiffness is to first determine the required load and then design the actuator such that it can barely, within a safety margin, sustain this load.

Future work

It seems that energy efficiency of soft pneumatic extension actuators is mainly increased by lowering axial stiffness and raising load. However, these are two conflicting concept since lowering the stiffness decreased the load bearing capabilities. To move towards more efficient actuators we should look into ways to combine a low axial stiffness with a high load capacity. A way to achieve this could be to modify the corrugated actuator by looking at the second design parameter described in section 2.1.1, the corrugation wavelength (λ). The actuator would initially be completely folded if we would decrease the wavelength to twice the wall thickness. This way, the actuator could perhaps carry bigger loads without buckling.

Additional research could be done investigating the rest of the design parameters that were disregarded during this project. We could also look into combinations of design parameters (e.g. by scaling down the entire actuator but keeping the same aspect ratios). Going one step further, we could even look into combinations of actuator designs (e.g. combining the chamber and corrugated designs). Beyond that there are the other classes of soft pneumatic actuators. All of which come with their own unique advantages and challenges.

Besides looking into other actuator designs we could also look into making changes to the experimental setup. For example, it could be interesting to look into ways to load and move the actuators outside of their intended movement pattern, although extension actuators might be least suitable for this purpose due to their inherent problems involving buckling. From the other types of actuators only the contraction actuators can be characterized using the current setup. To test bending or rotational actuators a completely new setup has to be developed.

A

Technical drawings

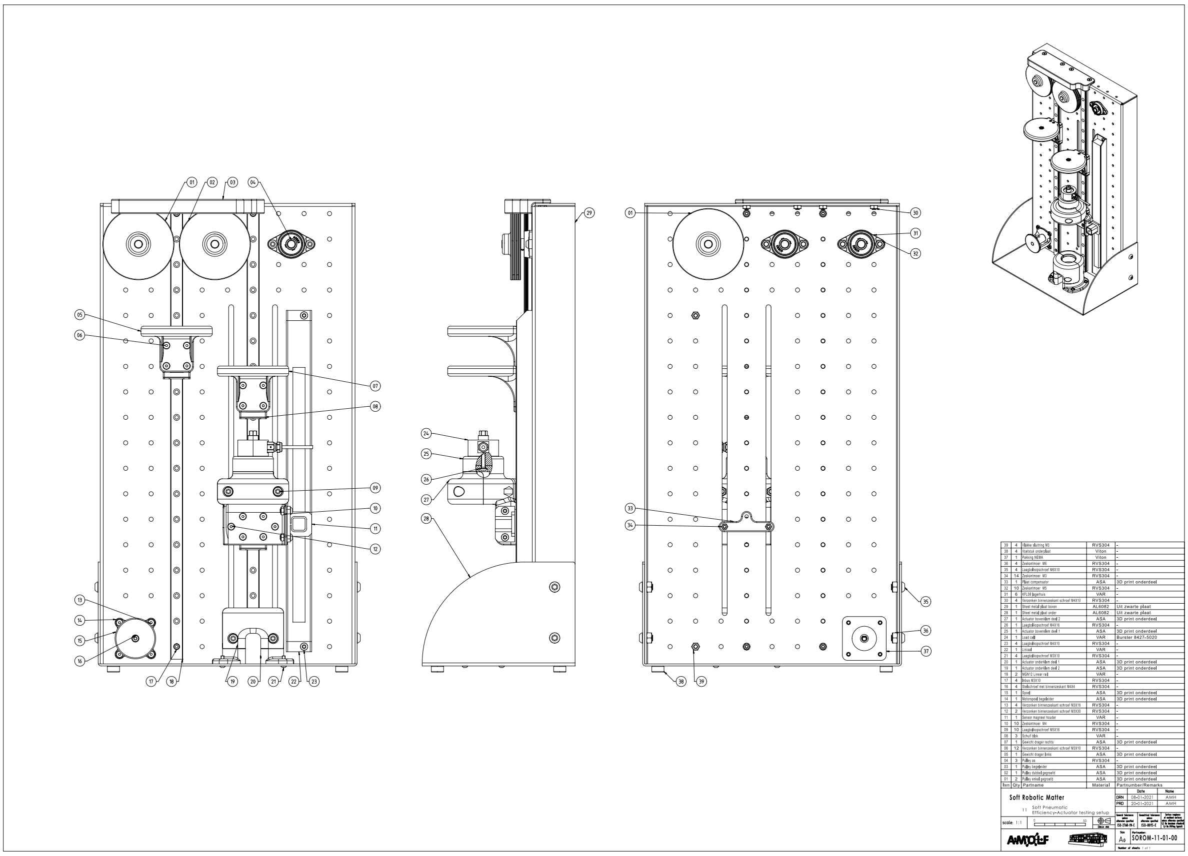

Figure A.1: Assembled setup

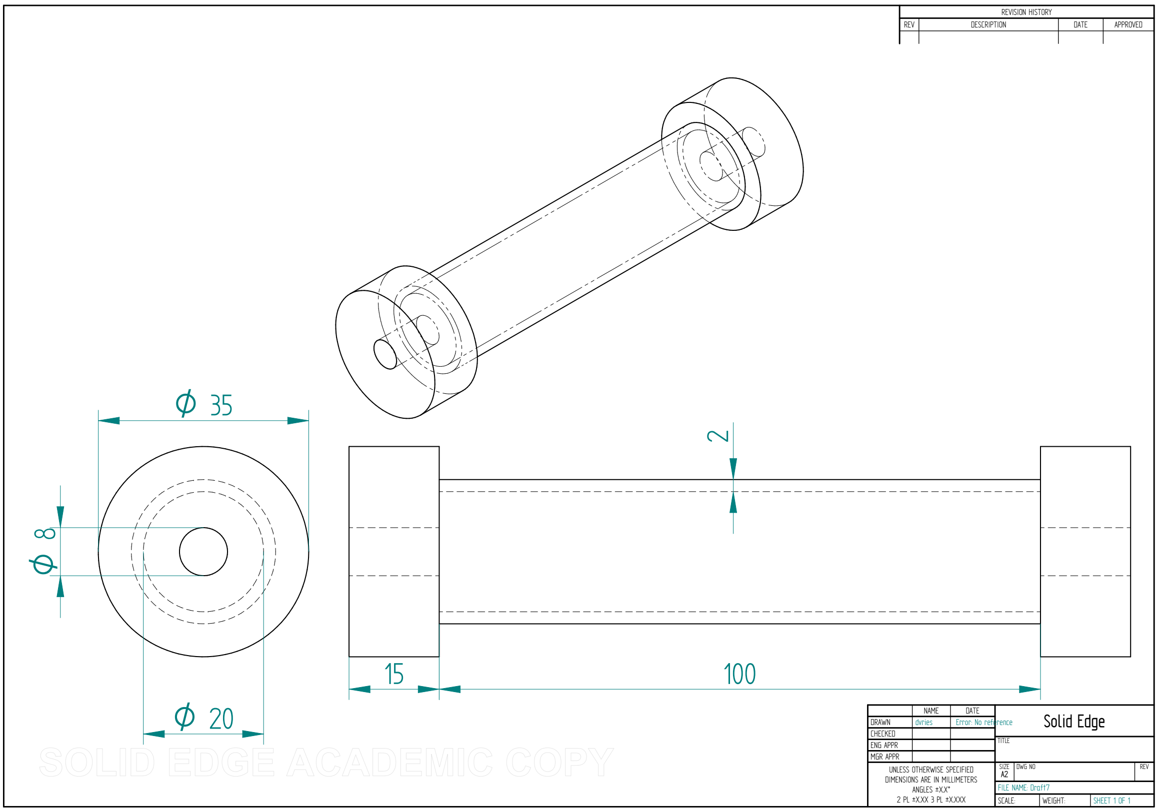

Figure A.2: Baseline actuator

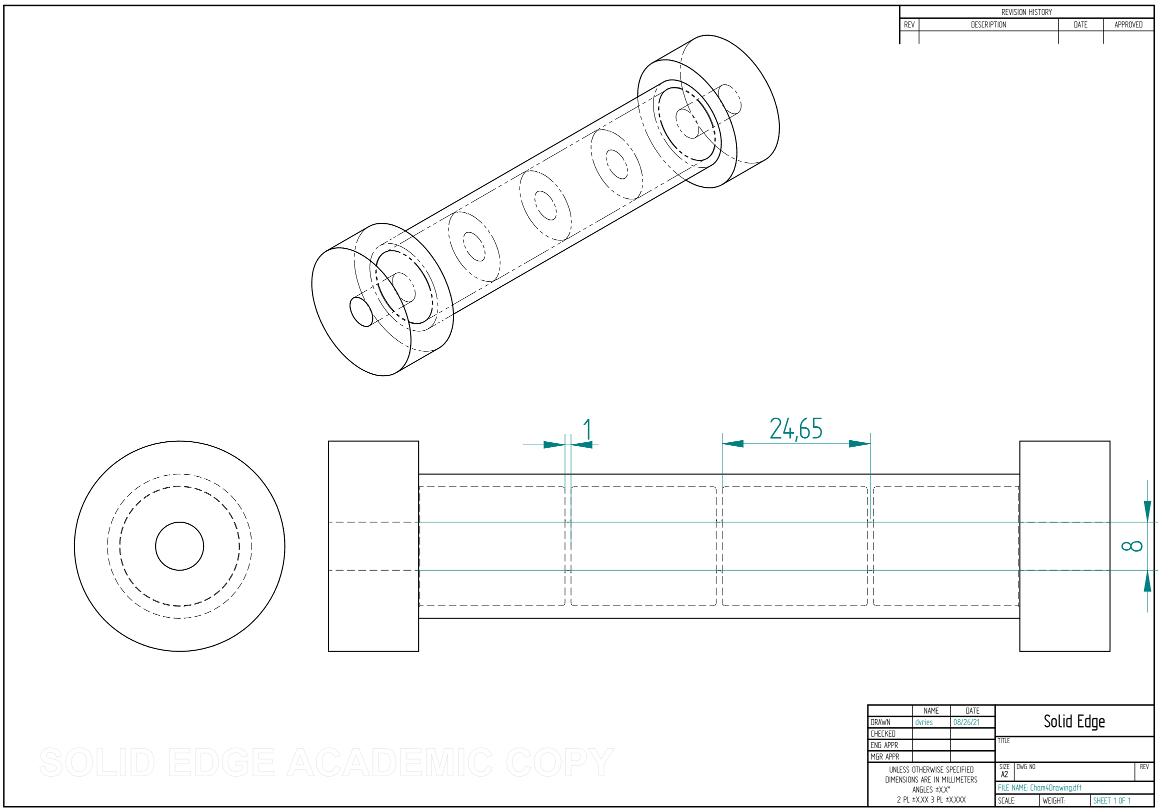

Figure A.3: Chamber design N4

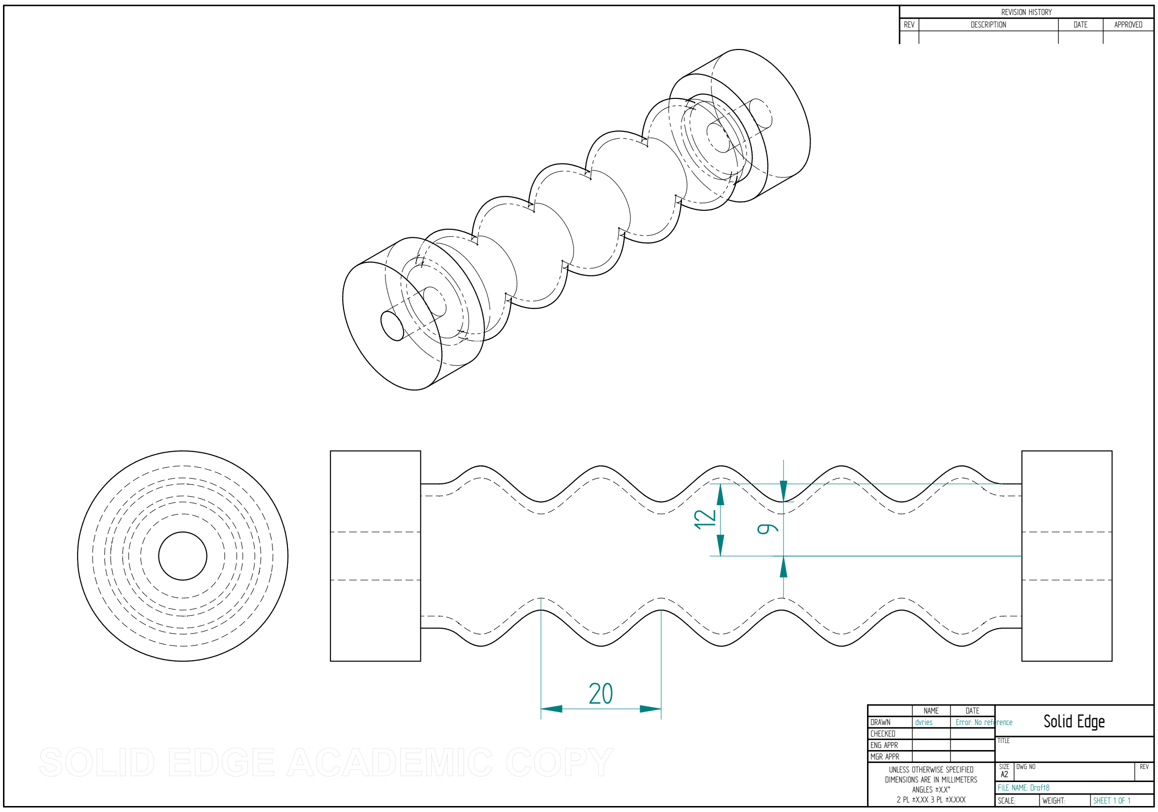

Figure A.4: Corrugated design A3

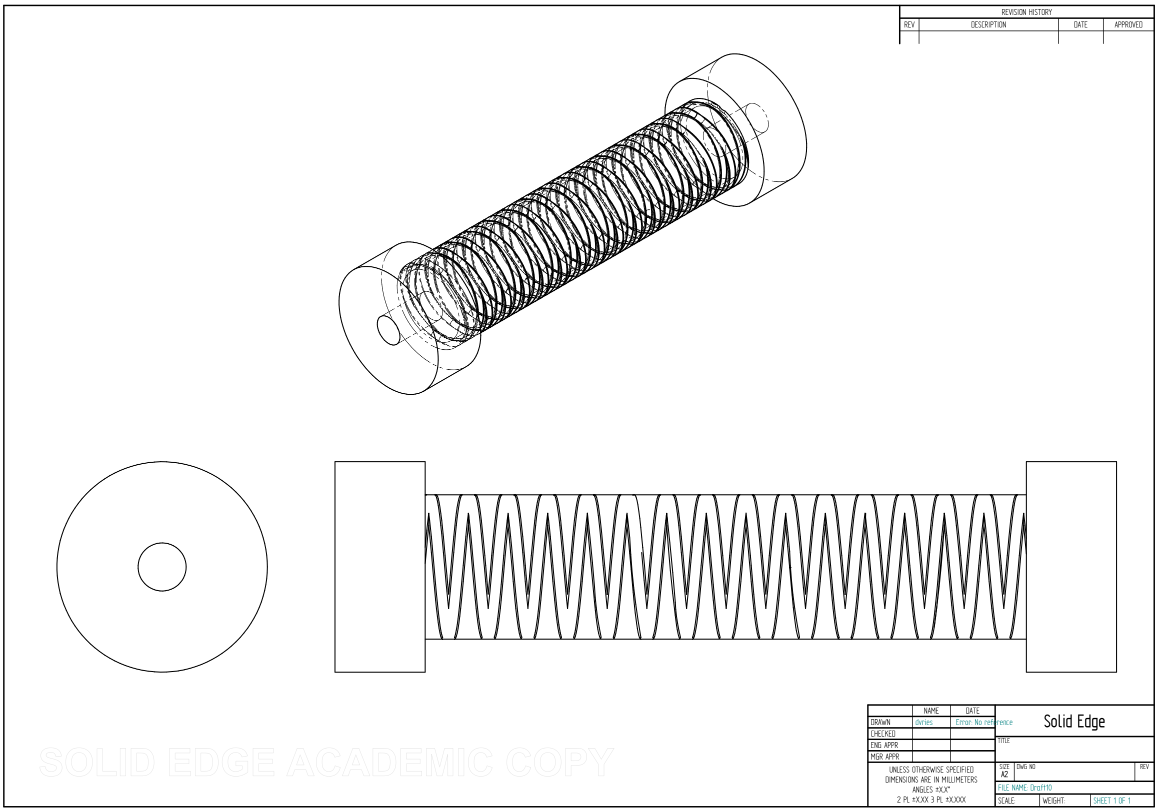

Figure A.5: Multi-material design

B

Matlab Code

```matlab
clc
clear
close all

%% Initialize and Load
addpath('Z:\group-folder\PROJECTS\Soft Pneumatic Efficiency (Jelle)\MATLAB\Functions');

Folders = {'20210413 Change fibers'};
point = 5;
Setups = {'FLUIDICS'};
Quantities = {'Load','Extension'};
File = [mfilename('fullpath'),'.m'];
if (contains(Folders,'cham','IgnoreCase',true)||contains(Folders,'corr','IgnoreCase',true))
    sep = true;
else
    sep = false;
end

[Data] = LoadData(Folders,Setups);
R0 = 10e-3;
for n = 1:length(Data.Samplenames)
    if contains(Folders,'length','IgnoreCase',true)
        L0(n) = str2double(extractBetween(Data.Samplenames{n},'L','-'))/1000;
    else
        L0(n) = 100e-3;
    end
    if contains(Folders,'cham','IgnoreCase',true)
        Vw(n) = (str2double(extractBetween(Data.Samplenames{n},'N','-'))-1)*1e-3*pi*...
                (R0^2-4e-3^2);
    else
        Vw(n) = 0;
    end
end
t0 = 2e-3;
V0 = pi*R0^2*L0-Vw;
Patm = 101325;

for i = 1:length(Data.Samplenames)
    Flow(i) = find(strcmp('BidirFlow',Data.FLUIDICSINFO.sensors(:,i)));
    Actuation(i) = find(strcmp('Actuation',Data.FLUIDICSINFO.sensors(:,i)));
    Deflation(i) = find(strcmp('Deflation',Data.FLUIDICSINFO.sensors(:,i)));
    Pressure(i) = find(strcmp('MPX5',Data.FLUIDICSINFO.sensors(:,i)));
    MFC(i) = find(strcmp('MFC',Data.FLUIDICSINFO.sensors(:,i)));
    Position(i) = find(strcmp('Ruler',Data.FLUIDICSINFO.sensors(:,i)));
    Force(i) = find(strcmp('Loadcell',Data.FLUIDICSINFO.sensors(:,i)));
end

R = 0.082057366080960;
n0 = V0*1e3/(R*293);
```

```
fun = @(m)sRGB_to_OSAUCS(m,true,true); % recommended OSA-UCS
colors = maxdistcolor(8,fun,'Lmin',0.45,'Lmax',0.7,'Cmin',0.25,'Cmax',0.75);
colors([1 2 5 6 7 ],:) = colors([7 6 2 1 5],:);
%% Remove dummy cycle
for n = 1:length(Data.Samplenames)
    start = 1+find(diff(Data.FLUIDICSDATA{Deflation(i),n}) == -1,1);
    for i = 1:length(Data.FLUIDICSDATA(:,n))
        Data.FLUIDICSDATA{i,n} = Data.FLUIDICSDATA{i,n}(start:end);
    end
end

%% Isolate run
Run = NaN;
if ~isnan(Run)
    for j = 1:length(Run)
        for i = 1:length(Data.FLUIDICSDATA(:,Run(j)))
            Data.FLUIDICSDATA{i,j} = Data.FLUIDICSDATA{i,Run(j)};
        end
        Data.Samplenames{j} = Data.Samplenames{Run(j)};
    end
    Data.FLUIDICSDATA(:,j+1:end) = [];
    Data.Samplenames(j+1:end) = [];
end

%% Calculations
for n = 1:length(Data.Samplenames)
    Cycend(:,n) = find(diff(Data.FLUIDICSDATA{Deflation(n),n}) == -1);
    nCyc = length(Cycend(:,n));
    for j = 1:length(Data.FLUIDICSDATA(:,n))
        Data.FLUIDICSDATA(j,n,1) = {Data.FLUIDICSDATA{j,n,1}(1:Cycend(end,n))};
        for i = 1:nCyc
            if i == 1
                Data.FLUIDICSDATA(j,n,i+1) = {Data.FLUIDICSDATA{j,n,1}(1:Cycend(i,n))};
            else
                Data.FLUIDICSDATA(j,n,i+1) = {Data.FLUIDICSDATA{j,n,1}...
                                              (1+Cycend(i-1,n):Cycend(i,n))};
            end
        end
    end
for i = 2:nCyc+1
    Actstart(n,i) = find(diff(Data.FLUIDICSDATA{Actuation(n),n,i}) == 1);
    Actend(n,i) = 0.2*Data.FLUIDICSINFO.SampleRate+1+...
                  find(diff(Data.FLUIDICSDATA{Actuation(n),n,i}) == -1);
    Defstart(n,i) = find(diff(Data.FLUIDICSDATA{Deflation(n),n,i}) == 1,1);
    Data.CALCDATA(1,n,i) = {((1:length(Data.FLUIDICSDATA{1,n,i}))/...
                           Data.FLUIDICSINFO.SampleRate)'};
    Data.CALCDATA(2,n,i) = {Data.FLUIDICSDATA{Flow(n),n,i}.*...
                           (1+Data.FLUIDICSDATA{Pressure(n),n,i}/1e5)*(293/273/60000)};
    Data.CALCDATA(3,n,i) = {V0(n)+ cumtrapz(Data.CALCDATA{1,n,i},Data.CALCDATA{2,n,i})};
    Temp = ((mean(Data.FLUIDICSDATA{Pressure(n),n,i}(1:4*Data.FLUIDICSINFO.SampleRate))...
           +Patm)./(Data.FLUIDICSDATA{Pressure(n),n,i}(1:Actstart(n,i))+Patm)-1)...
           *mean(Data.CALCDATA{3,n,i}(1:4*Data.FLUIDICSINFO.SampleRate));
    Data.CALCDATA(3,n,i) = {Data.CALCDATA{3,n,i}+[Temp; Temp(end)*...
                           ones(length(Data.CALCDATA{1,n,i})-Actstart(n,i),1)]};
    Temp2 = ((mean(Data.FLUIDICSDATA{Pressure(n),n,i}(Actend(n,i)+1:Actend(n,i)+...
            0.1*Data.FLUIDICSINFO.SampleRate))+Patm)./(Data.FLUIDICSDATA...
            {Pressure(n),n,i}(Actend(n,i)+1:Defstart(n,i))+Patm)-1)*mean(Data.CALCDATA...
            {3,n,i}(Actend(n,i)+1:Actend(n,i)+0.1*Data.FLUIDICSINFO.SampleRate));
    Data.CALCDATA(3,n,i) = {Data.CALCDATA{3,n,i}+[zeros(Actend(n,i),1); Temp2;...
                           Temp2(end)*ones(length(Data.CALCDATA{1,n,i})-Defstart(n,i),1)]};
    Data.CALCDATA(4,n,i) = {trapz(Data.CALCDATA{3,n,i}(Actstart(n,i):Actend(n,i)),...
                           Data.FLUIDICSDATA{Pressure(n),n,i}(Actstart(n,i):Actend(n,i)))};
    Data.CALCDATA(5,n,i) = {trapz(Data.CALCDATA{3,n,i}(Defstart(n,i):end),...
                           Data.FLUIDICSDATA{Pressure(n),n,i}(Defstart(n,i):end))};
    ntot(n,i) = n0(n)+trapz(Data.CALCDATA{1,n,i}(1:Actend(n,i)+2*...
                Data.FLUIDICSINFO.SampleRate)/60,Data.FLUIDICSDATA{Flow(n),n,i}...
                (1:Actend(n,i)+2*Data.FLUIDICSINFO.SampleRate))/(R*273);
    Data.CALCDATA(6,n,i) = {ntot(n,i)*R*293.*log(Patm./(Patm+...
                           max(Data.FLUIDICSDATA{Pressure(n),n,i})))};
    Data.CALCDATA(7,n,i) = {sum([Data.CALCDATA{4:5,n,i}])-trapz(Data.FLUIDICSDATA...
```

```
                                {Position(n),n,i},Data.FLUIDICSDATA{Force(n),n,i})};
    Data.CALCDATA(8,n,i) = {100*Data.CALCDATA{7,n,i}/Data.CALCDATA{4,n,i}};
    Data.CALCDATA(9,n,i) = {diff([Data.CALCDATA{5:6,n,i}])};
    Data.CALCDATA(10,n,i) = {Data.CALCDATA{5,n,i}/Data.CALCDATA{4,n,i}};
    Data.CALCDATA(11,n,i) = {trapz(Data.FLUIDICSDATA{Position(n),n,i},...
                             Data.FLUIDICSDATA{Force(n),n,i})};
    Data.CALCDATA(12,n,i) = {100*Data.CALCDATA{11,n,i}/Data.CALCDATA{4,n,i}};
    Data.CALCDATA(13,n,i) = {100*Data.CALCDATA{11,n,i}/sum([Data.CALCDATA{4:5,n,i}])};
    Data.CALCDATA(14,n,i) = {mean(Data.FLUIDICSDATA{Force(n),n,i}(((Actstart(n,i)+2*...
                             Actend(n,i))/3):Actend(n,i)))};
end
end

%% Averaging
repeats = 3;
for n = 1:length(Data.Samplenames)
    for i = 1:nCyc/repeats
        [¬,I(n,i,:)] = mink(abs(ntot(n,:)-ntot(n,i+1)),repeats);
        Input(n,i) = mean(ntot(n,I(n,i,:)))/n0(n)-1;
        Ecl(n,i) = mean([Data.CALCDATA{13,n,I(n,i,:)}]);
        Scl(n,i) = std([Data.CALCDATA{13,n,I(n,i,:)}]);
        Eol(n,i) = mean([Data.CALCDATA{12,n,I(n,i,:)}]);
        Sol(n,i) = std([Data.CALCDATA{12,n,I(n,i,:)}]);
        W(n,i) = mean([Data.CALCDATA{11,n,I(n,i,:)}]);
        Ws(n,i) = std([Data.CALCDATA{11,n,I(n,i,:)}]);
        Load(n,i) = mean([Data.CALCDATA{14,n,I(n,i,:)}]);
        Ediss(n,i) = mean([Data.CALCDATA{7,n,I(n,i,:)}]);
        Sdiss(n,i) = std([Data.CALCDATA{7,n,I(n,i,:)}]);
        Ein(n,i) = mean([Data.CALCDATA{4,n,I(n,i,:)}]);
    end
end

[Samples,Test,Isamp] = unique(extractBefore(Data.Samplenames,'-'));

for n = 1:length(Data.Samplenames)
    [¬,inputpoint(n,1)] = min(abs(Input(n,:)-point));
    inputs(n) = Input(n,inputpoint(n));
end
avginput = round(mean(inputs),1);

for i = 1:length(Samples)
    [Sampload{i},sorting] = sort(Load(sub2ind(size(Load),find(Isamp == i),...
                            inputpoint(Isamp == i))));
    Sampeff{i} = Ecl(sub2ind(size(Ecl),find(Isamp == i),inputpoint(Isamp == i)));
    Sampeff{i} = Sampeff{i}(sorting);
    Samperr{i} = Scl(sub2ind(size(Scl),find(Isamp == i),inputpoint(Isamp == i)));
    Samperr{i} = Samperr{i}(sorting);
    Sampeffo{i} = Eol(sub2ind(size(Eol),find(Isamp == i),inputpoint(Isamp == i)));
    Sampeffo{i} = Sampeffo{i}(sorting);
    Samperro{i} = Sol(sub2ind(size(Sol),find(Isamp == i),inputpoint(Isamp == i)));
    Samperro{i} = Samperro{i}(sorting);
    SampW{i} = W(sub2ind(size(W),find(Isamp == i),inputpoint(Isamp == i)));
    SampW{i} = SampW{i}(sorting);
    SampWs{i} = Ws(sub2ind(size(Ws),find(Isamp == i),inputpoint(Isamp == i)));
    SampWs{i} = SampWs{i}(sorting);
    SampEin{i} = Ein(Isamp == i,:);
    SampEdiss{i} = Ediss(Isamp == i,:);
end

if contains(Folders,{'mat','fibers'},'IgnoreCase',true)
    temp = Data.Samplenames;
    temp(contains(temp,'EF','IgnoreCase',true)) = eraseBetween(temp(contains(temp,'EF',...
                                                  'IgnoreCase',true)),3,3);
    [¬,sortruns] = sortrows([str2double(extractAfter(extractBefore(temp,'-'),2))'...
                   str2double(extractAfter(Data.Samplenames,'M'))']);
    temp = Samples;
    temp(contains(temp,'EF','IgnoreCase',true)) = eraseBetween(temp(contains(temp,'EF',...
                                                  'IgnoreCase',true)),3,3);
    [¬,SortSamples] = sort(str2double(extractAfter(temp,2)));
    if contains(Folders,{'fibers'},'IgnoreCase',true)
        Samples(contains(Samples,'DS10','IgnoreCase',true)) = ...
```

```
            strrep(Samples(contains(Samples,'DS10','IgnoreCase',true)),'DS10','None');
            Data.Samplenames(contains(Data.Samplenames,'DS10','IgnoreCase',true)) = ...
            strrep(Data.Samplenames(contains(Data.Samplenames,'DS10','IgnoreCase',true)),...
            'DS10','None');
        end
else
    [¬,sortruns] = sortrows([str2double(extractAfter(extractBefore(Data.Samplenames,...
                '-'),1))' str2double(extractAfter(Data.Samplenames,'M'))']);
    [¬,SortSamples] = sort(str2double(extractAfter(Samples,1)));
end
sortruns = sortruns';

Samples = Samples(SortSamples);


[Weights,¬,Iweights] = unique(extractAfter(Data.Samplenames,'-'));
[¬,sortWeights] = sort(str2double(extractAfter(Weights,1)));
Weights = Weights(sortWeights);

for n = 1:length(Weights)
    Seps{n} = extractBefore(Data.Samplenames(Iweights == n),'-');
    [¬,sorts{n}] = sort(str2double(extractAfter(Seps{n},1)));
    Seps{n} = Seps{n}(sorts{n});
    Sepin{n} = Input(Iweights == n,:);
    Sepin{n} = Sepin{n}(sorts{n},:)';
    [Sepin{n},sorts2] = sort(Sepin{n});
    [row,column]=size(sorts2);
    sorts2 = sub2ind([row column],sorts2,repmat(1:column,row,1));
    Sepcl{n} = Ecl(Iweights == n,:);
    Sepcl{n} = Sepcl{n}(sorts{n},:)';
    Sepcl{n} = Sepcl{n}(sorts2);
    Sepec{n} = Scl(Iweights == n,:);
    Sepec{n} = Sepec{n}(sorts{n},:)';
    Sepec{n} = Sepec{n}(sorts2);
    Sepol{n} = Eol(Iweights == n,:);
    Sepol{n} = Sepol{n}(sorts{n},:)';
    Sepol{n} = Sepol{n}(sorts2);
    Seper{n} = Sol(Iweights == n,:);
    Seper{n} = Seper{n}(sorts{n},:)';
    Seper{n} = Seper{n}(sorts2);
    SepW{n} = W(Iweights == n,:);
    SepW{n} = SepW{n}(sorts{n},:)';
    SepW{n} = SepW{n}(sorts2);
    SepWs{n} = Ws(Iweights == n,:);
    SepWs{n} = SepWs{n}(sorts{n},:)';
    SepWs{n} = SepWs{n}(sorts2);
end

Seps = Seps(sortWeights);
Sepin = Sepin(sortWeights);
Sepcl = Sepcl(sortWeights);
Sepec = Sepec(sortWeights);
Sepol = Sepol(sortWeights);
Seper = Seper(sortWeights);
SepW = SepW(sortWeights);
SepWs = SepWs(sortWeights);

%% Plot and Save
close all
fig1 = figure('Units','points','Position',[0 0 426 249]);
t1 = tiledlayout(2,3,'TileSpacing','None','Padding','None');
nexttile
[¬,pl] = sort(sortruns);
for j = 1:length(Samples)
    i = find(contains(Data.Samplenames,'M0')& contains(Data.Samplenames,[Samples{j} '-']));
    [sorted,sorting] = sort(Input(i,:));
    if sep == true
        errorbar(sorted,Ecl(i,sorting),Scl(i,sorting),'LineWidth',1.5)
    else
        errorbar(sorted,Ecl(i,sorting),Scl(i,sorting),'color',colors(j,:),'LineWidth',1.5)
    end
```

```
    hold on
end
grid on
yticks(linspace(6,10,5));
lh1 = legend(Samples,'Orientation','horizontal');
title('Closed Loop')
ylabel('$$\eta_{\mathrm{cl}}\: \mathrm{[\%]}$$','interpreter','latex')
xlabel('$$\frac{V_{\mathrm{input}}}{V_{\mathrm{act,0}}}$$','interpreter','latex');
set(gca,'linewidth',1,'FontSize',9)
if (contains(Folders,'fiber','IgnoreCase',true) || ...
    contains(Folders,'thicc','IgnoreCase',true))
    xlim([1.7 inf])
end

nexttile
for j = 1:length(Samples)
    i = find(contains(Data.Samplenames,'M0')& contains(Data.Samplenames,[Samples{j} '-']));
    [sorted,sorting] = sort(Input(i,:));
    if sep == true
        errorbar(sorted,Eol(i,sorting),Sol(i,sorting),'LineWidth',1.5)
    else
        errorbar(sorted,Eol(i,sorting),Sol(i,sorting),'color',colors(j,:),'LineWidth',1.5)
    end
    hold on
end
grid on
title('Open Loop')
yticks(linspace(0.9,1.2,4));
ylabel('$$\eta_{\mathrm{ol}}\: \mathrm{[\%]}$$','interpreter','latex')
xlabel('$$\frac{V_{\mathrm{input}}}{V_{\mathrm{act,0}}}$$','interpreter','latex');
set(gca,'linewidth',1,'FontSize',9)
if (contains(Folders,'fiber','IgnoreCase',true) || ...
    contains(Folders,'thicc','IgnoreCase',true))
    xlim([1.7 inf])
end

nexttile
for j = 1:length(Samples)
    i = find(contains(Data.Samplenames,'M0')& contains(Data.Samplenames,[Samples{j} '-']));
    [sorted,sorting] = sort(Input(i,:));
    if sep == true
        errorbar(sorted,W(i,sorting),Ws(i,sorting),'LineWidth',1.5)
    else
        errorbar(sorted,W(i,sorting),Ws(i,sorting),'color',colors(j,:),'LineWidth',1.5)
    end
    hold on
end
grid on
title('Work')
yticks(linspace(0,0.06,4));
ylabel('$$W\: \mathrm{[J]}$$','interpreter','latex')
xlabel('$$\frac{V_{\mathrm{input}}}{V_{\mathrm{act,0}}}$$','interpreter','latex');
set(gca,'linewidth',1,'FontSize',9)
if (contains(Folders,'fiber','IgnoreCase',true) || ...
    contains(Folders,'thicc','IgnoreCase',true))
    xlim([1.7 inf])
end

nexttile

for i = SortSamples
    errorbar(Sampload{i},Sampeff{i},Samperr{i},'color',colors(i == SortSamples,:),...
    'LineWidth',1.5)
    hold on
end
grid on
yticks(linspace(10,30,5));
%xticks(linspace(0,10,5));
xlabel('$$F\: \mathrm{[N]}$$','interpreter','latex')
ylabel('$$\eta_{\mathrm{cl}}\: \mathrm{[\%]}$$','interpreter','latex')
set(gca,'linewidth',1,'FontSize',9)
```

```
nexttile
for i = SortSamples
    errorbar(Sampload{i},Sampeffo{i},Samperro{i},'color',colors(i == SortSamples,:),...
    'LineWidth',1.5)
    hold on
end
grid on
yticks(linspace(1,4,4));
%ylim([1 inf]);
%xticks(linspace(0,10,5));
xlabel('$$F\: \mathrm{[N]}$$','interpreter','latex')
ylabel('$$\eta_{\mathrm{ol}}\: \mathrm{[\%]}$$','interpreter','latex')
set(gca,'linewidth',1,'FontSize',9)

nexttile
for i = SortSamples
    errorbar(Sampload{i},SampW{i},SampWs{i},'color',colors(i == SortSamples,:),...
    'LineWidth',1.5)
    hold on
end
grid on
yticks(linspace(0,0.15,4));
%xticks(linspace(0,10,5));
xlabel('$$F\: \mathrm{[N]}$$','interpreter','latex')
ylabel('$$W\: \mathrm{[J]}$$','interpreter','latex')
set(gca,'linewidth',1,'FontSize',9)

lh1.Layout.Tile = 'South';
title(t1,append('$$\mathrm{Top\:row}:F = F_{\mathrm{carrrier}}\\,\: \mathrm{Bottom\:row}
:\frac{V_{\mathrm{input}}}{V_{\mathrm{act,0}}} \approx ',num2str(avginput),'$$'),...
'interpreter','latex','FontSize',11)

fig2 = figure('Units','points','Position',[0 0 426 180]);
t2 = tiledlayout(1,3,'TileSpacing','None','Padding','None');
nexttile

for i = SortSamples
    errorbar(Sampload{i},Sampeff{i},Samperr{i},'color',colors(i == SortSamples,:),...
    'LineWidth',1.5)
    hold on
end
grid on
%xticks(linspace(1,2,5));
lh2 = legend(Samples,'Orientation','horizontal');
title('Closed Loop')
xlabel('$$F\: \mathrm{[N]}$$','interpreter','latex')
ylabel('$$\eta_{\mathrm{cl}}\: \mathrm{[\%]}$$','interpreter','latex')
set(gca,'linewidth',1,'FontSize',9)

nexttile
for i = SortSamples
    errorbar(Sampload{i},Sampeffo{i},Samperro{i},'color',colors(i == SortSamples,:),...
    'LineWidth',1.5)
    hold on
end
grid on
%xticks(linspace(1,2,5));
title('Open Loop')
xlabel('$$F\: \mathrm{[N]}$$','interpreter','latex')
ylabel('$$\eta_{\mathrm{ol}}\: \mathrm{[\%]}$$','interpreter','latex')
set(gca,'linewidth',1,'FontSize',9)

nexttile
for i = SortSamples
    errorbar(Sampload{i},SampW{i},SampWs{i},'color',colors(i == SortSamples,:),...
    'LineWidth',1.5)
    hold on
end
grid on
%xticks(linspace(1,2,5));
```

```
title('Work')
xlabel('$$F\: \mathrm{[N]}$$','interpreter','latex')
ylabel('$$W\: \mathrm{[J]}$$','interpreter','latex')
set(gca,'linewidth',1,'FontSize',9)

lh2.Layout.Tile = 'South';
title(t2,append('$$\frac{V_{\mathrm{input}}}{V_{\mathrm{act,0}}} \approx ',...
num2str(avginput),'$$'),'interpreter','latex','FontSize',11)

if sep == true
fig3 = figure('Units','points','Position',[0 0 426 336]);
t3 = tiledlayout(3,length(Weights),'TileSpacing','None','Padding','None');
for i = 1:length(Weights)
    nexttile(i)
    p1 = errorbar(Sepin{i},Sepcl{i},Sepec{i},'LineWidth',1.5);
    set(p1, {'color'}, num2cell(colors(1:length(Seps{i}),:),2));
    hold on
    grid on
    %yticks(linspace(0,40,5));
    if i == 1
        ylabel('$$\eta_{\mathrm{cl}}\: \mathrm{[\%]}$$','interpreter','latex')
        title('F = F_{carrier}')

    else
        title(['F = F_{carrier} + ' Weights{i}])
    end
    set(gca,'linewidth',1,'FontSize',9)

    nexttile(i+length(Weights))
    p2 = errorbar(Sepin{i},Sepol{i},Seper{i},'LineWidth',1.5);
    set(p2, {'color'}, num2cell(colors(1:length(Seps{i}),:),2));
    hold on
    grid on
    if i == 1
    ylabel('$$\eta_{\mathrm{ol}}\: \mathrm{[\%]}$$','interpreter','latex')
    %yticks(linspace(0,10,5));
    else
        %yticks(linspace(0,20,5));
    end
    set(gca,'linewidth',1,'FontSize',9)

    nexttile(i+2*length(Weights))
    p3 = errorbar(Sepin{i},SepW{i},SepWs{i},'LineWidth',1.5);
    set(p3, {'color'}, num2cell(colors(1:length(Seps{i}),:),2));
    hold on
    grid on
    xlabel('$$\frac{V_{\mathrm{input}}}{V_{\mathrm{act,0}}}$$','interpreter','latex');
    if i == 1
    ylabel('$$W\: \mathrm{[J]}$$','interpreter','latex')
    else
       % yticks(linspace(0,0.1,5));
    end
    set(gca,'linewidth',1,'FontSize',9)
end
lh3 = legend(Seps{1},'Orientation','horizontal','Numcolumns',length(Seps{1}));
lh3.Layout.Tile = 'South';

end

if sep == true
SaveData([fig2 fig3],Folders,Setups,File,[append(extractAfter(extractAfter(Folders,...
' '),' '),'oneinput'),append(extractAfter(extractAfter(Folders,' '),' '),'separate')]);
else
    SaveData([fig1 fig2],Folders,Setups,File,[append(extractAfter(extractAfter(Folders,...
    ' '),' '),'allruns'),append(extractAfter(extractAfter(Folders,' '),' '),'oneinput')]);
end
```

```
function [Data] = LoadData(Foldernames,Setups)
Data.Samplenames = {};

% Get a list of all files and folders in this folder.
files = dir(['Z:\group-folder\PROJECTS\Soft Pneumatic Efficiency (Jelle)\EXPERIMENTS\
        FLUIDICS\',Foldernames{m}]);
% Get a logical vector that tells which is a directory.
dirFlags = [files.isdir];
% Extract only those that are directories.
subFolders = files(dirFlags);
subFolders = subFolders(3:end); % exclude . and ..
subFolders = subFolders(¬contains({subFolders.name},'Processed'));

fid1 = fopen(['Z:\group-folder\PROJECTS\Soft Pneumatic Efficiency (Jelle)\EXPERIMENTS
    \FLUIDICS\',Foldernames{m},'\',subFolders(1).name,'\measurement.txt']);
for i=1:9
    SR = fgetl(fid1);
end
fclose(fid1);
Data(m).FLUIDICSINFO.SampleRate = str2double(SR(19:end));

for j = 1:length(subFolders)
    disp(['Loading... Folder ',num2str(m),' of ',num2str(length(Foldernames)),...
    ', Sample ',num2str(j),' of ',num2str(length(subFolders))])
    Data(m).Samplenames{end+1} = subFolders(j).name(17:end);
    fid1=fopen(['Z:\group-folder\PROJECTS\Soft Pneumatic Efficiency (Jelle)\EXPERIMENTS
    \FLUIDICS\',Foldernames{m},'\',subFolders(j).name,'\sensorvalues.txt']);
    legs=fgetl(fid1);
    legs=split(legs);
    numSensors=length(legs)/2;
    for i=1:numSensors
        sensors{i,1}=legs{i*2-1};
        units{i,1}=legs{i*2};
    end

    DAT=fscanf(fid1,'%f',[numSensors,inf])';
    for i = 1:numSensors
        switch sensors{i}
            case {'MPX5'}
                DAT(:,i) = DAT(:,i)-mean(DAT(1:9*Data(m).FLUIDICSINFO.SampleRate,i));
                DAT(:,i) = DAT(:,i)*2000/(5*0.018);
                DAT(:,i) = smooth(DAT(:,i),40,'loess');
                units{i} = '[Pa]';
                quantities{i} = 'Pressure';
            case {'Loadcell'}
                DAT(:,i) = DAT(:,i)-mean(DAT(1:9*Data(m).FLUIDICSINFO.SampleRate,i));
                DAT(:,i) = smooth(DAT(:,i),40,'loess');
                units{i} = '[N]';
                quantities{i} = 'Force';
            case {'Ruler'}
                DAT(:,i) = DAT(:,i)/1000;
                DAT(:,i) = smooth(DAT(:,i),40,'loess');
                DAT(:,i) = DAT(:,i)-mean(DAT(1:9*Data(m).FLUIDICSINFO.SampleRate,i));
                units{i} = '[m]';
                quantities{i} = 'Distance';
            case {'MFC'}
                DAT(:,i) = DAT(:,i)-mean(DAT(1:9*Data(m).FLUIDICSINFO.SampleRate,i));
                DAT(:,i) = smooth(DAT(:,i),40,'loess');
                quantities{i} = 'MFC';
            case {'HAF_bidir_flow0750'}
                load('bidirfit','bidirfitresult')
                DAT(:,i) = smooth(DAT(:,i),40,'loess');
                rawdata = DAT(:,i);
                data = rawdata-mean(DAT(1:9*Data(m).FLUIDICSINFO.SampleRate,i));
                DAT(:,i) = data.*bidirfitresult(data);
                units{i} = '[slpm]';
                quantities{i} = 'Flow';
                sensors{i,1} = 'BidirFlow';
            case {'Actuation'}
                data = DAT(:,i);
                DAT(data>2.5,i) = 1;
```

```
                DAT(data<2.5,i) = 0;
                DAT(1:9*Data(m).FLUIDICSINFO.SampleRate,i) = 0;
                units{i} = '[-]';
                quantities{i} = 'Actuation';
            case {'Deflation'}
                data = DAT(:,i);
                DAT(data>2.5,i) = 1;
                DAT(data<2.5,i) = 0;
                DAT(1:9*Data(m).FLUIDICSINFO.SampleRate,i) = 0;
                units{i} = '[-]';
                quantities{i} = 'Deflation';
            otherwise
                disp(['unknown sensor! ', sensors{i}])
        end
        if i == 1
            Data(m).FLUIDICSDATA{i,end+1}=DAT(:,i);
        else
            Data(m).FLUIDICSDATA{i,end}=DAT(:,i);
        end
    end
    fclose(fid1);

    if isfield(Data(m).FLUIDICSINFO,'sensors')
        Data(m).FLUIDICSINFO.sensors(1:length(sensors),end+1)=sensors;
        Data(m).FLUIDICSINFO.quantities(1:length(sensors),end+1) = quantities;
    else
        Data(m).FLUIDICSINFO.sensors(1:length(sensors),1)=sensors;
        Data(m).FLUIDICSINFO.quantities(1:length(sensors),1) = quantities;
    end
end
end

function SaveData(figs,Folders,Setups,File,names)
date = datestr(now,'yyyymmdd-HHMM');
Foldername = ['Processed-',date];
opt.figDPI = 300;
index = strfind(File,'\');
index = index(end);

for i = 1:length(Folders)
    for j = 1:length(Setups)
        mkdir(['Z:\group-folder\PROJECTS\Soft Pneumatic Efficiency (Jelle)\
        EXPERIMENTS\',Setups{j},'\',Folders{i}],Foldername)
        for n = 1:length(figs)
            if exist('names','var')
                printHigRes(figs(n),opt,names{n},['Z:\group-folder\PROJECTS\Soft Pneumatic
                Efficiency (Jelle)\EXPERIMENTS\',Setups{j},'\',Folders{i},'\',Foldername]);
            else
                printHigRes(figs(n),opt,['figure-',num2str(n)],['Z:\group-folder\PROJECTS\
                Soft Pneumatic Efficiency (Jelle)\EXPERIMENTS\',Setups{j},'\',...
                Folders{i},'\',Foldername]);
            end
        end
        copyfile(File,['Z:\group-folder\PROJECTS\Soft Pneumatic Efficiency (Jelle)\
        EXPERIMENTS\',Setups{j},'\',Folders{i},'\',Foldername,'\',File(index+1:end)]);
        copyfile('Z:\group-folder\PROJECTS\Soft Pneumatic Efficiency (Jelle)\MATLAB\
        Functions',['Z:\group-folder\PROJECTS\Soft Pneumatic Efficiency (Jelle)\
        EXPERIMENTS\',Setups{j},'\',Folders{i},'\',Foldername,'\Functions']);
    end
end
end

function printHigRes(f,opt,nam,nameFolder)
        name=[nameFolder,'/',nam,'_highres'];
        figpos=getpixelposition(f);
        resolution=get(0,'ScreenPixelsPerInch');
        set(f,'paperunits','inches','papersize',figpos(3:4)/resolution,...
        'paperposition',[0 0 figpos(3:4)/resolution]);
        print(f,name,'-dpdf',['-r',num2str(opt.figDPI)],'-opengl')
end
```

Bibliography

[1] Momme Adami and Arthur Seibel. “On-board pneumatic pressure generation methods for soft robotics applications”. In: *Actuators* 8.1 (2019). ISSN: 20760825. DOI: 10.3390/act8010002.

[2] G Agarwal et al. “Design and Computational Modeling of a Modular, Compliant Robotic Assembly for Human Lumbar Unit and Spinal Cord Assistance”. In: *Scientific Reports* 7.1 (2017). DOI: 10.1038/s41598-017-14220-3.

[3] G Agarwal et al. “Stretchable Materials for Robust Soft Actuators towards Assistive Wearable Devices”. In: *Scientific Reports* 6 (2016). DOI: 10.1038/srep34224.

[4] J Bishop-Moser and S Kota. “Design and Modeling of Generalized Fiber-Reinforced Pneumatic Soft Actuators”. English. In: *IEEE Transactions on Robotics* 31.3 (2015), pp. 536–545. ISSN: 15523098 (ISSN). DOI: 10.1109/TRO.2015.2409452.

[5] P Boyraz, G Runge, and A Raatz. “An overview of novel actuators for soft robotics”. English. In: *Actuators* 7.3 (2018). ISSN: 20760825 (ISSN). DOI: 10.3390/act7030048.

[6] V Cacucciolo et al. “Electrically-Driven Soft Fluidic Actuators Combining Stretchable Pumps With Thin McKibben Muscles”. In: *Frontiers in Robotics and AI* 6 (2020). DOI: 10.3389/frobt.2019.00146.

[7] W Chen et al. “Fabrication and Dynamic Modeling of Bidirectional Bending Soft Actuator Integrated with Optical Waveguide Curvature Sensor”. English. In: *Soft Robotics* 6.4 (2019), pp. 495–506. ISSN: 21695172 (ISSN). DOI: 10.1089/soro.2018.0061.

[8] Ho Tak D. Chun et al. “Towards more energy efficient pneumatic soft actuators using a port-hamiltonian approach”. In: *RoboSoft 2019 - 2019 IEEE International Conference on Soft Robotics* May (2019), pp. 277–282. DOI: 10.1109/ROBOSOFT.2019.8722709.

[9] Matteo Cianchetti et al. “Biomedical applications of soft robotics”. In: *Nature Reviews Materials* 3.6 (2018), pp. 143–153. ISSN: 20588437. DOI: 10.1038/s41578-018-0022-y.

[10] A Costas et al. “Design, development and characterization of linear, soft actuators via additive manufacturing”. In: *ASME 2018 Conference on Smart Materials, Adaptive Structures and Intelligent Systems, SMASIS 2018*. Vol. 1. 2018. DOI: 10.1115/SMASIS2018-8097.

[11] Stephen Coyle et al. “Bio-inspired soft robotics: Material selection, actuation, and design”. In: *Extreme Mechanics Letters* 22 (2018), pp. 51–59. ISSN: 23524316. DOI: 10.1016/j.eml.2018.05.003.

[12] Dylan Drotman et al. “3D printed soft actuators for a legged robot capable of navigating unstructured terrain”. In: *Proceedings - IEEE International Conference on Robotics and Automation* (2017), pp. 5532–5538. ISSN: 10504729. DOI: 10.1109/ICRA.2017.7989652.

[13] J M Florez et al. “Rehabilitative Soft Exoskeleton for Rodents”. English. In: *IEEE Transactions on Neural Systems and Rehabilitation Engineering* 25.2 (2017), pp. 107–118. ISSN: 15344320 (ISSN). DOI: 10.1109/TNSRE.2016.2535352.

[14] Benjamin Gorissen et al. “Elastic Inflatable Actuators for Soft Robotic Applications”. In: *Advanced Materials* 29.43 (2017), pp. 1–14. ISSN: 15214095. DOI: 10.1002/adma.201604977.

[15] Michael D. Grissom et al. “Design and experimental testing of the OctArm soft robot manipulator”. In: *Unmanned Systems Technology VIII* 6230.May 2006 (2006), 62301F. ISSN: 0277786X. DOI: 10.1117/12.665321.

[16] E W Hawkes, D L Christensen, and A M Okamura. “Design and implementation of a 300% strain soft artificial muscle”. In: *Proceedings - IEEE International Conference on Robotics and Automation*. Vol. 2016-June. 2016, pp. 4022–4029. DOI: 10.1109/ICRA.2016.7487592.

[17] A Al-Ibadi, S Nefti-Meziani, and S Davis. “Novel models for the extension pneumatic muscle actuator performances”. In: *ICAC 2017 - 2017 23rd IEEE International Conference on Automation and Computing: Addressing Global Challenges through Automation and Computing*. 2017. DOI: 10.23919/IConAC.2017.8081973.

[18] Z Jiao et al. “Vacuum-Powered Soft Pneumatic Twisting Actuators to Empower New Capabilities for Soft Robots”. English. In: *Advanced Materials Technologies* 4.1 (2019). ISSN: 2365709X (ISSN). DOI: 10.1002/admt.201800429.

[19] W Jung et al. “Biocompatible micro, soft bellow actuator rapidly manufactured using 3D-printed soluble mold”. In: *Journal of Micromechanics and Microengineering* 29.12 (2019). DOI: 10.1088/1361-6439/ab477f.

[20] Robert K. Katzschmann et al. “Exploration of underwater life with an acoustically controlled soft robotic fish”. In: *Science Robotics* 3.16 (2018), pp. 1–13. ISSN: 24709476. DOI: 10.1126/SCIROBOTICS.AAR3449.

[21] Cecilia Laschi and Matteo Cianchetti. “Soft robotics: New perspectives for robot bodyware and control”. In: *Frontiers in Bioengineering and Biotechnology* 2.JAN (2014), pp. 1–5. ISSN: 22964185. DOI: 10.3389/fbioe.2014.00003.

[22] Cecilia Laschi, Barbara Mazzolai, and Matteo Cianchetti. “Soft robotics: Technologies and systems pushing the boundaries of robot abilities”. In: *Science Robotics* 1.1 (2016), pp. 1–12. ISSN: 24709476. DOI: 10.1126/scirobotics.aah3690.

[23] Jin Gyu Lee and Hugo Rodrigue. “Origami-Based Vacuum Pneumatic Artificial Muscles with Large Contraction Ratios”. In: *Soft Robotics* 6.1 (2019), pp. 109–117. ISSN: 21695180. DOI: 10.1089/soro.2018.0063.

[24] Y Lin, J Zou, and H Yang. *A Vacuum-Powered Soft Linear Actuator Strengthened by Granular Jamming*. 2019. DOI: 10.1007/978-3-030-27532-7_47.

[25] Quan Liu et al. “Design and control of soft rehabilitation robots actuated by pneumatic muscles: State of the art”. In: *Future Generation Computer Systems* 113 (2020), pp. 620–634. ISSN: 0167739X. DOI: 10.1016/j.future.2020.06.046.

[26] L Manfredi et al. “4 DOFs hollow soft pneumatic actuator–hose”. In: *Materials Research Express* 6.4 (2019). DOI: 10.1088/2053-1591/aaebea.

[27] Michael J. Moran and Howard N. Shapiro. *Fundamentals of Engineering Thermodynamics.* Vol. 5th ed. John Wiley and Sons, Inc, 2006. ISBN: 9780470030370.

[28] B Mosadegh et al. “Pneumatic networks for soft robotics that actuate rapidly”. In: *Advanced Functional Materials* 24.15 (2014), pp. 2163–2170. DOI: 10.1002/adfm.201303288.

[29] P Moseley et al. “Modeling, Design, and Development of Soft Pneumatic Actuators with Finite Element Method”. In: *Advanced Engineering Materials* 18.6 (2016), pp. 978–988. DOI: 10.1002/adem.201500503.

[30] P Polygerinos et al. “Modeling of Soft Fiber-Reinforced Bending Actuators”. In: *IEEE Transactions on Robotics* 31.3 (2015), pp. 778–789. DOI: 10.1109/TRO.2015.2428504.

[31] Panagiotis Polygerinos et al. “Soft robotic glove for combined assistance and at-home rehabilitation”. In: *Robotics and Autonomous Systems* 73 (2015), pp. 135–143. ISSN: 09218890. DOI: 10.1016/j.robot.2014.08.014.

[32] Panagiotis Polygerinos et al. “Soft Robotics: Review of Fluid-Driven Intrinsically Soft Devices; Manufacturing, Sensing, Control, and Applications in Human-Robot Interaction”. In: *Advanced Engineering Materials* 19.12 (2017). ISSN: 15272648. DOI: 10.1002/adem.201700016.

[33] Steven I. Rich, Robert J. Wood, and Carmel Majidi. “Untethered soft robotics”. In: *Nature Electronics* 1.2 (2018), pp. 102–112. ISSN: 25201131. DOI: 10.1038/s41928-018-0024-1.

[34] Robert F. Shepherd et al. “Multigait soft robot”. In: *Proceedings of the National Academy of Sciences of the United States of America* 108.51 (2011), pp. 20400–20403. ISSN: 00278424. DOI: 10.1073/pnas.1116564108.

[35] Jun Shintake et al. “Soft Robotic Grippers”. In: *Advanced Materials* 30.29 (2018). ISSN: 15214095. DOI: 10.1002/adma.201707035.

[36] Langquan Shui et al. “Energy efficiency of mobile soft robots”. In: *Soft Matter* 13.44 (2017), pp. 8223–8233. ISSN: 17446848. DOI: 10.1039/c7sm01617d.

[37] Z.-S. Sun, Z.-H. Guo, and W Tang. “Design of wearable hand rehabilitation glove with soft hoop-reinforced pneumatic actuator”. In: *Journal of Central South University* 26.1 (2019), pp. 106–119. DOI: 10.1007/s11771-019-3986-x.

[38] C Tawk et al. “3D Printable Linear Soft Vacuum Actuators: Their Modeling, Performance Quantification and Application in Soft Robotic Systems”. In: *IEEE/ASME Transactions on Mechatronics* 24.5 (2019), pp. 2118–2129. DOI: 10.1109/TMECH.2019.2933027.

[39] C Tawk et al. “Fully 3D printed monolithic soft gripper with high conformal grasping capability”. In: vol. 2019-July. 2019, pp. 1139–1144. ISBN: 9781728124933 (ISBN). DOI: 10.1109/AIM.2019.8868668.

[40] Michael T. Tolley et al. “A Resilient, Untethered Soft Robot”. In: *Soft Robotics* 1.3 (2014), pp. 213–223. ISSN: 21695180. DOI: 10.1089/soro.2014.0008.

[41] Deepak Trivedi et al. “Soft robotics: Biological inspiration, state of the art, and future research”. In: *Applied Bionics and Biomechanics* 5.3 (2008), pp. 99–117. ISSN: 17542103. DOI: 10.1080/11762320802557865.

[42] T Wang, W Song, and S Zhu. “Analytical research on energy harvesting systems for fluidic soft actuators”. In: *International Journal of Advanced Robotic Systems* 15.1 (2018). DOI: 10.1177/1729881418755876.

[43] M Wehner et al. “Experimental characterization of components for active soft orthotics”. In: *Proceedings of the IEEE RAS and EMBS International Conference on Biomedical Robotics and Biomechatronics*. 2012, pp. 1586–1592. DOI: 10.1109/BioRob.2012.6290903.

[44] R Xie et al. “3D-PSA: A 3D Pneumatic Soft Actuator with Extending and Omnidirectional Bending Motion”. In: *2018 IEEE International Conference on Robotics and Biomimetics, ROBIO 2018*. 2018, pp. 618–623. DOI: 10.1109/ROBIO.2018.8665051.

[45] J Yan et al. “A New Spiral-Type Inflatable Pure Torsional Soft Actuator”. In: *Soft Robotics* 5.5 (2018), pp. 527–540. DOI: 10.1089/soro.2017.0040.

[46] H K Yap, H Y Ng, and C.-H. Yeow. “High-Force Soft Printable Pneumatics for Soft Robotic Applications”. In: *Soft Robotics* 3.3 (2016), pp. 144–158. DOI: 10.1089/soro.2016.0030.

[47] H K Yap et al. “Characterisation and evaluation of soft elastomeric actuators for hand assistive and rehabilitation applications”. In: *Journal of Medical Engineering and Technology* 40.4 (2016), pp. 199–209. DOI: 10.3109/03091902.2016.1161853.

[48] J Yi et al. “Fiber-Reinforced Origamic Robotic Actuator”. In: *Soft Robotics* 5.1 (2018), pp. 81–92. DOI: 10.1089/soro.2016.0079.

Mand.